Magnetostructural characterisation of biological materials: Detection and quantification of nanometric iron-containing species

Lucía Gutiérrez Marruedo

Caracterización magnetoestructural de materiales biológicos: Detección y cuantificación de especies nanométricas que contienen hierro

Tesis presentada por
Lucía Gutiérrez

Director de la tesis
Francisco J. Lázaro

Departamento de Ciencia y Tecnología de Materiales y Fluidos

Universidad de Zaragoza

Septiembre 2008

Magnetostructural characterisation of biological materials: Detection and quantification of nanometric iron-containing species

Thesis presented by
Lucía Gutiérrez

Thesis advisor
Francisco J. Lázaro

Departamento de Ciencia y Tecnología de Materiales y Fluidos

Universidad de Zaragoza

September 2008

Resumen

En esta tesis se ha investigado la especiación del hierro en sistemas biológicos prestando especial atención a las especies en las que el hierro se encuentra formando parte de partículas de óxidos y oxohidróxidos de tamaño nanométrico tanto biogénicas (ferritina y hemosiderina) como no biogénicas (suplementos de hierro y agentes de contraste).

Se han caracterizado ocho suplementos de hierro utilizados en el tratamiento de la anemia ferropénica. El estudio de estos fármacos, además de proporcionar información estructural de cada compuesto, que puede estar relacionado con sus propiedades farmacocinéticas, es el paso previo necesario para su posterior monitorización en el organismo.

Las especies minerales de hierro de origen biogénico se han estudiado en el marco de las enfermedades de sobrecarga de hierro para lo que se han utilizado dos modelos animales distintos.

El primer modelo estudiado se ha generado a partir de la administración de una dosis única de un suplemento de hierro (hierro dextrano) a ratas. Este fármaco está constituido por nanopartículas de un oxohidróxido de hierro llamado akaganeita. Las transformaciones sufridas por el fármaco en el hígado y músculo de la zona cercana a la inyección se han monitorizado magnéticamente a lo largo de tres meses, observándose la disminución de la cantidad de partículas de akaganeita y el aumento de la cantidad de hierro en forma de ferritina. Además, se ha detectado también la acumulación de hierro en el bazo, corazón y riñones de los animales. La identificación de este tipo de especies en los tejidos a partir de la caracterización magnética ha sido posible gracias al estudio de las propiedades magnéticas tanto del fármaco inyectado como de la ferritina de hígado de rata.

El segundo modelo animal de sobrecarga de hierro utilizado ha consistido en ratones modificados genéticamente (knockout $Hfe^{-/-}$) que, a pesar de tener una dieta normal, acumulan grandes cantidades de hierro en el organismo. Este modelo simula mejor las enfermedades humanas y de ahí su especial interés para el estudio de los depósitos de hierro en patologías de sobrecarga de hierro. Se han estudiado magnéticamente tres tejidos diferentes: Hígados, bazos y corazones, habiéndose encontrado una acumulación anómala de hierro en el tejido hepático. Mediante el estudio por Microscopía Electrónica de Transmisión se han observado depósitos de hierro en forma de ferritina o lisosomas que contienen ferritina parcialmente degradada. Sin embargo, se ha detectado también la presencia de otro tipo de depósitos, con un tamaño y una estructura

cristalina diferente a los usualmente observados en estos procesos de sobrecarga, que necesitan un mayor estudio ya que podrían estar relacionados con el aspecto sano de los tejidos a pesar de la gran cantidad de hierro acumulada.

Se incluye también en esta tesis un estudio de la monitorización magnética de un agente de contraste comúnmente utilizado en Imagen por Resonancia Magnética Nuclear. El interés del estudio de la biodistribución de este compuesto por medios magnéticos radica en que, debido a que la cantidad de hierro administrada con el fármaco es muy pequeña en comparación con el hierro biogénico, su estudio por otras técnicas es complicado de realizar. La presencia del agente de contraste ha sido detectada en el hígado y el bazo pero no se ha observado en el corazón ni en los riñones. Además, se ha desarrollado un protocolo para la cuantificación de la cantidad de hierro que está formando parte tanto del agente de contraste como de la ferritina biogénica presente en los tejidos a partir de las medidas magnéticas, que ha servido para proporcionar información cuantitativa sobre la cantidad de hierro que forma parte de estas dos especies en los tejidos. El estudio de la influencia de las interacciones dipolares en muestras del agente de contraste de diferentes concentraciones ha permitido, además, obtener información acerca del grado de agregación de este compuesto en los tejidos, observándose diferencias entre hígado y bazo.

El estudio de las propiedades magnéticas de los tejidos, especialmente en situaciones de sobrecarga de hierro, es de especial interés para el desarrollo de tecnologías no invasivas basadas en el magnetismo para la cuantificación de los depósitos de hierro.

Summary

In this thesis, the iron speciation in biological systems has been investigated paying special attention to those species in which iron is found forming part of nanometric oxides and oxyhydroxides, from biogenic (ferritin and haemosiderin) and non-biogenic (iron supplements and contrast agents) origin.

Eight iron supplements used for the treatment of iron deficiency anaemia have been characterised. The study of these drugs, besides providing structural information about each compound, which can be related to their respective pharmacological properties, is the necessary previous step for their monitorisation in the organism.

Mineral iron species from biogenic origin have been studied in the frame of iron-overload pathologies for which two different animal models have been used.

The first studied model has been generated by the single administration of an iron supplement (iron dextran) to rats. This drug contains nanoparticles of an iron oxide called akaganéite. The transformations of the drug in the liver and the muscle near the place of injection have been magnetically monitorised during three months. The decrease of the number of akaganéite particles, and the increase of the amount of iron in the form of ferritin has been observed. Besides, the accumulation of iron in the spleen, heart and kidneys of the animals has been detected. It has been possible to identify this kind of species in the tissues by magnetic means because the magnetic properties of the injected drug and rat liver ferritin where previously characterised.

The second animal model of iron overload consists on genetically modified mice ($Hfe^{-/-}$ knockout) that, besides having a normal diet, accumulate a great amount of iron in the organism. This model simulates in a better way the human disease so it is of special interest for studies of the iron deposits in overload pathologies. Three different tissues have been magnetically characterised: liver, spleen and heart, and an anomalous accumulation of iron in the hepatic tissue has been detected. Ferritin and lysosomes containing partially degraded ferritin have also been observed by Transmission Electron Microscopy. However, the presence of a different kind of deposit, with a size and crystalline structure different from the typical deposits in overload situations, needs deeper studies as they may be related with the healthy aspect of the tissues in spite of the big amount of iron accumulated.

It has also been included in this thesis a study of the magnetic monitorisation, in biological tissues, of a contrast agent commonly used for Magnetic Resonance Imaging. Due to the small amount of iron administered with this drug in comparison with the biogenic iron, the study of its biodistribution by techniques different from the magnetic characterisation is more complicated. The presence of the contrast agent has been detected in the liver and the spleen but not in the heart and kidneys. Besides, a protocol for the quantification of the amount of iron that is forming part of the contrast agent and the biogenic ferritin present in the tissues has been developed from the magnetic measurements, providing quantitative information about the amount of iron in these two species in the tissues. The study of the influence of dipolar interactions in samples of different concentrations of the contrast agent has allowed to analyse the degree of aggregation of this compound in the tissues providing different results for liver and spleen.

The study of the magnetic properties of the tissues, especially in iron overload situations, is of special interest for the development of non-invasive techniques based on magnetism for the quantification of iron deposits.

Contents

Introduction

Nowadays science is living the revolution of multidisciplinary work. Scientific disciplines have stopped from being independent of each other and the interchange of ideas between different fields is now being promoted.

One of these synergies that are producing interesting results is the use of magnetism in biological and biomedical fields. In the field of diagnosis, it is absolutely recognised the role played today by Magnetic Resonance Imaging (MRI) as a wonderful noninvasive mean to differentiate, with spatial resolution, among soft tissues. But this is just the most elemental case, as a great number of nuclear magnetic resonance - based techniques, from, e.g., nuclear spectroscopy, to functional MRI by means of blood oxygenation detection techniques are currently used in

biomedicine. In other cases, in the so-called biosusceptometry, the direct measurement of the magnetic susceptibility of given organs of the patient is used to detect extraordinary iron-containing deposits in pathologies of iron overload. Not to forget also the present research efforts on using magnetic biocompatible materials and nanoparticles for cancer treatment purposes as hyperthermia, drug delivery or as MRI contrast agents.

In this scenario, as there exist either biogenic and administered species with differentiated magnetic properties, one can envisage the idea of using magnetic characterisation techniques, commonly used in Material Science, in order to solve biomedical and biological problems. In fact, only research groups with expertise on using characterisation techniques able to correlate the magnetic properties with the *biological* microstructure will have the necessary background to solve these problems. One of the main aims of this work was to detect in which biological problems the magnetic point of view may be able to contribute with relevant results.

One of the key common points between magnetism and biology is iron. The state of iron in biological systems usually corresponds to what is usually called a magnetic nanodisperse system. This means that the magnetic species are in the nanometric range (1 – 100 nm), usually single-domain, and besides, that they are far enough from each other in a way that the interparticle interactions are negligible. For these reasons, the interpretation of the magnetic characterisation results is simpler than in other cases. Another advantage of characterising magnetically a biological system is that, apart from iron, usually, there are no other magnetogenic elements present in a sufficient concentration to influence its magnetic behaviour so the magnetic properties of the sample can be interpreted as only due to iron. Moreover, the magnetic characterization

of tissues usually involves an amount of sample usually of the order of ≈ 50 mg, in such a way that the obtained information is more representative of the organ in comparison with other techniques as optical or electron microscopical analyses.

The magnetic characterisation of biological systems presents however some obvious difficulties. Although indispensable for life, iron is a trace element in the body. According to the IUPAC (International Union of Pure and Applied Chemistry) trace elements are those having an average concentration of less than about 100 parts per million atoms or less than 100 μg/g. Besides, in physiological conditions, the iron-containing species present in the tissues are usually paramagnetic, diamagnetic or superparamagnetic particles of antiferromagnetic iron oxyhydroxides, which correspond to the lowest efficient magnetic states. For these two reasons, sometimes, the magnetic measurements of biological samples will be close to the detection limits of the technique.

Given the centrality of iron in many metabolic pathways, it is unsurprising that human diseases are commonly linked to fundamental problems in iron metabolism. There are still many unknown iron metabolism issues in which the magnetic characterisation may contribute with new results. There are two particular situations in which, apart from solving a problem of general interest, the magnetic analysis results easier. The first one is the case of iron-overload pathologies because, in these situations, the iron concentration is higher, facilitating the magnetic measurements. The second one is the study of the metabolism of magnetic carriers, whose magnetic signal may be three orders of magnitude higher than the endogenous iron. So, in order to start with the most suitable scenarios for the application of magnetism to solve biological problems, these two special situations were analysed.

The structure of the thesis is as follows. Before presenting any result, a brief introduction to the magnetic properties of matter and the iron-containing species present in the body, together with an introduction to the magnetic characterisation techniques in biological samples is provided in Chapter 1. In Chapter 2, the magnetic characterisation of iron supplements used in the treatment of iron-deficiency anaemia is presented. The study of the magnetic properties of these drugs is the key step to study its metabolism in the body. In Chapter 3, it is presented the study of one of these iron supplements in an animal model of iron overload, to study the changes in the iron speciation. Chapter 4 describes the magnetic characterisation of other animal model of iron overload although, in this case, the iron overload has a genetic origin, in order to better mimicking the human case. Chapter 5 describes the application of the magnetic characterisation to study the biodistribution of a magnetic carrier, in this case a contrast agent commonly used in MRI. For this study, an especial protocol for the quantification of different iron-containing species in the tissues has been developed.

The work presented in this thesis contemplates the study of the iron metabolism and the biomineralisation in the tissues by magnetic means. The common purpose of the different chapters does not aim at studying a given disease but to follow, by combination of magnetic and structural characterisation techniques, the transformation of iron-containing species in the biological medium. The study of these transformations will provide data of relevance for the further understanding of the iron metabolic mechanisms and will also supply important magnetic data for the interpretation of diagnostic results and treatment techniques.

1. Elements of iron in biological systems and analytical techniques

In this chapter, as the work presented in this thesis is an intrinsically multidisciplinary research study, some basic tools on the different fields involved are provided. The general properties of the magnetic materials (relevant for the thesis) are described in section 1.1. Then, a brief summary of the iron-containing species present in the tissues is provided in section 1.2. Section 1.3 includes a brief description of the iron oxides and oxyhydroxides that can be present in biological samples. After this, an introduction to the different techniques employed in this thesis is provided. Section 1.4 is related to the magnetic measurements, focused in the characterization of biological samples. The

last two sections (1.5 and 1.6) include just some brief comments on the application of Transmission Electron Microscopy (TEM) and Inductively-Coupled-Plasma Atomic Emission Stpectroscopy (ICP AES) to biological samples.

1.1. Origin of magnetism and classification of the different magnetic behaviours

The microscopic origin of all magnetic properties in matter lies in the orbital and spin motions of electrons (Martin 1967). To explain it just in few words, electronic magnetism arises from the spin and angular momenta of individual electrons and their associated magnetic moments. Depending if these moments interact with one another it would result in long-range magnetic order below a certain critical temperature.

Materials are classified on the basis of their magnetic behaviour in response to magnetic fields at different temperatures. These types of magnetic behaviours are called diamagnetism, paramagnetism, ferromagnetism, ferrimagnetism and antiferromagnetism (Jiles 1991). In what follows, a brief description of the origin of the different magnetic behaviours is provided together with an introduction to superparamagnetism, a special behaviour of some nanometric materials.

1.1.1. Diamagnetism

Diamagnetism is a fundamental property of all matter, although it is usually very weak. Diamagnetic substances contain no unpaired electrons, which imply that all the magnetic moments of the electrons are

compensated and the atoms do not have a net magnetic moment. In absence of a magnetic field, diamagnetic substances have a net magnetic moment equal to zero. However, when a field is applied, the variation of the flux induces a moment in a way that it is opposed to the applied field.

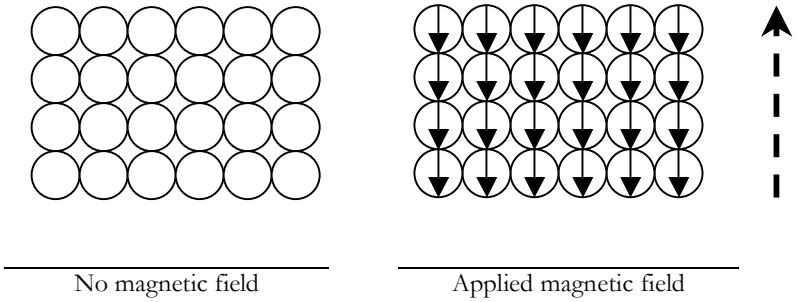

Fig. 1. Diamagnetic substances are composed of atoms which have no net magnetic moments. However, when exposed to a magnetic field (dashed arrow) magnetic moments are induced in the opposite direction of the field.

The response of a material to a magnetic field is defined as the magnetic susceptibility. Diamagnetic substances present a negative susceptibility, as the induced magnetic moments are oriented in the opposite direction of the applied field.

1.1.2. Paramagnetism

In paramagnetic state, some of the atoms or ions have a net magnetic moment due to unpaired electrons in partially filled orbitals.

In absence of a magnetic field, the moments are randomly oriented so the magnetization is zero. The application of a magnetic field causes the alignment of the magnetic moments of the atoms parallel to the

field resulting in a net positive magnetization and positive susceptibility. However, the efficiency of the field in aligning the moments is opposed by the randomizing effects of temperature.

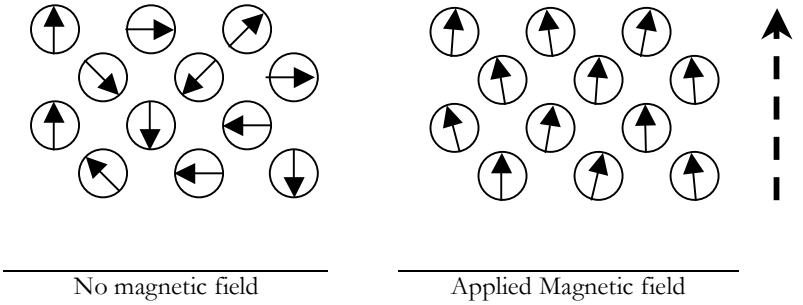

Fig. 2. Schematic representation of the magnetic moments of a paramagnetic material. In absence of a magnetic field the atomic magnetic moments will be randomly oriented. The presence of a magnetic field (dashed arrow) tends to align the atomic magnetic moments in the direction of the field.

1.1.3. Ferro-, ferri- and antiferromagnetism

These states have some atoms or ions with a net magnetic moment and moreover there is an interaction between them produced by electronic exchange forces. The differences between these behaviours depend on the relative orientation of the magnetic moments. Ferromagnetic materials exhibit parallel alignment of moments resulting in large net magnetization even in the absence of a magnetic field. In contrast, ferrimagnetic and antiferromagnetic materials present an antiparallel alignment of the moments. In antiferromagnetic materials, the moments that are in different sublattices are equal but opposite giving rise to a total compensation of the moments, while in ferrimagnetic materials,

the moments that are in the different sublattices are not equal, or there are more in one direction than in the other giving rise to a net magnetic moment in a given domain.

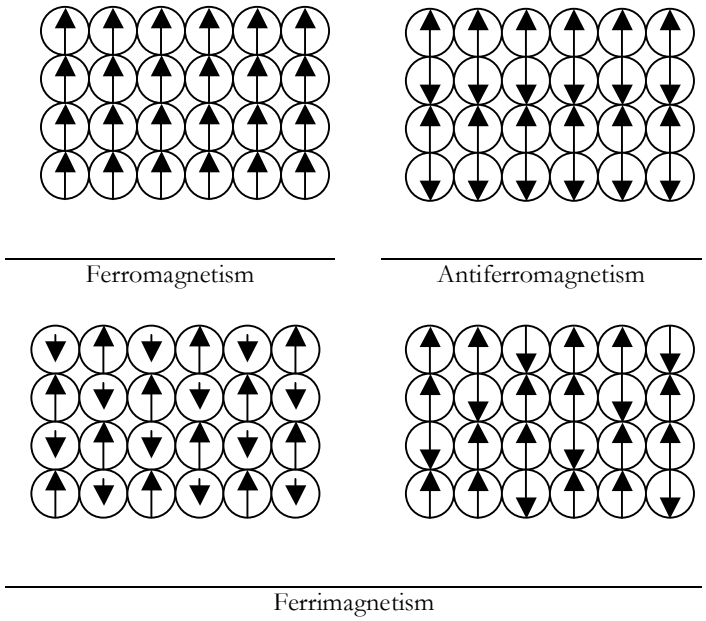

Fig. 3. Schematic representation of the magnetic moments of ferromagnetic, antiferromagnetic and ferrimagnetic materials at microscopic scale.

1.1.4. Superparamagnetism

Bulk ferromagnetic, ferrimagnetic or antiferromagnetic materials are composed of small regions called magnetic domains within which the direction of the magnetic moments is the same. Magnetic domains are separated by domain walls in which the orientation of the magnetization changes gradually from the one in a particular domain to the orientation in the neighboring domain (Jiles 1991).

If the volume of these materials is reduced, a situation in which the particles contain just one domain is reached.

If the volume of the particles is small enough, or the temperature is high enough, the thermal energy will be sufficient to overcome the anisotropy energy and cause a spontaneous reversal of magnetization. This magnetic behaviour is called superparamagnetism and means that the net magnetic moment (in zero field and at high enough temperatures) of a system containing superparamagnetic particles will be zero. In the presence of a field, there will be a net statistical alignment of magnetic moments, analogous to what happens to paramagnetic materials, except that now the magnetic moment is not that of a single atom but of the particle containing various atoms (Tarling et al. 1993).

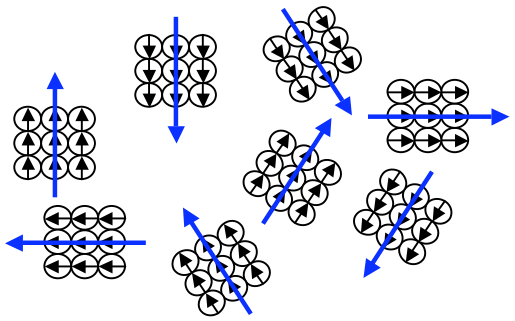

Fig. 4. Schematic representations of a superparamagnetic material. See that although the moments within each particle are ordered, the net magnetic moment of the material is zero in absence of a magnetic field.

1.2. Iron-containing species in the tissues

As the amount of other magnetogenic elements different from iron in biological systems is usually negligible in order to study a

biological system by magnetic means, it is necessary to know which are the most abundant iron-containing species in the system that we want to characterise and furthermore, which are their magnetic properties.

Despite the dependence of life on this element, free iron atoms are extremely toxic via the Fenton reaction in biological media (Fig. 5). For this reason, in physiological conditions, iron will be usually associated to proteins to avoid its toxicity (Testa 2002).

$$Fe^{2+} + H_2O_2 \rightarrow OH^{\bullet} + OH^{-} + Fe^{3+}$$

Fig. 5. The Fenton reaction generates the radical $OH^{\bullet}$ which besides being toxic, enhances oxygen toxicity (Crichton 2001).

Iron-containing proteins can be classified into three groups: (i) haemoproteins, (ii) iron-sulphur proteins and (iii) other iron-containing proteins (Crichton 2001). This third group is quite heterogeneous and includes the proteins that are involved in the transport and storage of iron: Transferrin and ferritin. Anyway, in spite of the great amount of iron-containing proteins that can be present in animals, only a few of them contain most of the iron in the organism. For this reason, a list with the species that contain most of the human-body iron is detailed in Table 1 as an example of the distribution of iron among the different proteins.

Although there can be differences between the concentration of the different iron-containing proteins depending on the gender and age of the individuals, it is clear that nearly two thirds of the total iron of humans is in the form of haemoglobin (Table 1). Then, around a quarter of the total iron in the body is contained by the iron storage protein, ferritin. Finally, although less abundant, there are also other two species, myoglobin and transferrin, that contain an important quantity of the total

iron in the body. The contribution to the total iron content of the rest of the iron-containing proteins is small.

As the biomineralisation, oxidation state and coordination of iron in each protein affects to their respective magnetic properties, a brief description of the three groups of proteins, making emphasis in the most abundant iron-containing proteins in the body included in the table is given below. At this point of the description, it has to be said that in pathological conditions other not so well-defined iron-containing species (non-transferrin-bound-iron and haemosiderin) can also be present in the body. For this reason, at the end of this section, a brief introduction to these species will also be provided.

SPECIES	**CONCENTRATION (mg Fe/kg body weight)**
Haemoglobin	30
Ferritin and haemosiderin	10-12 in men 5 in women
Myoglobin	4
Transferrin	3
Other haemoproteins, iron-sulphur proteins and other iron-containing proteins...	2
TOTAL	**40-50**

Table 1. Concentration of iron associated to the different iron-containing species present in the tissues (Crichton 2001).

1.2.1. Haemoproteins

Haemoproteins are distinguished from the rest of the iron-containing proteins as they have at least one haem prosthetic group, which consists of an iron atom at the centre of a large heterocyclic organic ring called porphyrin (Fig. 6).

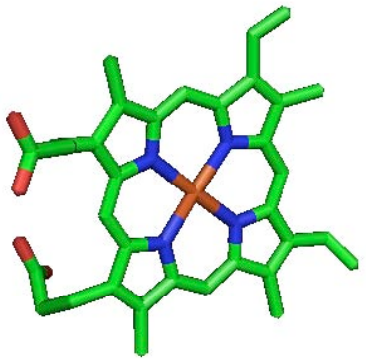

Fig. 6. Scheme of the coordination of iron in a porphyrin group. Each element has been plotted in a different colour: Iron in brown, nitrogen in blue, carbon in green and oxygen in red.

In these proteins iron is bound to four nitrogen atoms from the porphyrin molecule and to one or two axial ligands from the protein (Fig. 7). The iron atom can also bound other ligands as H_2O, CO_2, O_2 or NH_3.

In the haem group, iron has octahedral coordination geometry, and can be in its ferric (Fe^{3+}: $[Ar]3d^64s^0$) or ferrous (Fe^{2+}: $[Ar]3d^54s^0$) states. In the octahedral geometry, the 3d-orbitals split into two sets of different energy. Depending on the energy gap, the electrons of the 3d orbitals will be arranged with the configurations shown in Fig. 8.

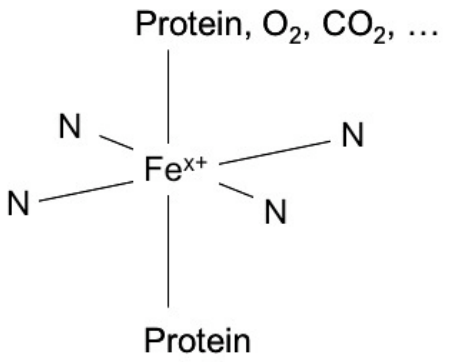

Fig. 7. Octahedral coordination geometry of iron in the haem group. Apart from the four nitrogen atoms from the porphyrin and the protein that contains the haem group, iron can be bounded to other different ligands.

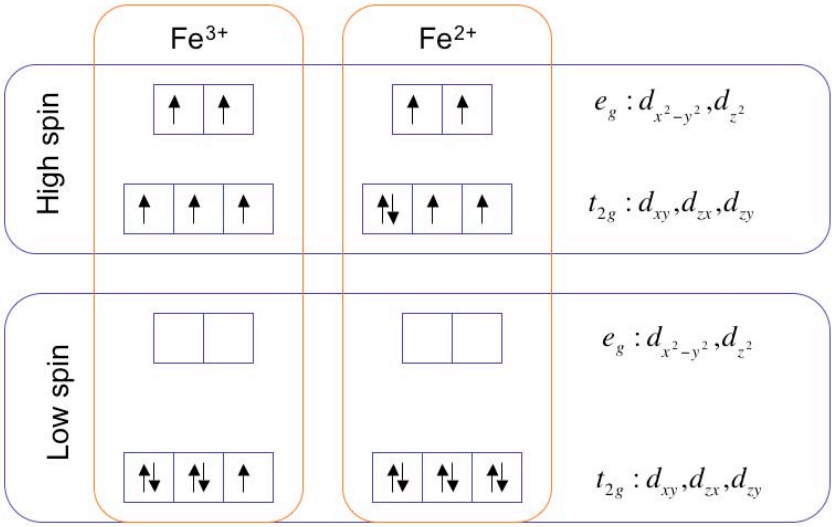

Fig. 8. Schematic representation of the energy levels of the 3d electrons in the high and low spin configurations of the Fe^{2+} and Fe^{3+} ions in octahedral coordination geometry.

In the low spin configuration the energy gap between the two sets of orbitals is high so the electrons are located in the low energy orbitals.

In contrast, in the high spin configuration, the energy gap is smaller and it is energetically favourable to have one electron in each orbital before any pairing occurs in agreement with Hund's rule. The size of the energy gap between the two sets of orbitals depends on several factors, including the ligands and geometry of the complex.

As it can be observed in Fig. 8, the presence of unpaired electrons in the 3d orbitals of the high spin configurations of both oxidation states and the low spin configuration of Fe^{3+} will lead to paramagnetic behaviour. In contrast, haemoproteins containing low spin Fe^{2+} will have diamagnetic behaviour, as there are no unpaired electrons (see previous section).

Haemoproteins have diverse biological functions including the transportation of gases, chemical catalysis and electron transfer. This kind of proteins can also be subdivided into three groups: (i) haemoglobins, (ii) myoglobins and (iii) cytochromes (Crichton 2001).

Haemoglobins contain most of the body iron, so their magnetic properties are of special interest for the interpretation of the tissues magnetic properties. In general, the contributions to the tissue susceptibility of the other haemoproteins, especially of the cytochromes, will be much lower than that coming from haemoglobins.

1.2.1.1. Haemoglobins

Haemoglobin is a protein found in erythrocytes where it is responsible for binding oxygen in the lung and transporting it throughout the body to the peripheral tissues. In addition, haemoglobin molecules play also an important role in transporting CO_2 in the opposite direction.

This protein is formed by four identical subunits (Fig. 9) each of which consists of two parts: a globin molecule and a haem prosthetic group. In haemoglobin, iron is bound to the four nitrogen atoms from the porphyrin and one histidine from the globin. The sixth coordination site of iron is the oxygen-binding site.

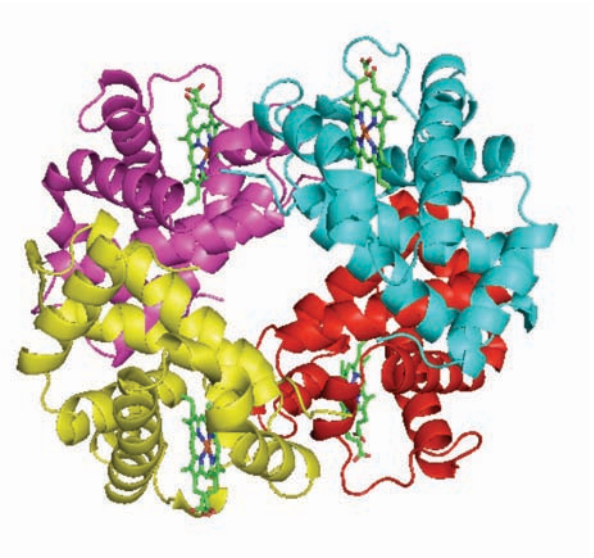

Fig. 9. Structure of human deoxyhaemoglobin. The four different subunits are shown in different colours. The haeme groups can be observed with the same colour code as in Fig. 6. This figure was made in PYMOL using PDB[#] ID: 1a3n (Tame et al. 2000).

The predominant forms of haemoglobins in intact red blood cells, contain iron in its ferrous state (Fe^{+2}), however there can also be Fe^{3+}-containing haemoglobins.

[#] PDB stands for Protein Data Bank (Berman, H., K. Henrick and H. Nakamura (2003). "Announcing the worldwide Protein Data Bank." Nature Structural Biology 10(12): 980-980.

The chemical coordination of iron in this protein, which affect to its magnetic properties, changes if it has bound oxygen (oxyhaemoglobin) or not (deoxyhaemoglobin). The deoxyhaemoglobin variant presents paramagnetic behaviour with an effective moment per iron ion of 5.46 μ_B while oxyhaemoglobin appears to be diamagnetic (Pauling et al. 1936; Alpert et al. 1975; Pauling 1977). This is explained as oxyhaemoglobin is a low-spin system that has no unpaired electrons while deoxyhaemoglobin is a high-spin system with four unpaired electrons (Bush 2000) (see Fig. 8).

A different kind of haemoglobin, called methahaemoglobin, which instead of containing Fe^{2+} contains Fe^{3+}, is usually formed by oxidation processes for example in haematomas. In this molecule the iron atoms contain five unpaired electrons, and, as it happens with deoxyhaemoglobin, it is paramagnetic (Bush 2000).

1.2.1.2. Myoglobin

Myoglobin is a monomeric haemoprotein found mainly in muscle tissues where it serves as an intracellular storage site for oxygen. Each myoglobin molecule contains one haem prosthetic group, which means that each protein contains just one iron atom.

As it happens to haemoglobin, its magnetic behaviour depends on the binding of oxygen to the iron atom in the haem group. The magnetic behaviour of deoxymyoglobin, is similar to that of deoxyhaemoglobin, as it has an effective moment of 4.90 μ_B, becoming diamagnetic after oxygen binding (Roder et al. 1984).

Fig. 10. Structure of human myoglobin. The haeme group can be observed with the same colour code as in Fig. 6. This figure was made in PYMOL using PDB ID: 2mm1 (Hubbard et al. 1990).

1.2.1.3. Cytochromes

The group of haemoproteins that serve as electron-carriers are called cytochromes so, according to this definition, a wide and diverse family of proteins are included under the same name. The cytochromes are classified into four major groups called a, b, c and d, which differ in the nature of the side chains of the porphyrins from the haem prosthetic groups and their linkage to the protein.

In most of the cytochromes, iron is bounded to the four nitrogen atoms from the porphyrin and to two axial aminoacids coming from the protein. It has been described that the most common aminoacids to which iron is bounded in the cytochromes are hystidin and metionin, and it is known that these ligands give low spin configurations of iron (see Fig. 8). However there can be some exceptions as the cytochrome P_{450}s, which is

found in most of the human tissues, and that contains iron bounded to the porphyrin and just one cysteine residue. The sixth coordination site (trans to the cysteine residue) can bind water, O_2, CO, isocyanides, and other ligands or it can also be free, generating a pentacoordinate configuration (Crichton 2001).

The iron state in most of the cytochromes may change during their activity between Fe^{3+} and Fe^{2+} and depending on the oxidation state and the coordination (five or six ligands) of iron, it may be high spin or low spin leading to different magnetic properties. However, in comparison with the abundance of the other haemoproteins, iron coming from the cytochromes would have a very little contribution to the total magnetic susceptibility of the tissues.

1.2.2. Iron-sulphur proteins

Iron-sulphur proteins constitute a heterogeneous group of proteins and their roles include the electron transport, redox functions, DNA repair, etc (Crichton 2001). These proteins contain various iron atoms bound to sulphur atoms forming clusters in which iron can have different oxidation states. Sulphur atoms can come from an aminoacid from the protein chain or act as bridges between the iron atoms. In any case, the contribution of these proteins to the total body iron content is very low.

1.2.3. Other iron-containing proteins

There is a heterogeneous collection of proteins that contain iron in a non-haem, non iron-sulphur form. This group includes a wide variety

of enzymes that have a diverse biological activity characterised by the presence of iron (e.g dioxygenases, hydroxylases, lipoxygenases...) which are present in a very low concentration in the body. However, in this group there are also included two proteins that have a big contribution to the total body iron content: transferrin and ferritin.

1.2.3.1. Transferrins

Transferrins are a family of iron-binding proteins found in many body fluids as serum, milk, tears and saliva (Crichton 2001). These proteins, which include serum transferrin (siderophilin), lactoferrin and melanotransferrin are thought to control the iron concentration in the fluids, working as antibiotic agents, since iron availability is a major limiting factor in bacterial growth.

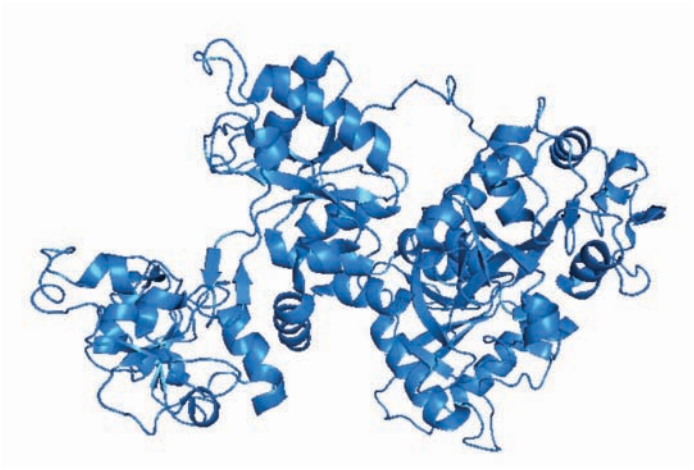

Fig. 11. Structure of human apotransferrin. This figure was made in PYMOL using PDB ID: 2hau (Wally et al. 2006).

However, the most abundant of the proteins of this family in the human body is serum transferrin, which is also in charge of binding and transporting iron from the site of absorption (intestinal mucosa) to the cells. Serum transferrin is formed by two homologous globular domains called N and C, each of which can bind reversibly one iron atom (Testa 2002) so it is possible to find apotransferrin, monosaturated transferrin and disaturated transferrin.

Iron in transferrin is in its Fe^{3+} state and is bounded to six ligands: four aminoacids, that in humans are Asp, Tyr, Tyr and His (Testa 2002), and two oxygen atoms coming from a carbonate co-anion in a nearly octaedrical coordination structure (Fig. 12).

The Fe^{3+} iron atoms are in a high spin state, (Fig. 8) so monosaturated or disaturated serum transferrins will be paramagnetic.

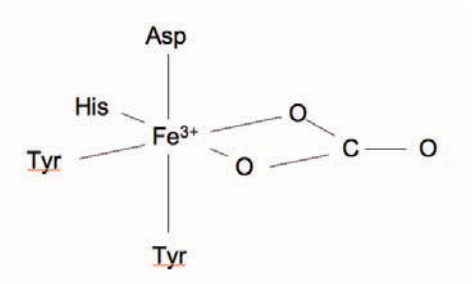

Fig. 12. Coordination of iron in transferrin. The iron atom is bounded to four aminoacids and two oxygen atoms.

1.2.3.2. Ferritin

Ferritin stores iron in a non-toxic form. Its role is so important for life that it has been conserved during evolution being present not only in

mammals but also in nearly all living forms, from bacteria to eukaryotic organisms.

The mammalian apoferritin molecule is nearly spherical (∅ ≈ 12.5 nm), and is composed of 24 subunits of two homologous polypeptides called L and H. These subunits are arranged forming a hollow, the internal cavity where iron is stored, and that has 8 nm of diameter.

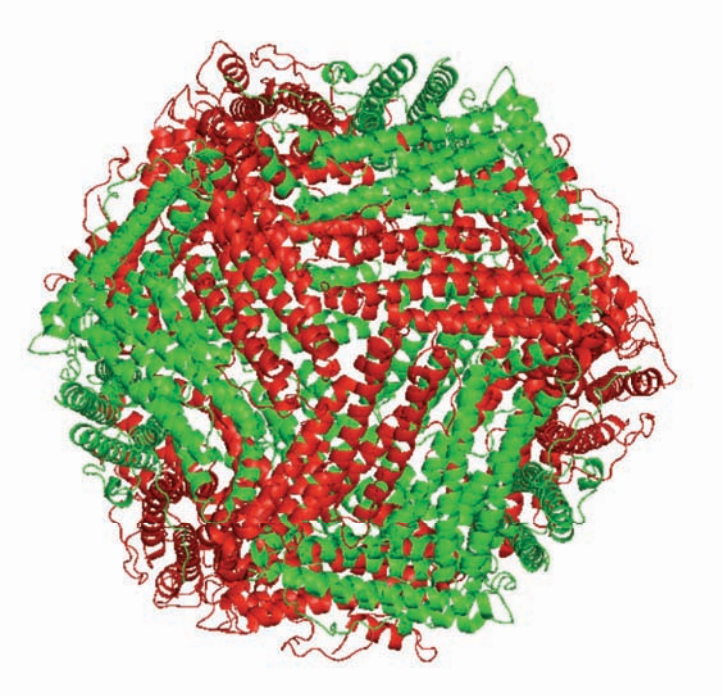

Fig. 13. Apoferritin structure from *Trichlplusia ni*. Heavy chains are in red and light chains are in green. This figure was made in PYMOL using PDB ID: 1z6o (Hamburger et al. 2005).

Up to around 5000 iron atoms can enter to the protein cavity trough channels in the protein shell to form a mineral phase whose size is limited by the cavity size. In physiological conditions the major phase of

the nanocrystals formed inside the protein shell has a structure very similar to the iron oxyhydroxide ferrihydrite (Massover 1993; Chasteen et al. 1999; Cowley et al. 2000). Nevertheless, the biomineralisation of iron inside the ferritin core is not unique, and other different iron oxides and oxyhydroxides (magnetite, haematite, goethite, etc.) have been observed to be formed inside ferritin (Cowley et al. 2000; Quintana et al. 2004).

The magnetic properties of ferritin have been studied since 1943 (Michaelis et al. 1943), when its structure was still not clear. Due to the limited size of the protein, the iron-containing particles inside it are single domain and have superparamagnetic behaviour at room temperature (Blaise et al. 1967; Mohieeldin et al. 1994; Tejada et al. 1994; Gider et al. 1995; Kilcoyne et al. 1995; Makhlouf et al. 1997; Luis et al. 1999; Allen et al. 2000; Gilles et al. 2002). In the last years, the magnetic properties of ferritin have acquired special interest for the non-invasive determination of liver iron deposits by MRI analysis or biosusceptometry measurements (Jensen 2004).

It has to be also pointed out that in the last decade, an intense effort on the study of the role of ferritin in neurological disorders is being performed (Dobson et al. 1996; Dubiel et al. 1999; Quintana et al. 2004; Brem et al. 2005; Quintana et al. 2005; Quintana et al. 2007).

1.2.4. Other iron-containing species

There are other not so well defined species present in the tissues that can contain iron: haemosiderin and non-transferrin bound iron (NTBI). Especially in iron overload situations, these species may contain a big amount of the total iron content in a given organism.

1.2.4.1. Haemosiderin

Historically, this term was initially employed to describe Prussian blue-positive granules that were observed in the tissues under the optical microscope (for a review see (Wixom et al. 1980) and references therein). However, the term haemosiderin has been lately used to name iron-containing bodies of different origin that were present in the tissues, as those coming from the digestion of ferritins ((Fischbach et al. 1971) and references therein) or from deposits of administered iron compounds (Richter 1959).

Nowadays, the term haemosiderin is usually ascribed to "a poorly defined iron-protein complex that forms an insoluble iron storage system thought to be derived from the lysosomal degradation of the ferritin protein shell" (Testa 2002). Haemosiderin is typically found in secondary lysosomes called siderosomes (Richter 1984) in tissues with iron overload.

Differences between the biomineralisation of iron in haemosiderins corresponding to various pathological tissues and animals have been detected (St Pierre et al. 1987; Dickson et al. 1988a; Mann et al. 1988; Chuaanusorn et al. 1994; Ward et al. 1994; Ward et al. 2000). For this reason, it is important to know the conditions, pathology and treatments, under which these deposits have been formed (Andrews et al. 1988).

Although the magnetic properties of some haemosiderins have been studied (Michaelis et al. 1943; Allen et al. 2000), it is complicated to define a unique magnetic behaviour. However, it can be assumed that haemosiderins coming from the first stages of the degradation of ferritins (what some authors have named pre-haemosiderin (St Pierre et al. 1987))

would have a similar magnetic behaviour to the particles inside ferritin. Nevertheless, haemosiderins from some iron overload diseases may contain particles with a biomineralisation different than that of physiological ferritin depending on the way in which iron is delivered and deposited in the tissues (Andrews et al. 1988).

1.2.4.2. Non-transferrin bound iron

Non-transferrin bound iron is, as it happens with haemosiderin, a not well-defined iron-containing species. NTBI is the name given to a percentage of the serum iron, which is not associated to known proteins as transferrin, serum ferritin or haemoglobins.

The existence of NTBI of different molecular weight leads to the idea that the composition of this kind species is quite heterogeneous (for a review see (Hider 2002) and references therein). As a consequence of this, it is possible that some forms of NTBI can be highly toxic, possible leading to free radical generation. Besides, it also seems that the nature of NTBI may be associated with the different iron overload pathologies, so, as it happens with haemosiderin, in future studies it will also be necessary to specify the conditions, pathology and treatments, under which it has been studied.

1.3. Iron oxides and oxyhydroxides

Mineralised iron that can be present in biological systems, from endogenous or exogenous origin, is usually in the form of iron oxides or oxyhydroxides (Mann 2001). Although the stoichiometric composition of

this kind of compounds may be very similar in some cases, their different crystalline structure results in different magnetic behaviours (Cornell et al. 1996).

In what follows, a list of the magnetic properties of the most common iron oxides and oxyhydroxides in biological systems together with some examples of their occurrence is provided in Table 2.

Mineral	Formula	Magnetic behaviour	Biological occurrence
Goethite	α-FeOOH	Antiferromagnetic	Limpets Human (liver)
Lepidocrocite	γ-FeOOH	Antiferromagnetic	Sponges Chitons
Akaganéite	β-FeOOH	Antiferromagnetic	Iron supplements*
Ferrihydrite	$Fe_5HO_8 \cdot 4H_2O$	Speromagnetic	Ferritin Chitons
Haematite	α-Fe_2O_3	Antiferromagnetic or weakly ferromagnetic	Ferritin
Magnetite	Fe_3O_4	Ferrimagnetic	Bacteria Ferritin Animals (magnetic navigation)
Maghaemite	γ-Fe_2O_3	Ferrimagnetic	Ferritin
Wüstite	FeO	Antiferromagnetic	Ferritin

Table 2. Chemical formula and magnetic behaviour of the most common iron oxides and oxyhydroxides in biological systems [Adapted from (Cornell et al. 1996; Mann 2001; Quintana et al. 2004)]. *Iron supplements have been included in the table as their characterisation will be described in the next chapter.

As observed in Table 2, biomineralised iron can be present in different organisms being its role quite heterogeneous (Mann 2001):

- Linear chains of magnetite particles have been found in bacteria. These particles allow the bacteria to orient and migrate along the geomagnetic field towards favourable habitats, a behaviour known as magnetotaxis (Blakemore 1982). Furthermore, and also related to their orientation in the Earth's magnetic field, magnetite particles have also been found in honeybees, salmon, trout, pigeons, and several other animals (Kirschvink et al. 2001).

- Goethite, lepidocrocite and magnetite have been observed in the teeth of some molluscs as limpets and chitons. The role of these compounds in these cases is to make their teeth harder enabling them to extract and eat algae from within the surface of rocks (Mann 2001).

- The role of the iron-containing nanoparticles accumulated inside ferritin is to store iron in a non-toxic form. As mentioned before, ferrihydrite is the major phase found in physiological ferritin however particles of magnetite, maghaemite, haematite and goethite have also been detected inside it (Cowley et al. 2000; Quintana et al. 2004). The biomineralisation of iron inside ferritin is of special interest because a greater proportion of iron oxides and oxyhydroxides different from ferrihydrite has been observed in neurodegenerative diseases (Cowley et al. 2000; Quintana et al. 2004).

1.4. Magnetic characterisation

The special interest in studying iron in biological systems by magnetic means is based in the next two reasons. First, the magnetic

properties of biological systems can usually be related to the iron-containing species present in it, due to the low amount of other magnetogenic elements. Furthermore, given that biological samples usually constitute nanodisperse systems, their magnetic properties are easier to interpret.

Nowadays, many different magnetic characterisation techniques exist (Evans et al. 2003), and a wide variety of magnetic parameters can be measured in a given sample in order to characterise the presence of different iron oxides and oxyhydroxides (Cornell et al. 1996).

In this thesis most of the work has been focused on the use of AC magnetic susceptibility measurements in order to characterise different samples of biological origin. Besides, in some cases, field dependent magnetisation measurements have also been performed. The special interest of the AC magnetic susceptibility characterisation of biological samples is that it can provide information about some of the different iron-containing species, and, in some cases, about particle size distributions.

In what follows, an introduction to the field dependent magnetisation and AC magnetic susceptibility measurements is provided. The aim of these forthcoming sections is not to present new equations that describe the different magnetic behaviours, but to describe the application of an already existing theoretical background [see (Garcia-Palacios 2000) and references therein] to the specific case of biological samples. The main idea is to provide the tools needed for the interpretation of the magnetic measurements described in the following chapters.

1.4.1. Field Dependent Magnetisation

Field dependent magnetisation measurements indicate the variation of the magnetisation (M) of a given sample when a magnetic field (H) is applied. It has to be taken into account that the thermal energy tends to randomize the alignment of the moments, so the magnetisation of a given sample will be temperature dependent.

In the classical approximation in which the magnetic moments can adopt all the directions, the magnetisation is described as

$$M = N\mu \mathrm{L}\left(\frac{\mu_0 \mu H}{kT}\right) \qquad \text{Eq. 1}$$

where N is the number of magnetic moments (μ) per unit volume, μ_0 is the permeability of the empty space, k is the Boltzmann constant, T the absolute temperature and $L(x)$ is the Langevin function (Jiles 1991).

$$\mathrm{L}(x) = \coth(x) - \frac{1}{x} \qquad \text{Eq. 2}$$

However, as a result of quantization phenomena, the magnetic moments can only be oriented in discrete directions, so equation 1 is slightly modified, being the Langevin function substituted by the Brillouin, $B_J(x)$, one.

$$M = N\mu.\mathrm{B}_J\left(\frac{\mu_0 \mu H}{kT}\right) \qquad \text{Eq. 3}$$

where

$$\mathrm{B}_J(x) = \frac{2J+1}{2J} \cdot \coth\left[\frac{(2J+1).x}{2J}\right] - \frac{1}{2J}\coth\frac{x}{2J} \qquad \text{Eq. 4}$$

and where J is the total angular momentum quantum number. It has to be noted that if $J \to \infty$, $B_J(x) = L(x)$.

According to the previous equations and as far as the magnetic moment can be considered a temperature independent magnitude, the M(H/T) curves corresponding to different temperatures will superimpose into a single master curve. However, for increasing anisotropic contributions, not all the moment orientations are equally probable and M (H/T) scaling is not valid anymore. It has been found (Garcia-Palacios 2000) that at low fields, if the anisotropy axes are randomly orientated, the susceptibility will be independent of the anisotropy term.

1.4.2. AC Magnetic susceptibility

The magnetic susceptibility (χ) is defined as the response of a material to a magnetic field ($M=\chi H$). In AC magnetic measurements, an AC field is applied to a sample and the resulting AC moment is measured. Because the induced sample moment is time-dependent, the AC magnetic susceptibility measurement yields two quantities: the magnitude of the susceptibility, and the phase shift. Thus, the susceptibility is described as having an in-phase, or real, component (χ') and an out-of-phase, or imaginary, component (χ'').

In this section, the different contributions to the AC magnetic susceptibility that may appear when characterising tissues have been described. At the end of this section, the description of the calculations to obtain more information from the susceptibility measurements and some special features on the characterisation of samples with a very low magnetic signal, as it happens in biological samples, will be described.

1.4.2.1. Paramagnetic species

Some of the most abundant iron-containing species in the body are paramagnetic (e.g. deoxyhaemoglobin, deoxymyoglobin, etc.). The magnetic susceptibility of these species is positive and small, and varies with temperature, due to the influence of the thermal agitation in the alignment of the moments by the field.

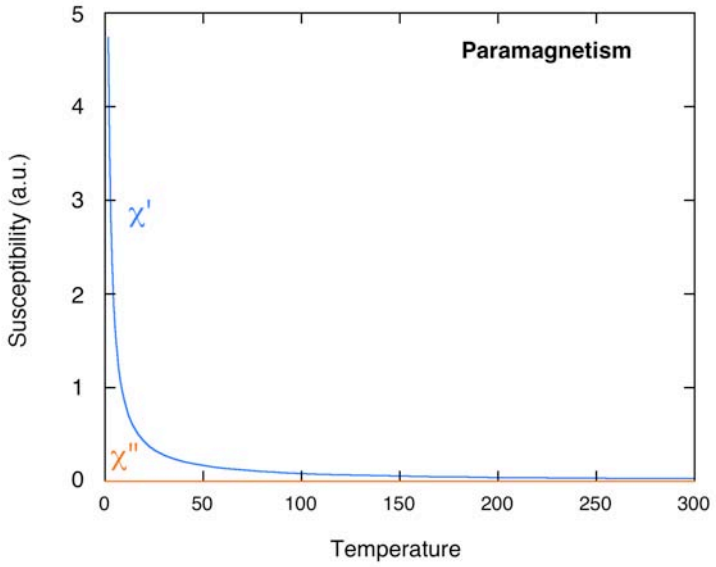

Fig. 14. Scheme of temperature dependence of the in phase and out-of-phase components of the AC susceptibility of a paramagnetic substance.

In the limit of small applied magnetic fields, as it is the case of the experiments presented in this thesis, $L(x) \rightarrow x/3$, so from Eq. 1 it can be concluded that the temperature dependence of the susceptibility of paramagnetic species will follow Eq. 5, called the Curie law,

$$\chi = \frac{\mu_0 N \mu_{eff}^2}{3kT} \qquad \text{Eq. 5}$$

where *N* is the number of magnetic ions per unit volume and μ_{eff} is the so-called effective moment. The temperature dependence of the susceptibility of a paramagnetic species has been schematically plotted in Fig. 14. It is important to emphasize that there is no contribution of these species to the out-of-phase susceptibility.

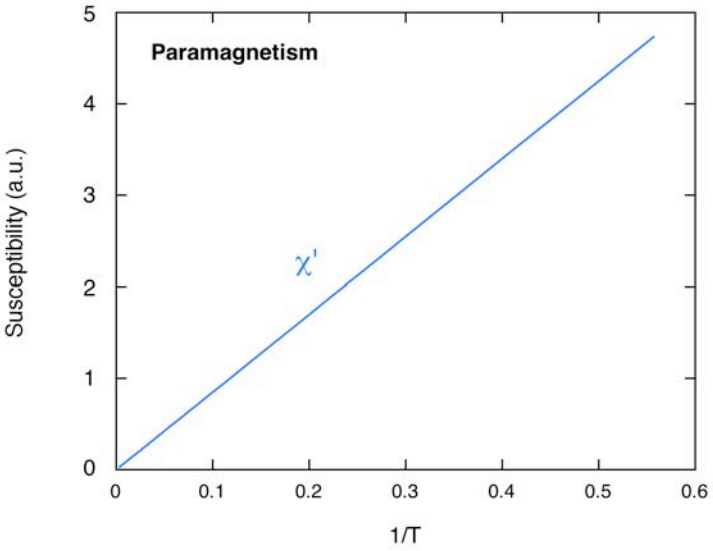

Fig. 15. Scheme of the χ' vs 1/T representation of a paramagnetic substance. The value of the Curie constant can be obtained form the slope of the line in this representation.

The value of the effective moment per iron ion informs about the iron speciation in a given sample. To calculate this value it is customary to make a fit of the susceptibility measurements to a Curie law by assuming *N* equal to the total number of magnetic ions, a value that can be determined from elemental analysis of the sample. A straight line will be obtained in the χ' vs 1/T representation (Fig. 15), from whose slope it can be obtained the value of the Curie constant (C), that allows the calculation of the effective moment per ion (μ_{eff}).

$$C = \frac{\mu_0 N \mu_{eff}^2}{3k} \qquad \text{Eq. 6}$$

The values of the effective moment per iron ion in paramagnetic substances are around 5.5 and 5.8 μ_B for Fe^{2+} and Fe^{3+} respectively (Martin 1967), so it can be assumed that the magnetic moment of iron-containing paramagnetic species should be around 5 - 6 μ_B.

1.4.2.2. Antiferromagnetic compounds

The dynamic AC susceptibility of these substances (Fig. 16) will show a peak at the Neel temperature (T_N) in $\chi'(T)$. T_N indicates the transition at which the antiparallel coupling of the moments is disrupted by heating.

Above the temperature of the χ' peak maxima, the $\chi'(T)$ data can be fitted with a Curie-Weiss equation (Jiles 1991).

$$\chi = \frac{C}{T + \theta} \qquad \text{Eq. 7}$$

When measuring this kind of samples, the value of the Curie constant and θ can be obtained from the $1/\chi'$ vs T representation, supposing the diamagnetic contributions to be negligible. The positive sign of θ will confirm the antiferromagnetic behaviour.

The value of the Curie constant may be used to determine the effective moment per iron ion, μ_{eff}, calculated from Eq.6. The μ_{eff} values, calculated in the temperature region well above T_N should coincide with those reported for the paramagnetic ions.

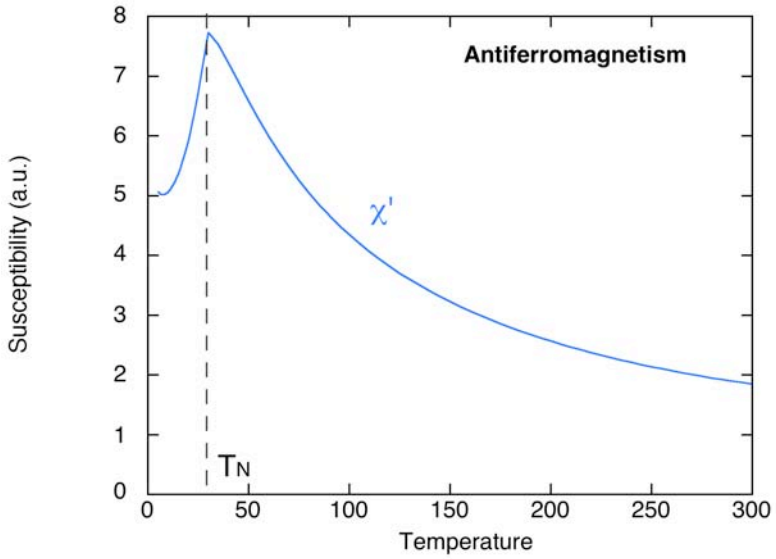

Fig. 16. Scheme of temperature dependence of the in phase and out-of-phase components of the AC susceptibility of an antiferromagnetic substance

1.4.2.3. Superparamagnetic iron oxides and oxyhydroxides nanoparticles

The presence of iron oxides and oxyhydroxides nanoparticles in the tissues may have different origins. On one hand, endogenous iron-containing nanoparticles can be found inside the protein shell of ferritin and also similar species may form part of haemosiderin deposits in iron overload situations. On the other hand, exogenous iron-containing nanoparticles can be present in the tissues after the administration of iron supplements or magnetic carriers. As the size of the particles that may be present in the tissues is in the nanometric range, they will present superparamagnetic behaviour at high enough temperatures.

A schematic representation of the AC susceptibility of these particles is represented in Fig. 17.

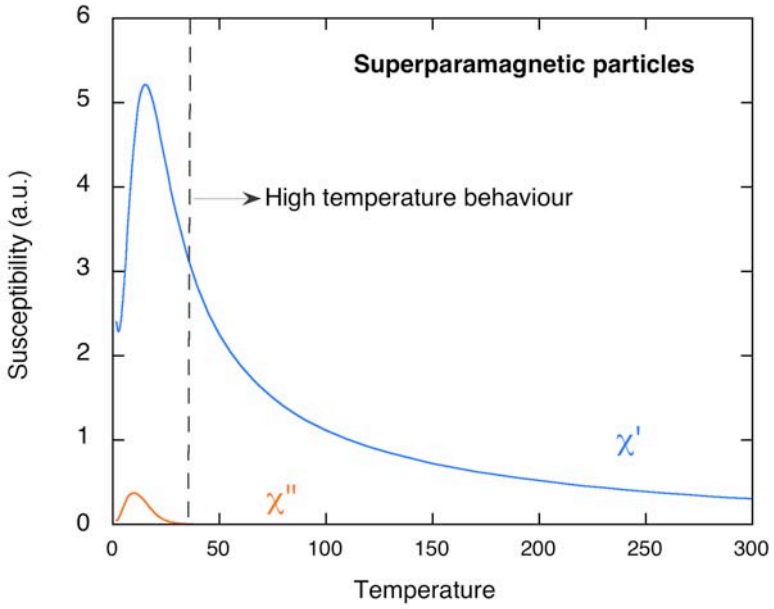

Fig. 17. Scheme of temperature dependence of the in phase and out-of-phase components of the AC susceptibility of a superparamagnetic substance.

As it can be observed in Fig. 17, the behaviour at high and low temperatures can be distinguished.

In the high temperature region and assuming negligible dipolar interparticle interactions, the particle magnetic moments have enough experimental time to overcome their anisotropy energy barriers $\sigma = Kv/kT$ (where K is the effective anisotropy constant and v the particle volume). In this situation, the in-phase susceptibility will follow the Curie law ($\chi' = C/T$), as in paramagnetic materials, although in this case the magnetic moments that would thermally fluctuate would be the particle

moments instead of the single ion moments (Bean et al. 1956). It has to be noted that the out-of-phase susceptibility is zero in this temperature range.

It would be possible to calculate the Curie constant from the slope, in the high temperature range, of the χ' vs 1/T representation (Fig. 18) in order to obtain the value of the effective moment per iron ion, as it happened with paramagnetic species.

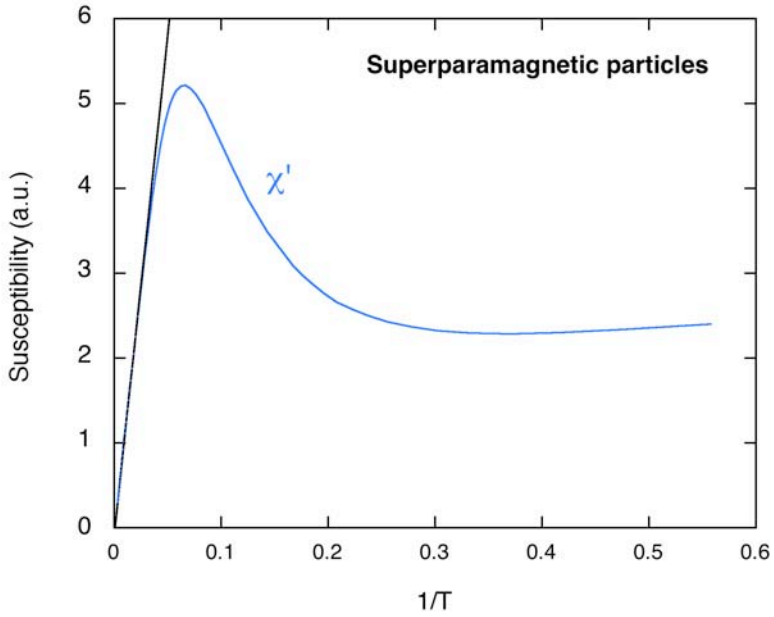

Fig. 18. Scheme of the χ' vs 1/T representation of a superparamagnetic substance. The Curie constant can only be obtained form the slope of the curve in the temperature region where $\chi''=0$.

For small particles constituted by a material that is antiferromagnetic in the bulk state, it may be observed a non-zero particle magnetic moment coming from a non complete spin compensation (Neel 1962) most likely due to magnetic ion vacancies in the inner volume or at the particle surface. The volume or surface spin uncompensation models

predict, for assemblies of antiferromagnetic particles, a μ_{eff} equal to μ or $\mu n^{-1/6}$ respectively, where n is the number of ion spins per particle (López et al. 1997). This means that if the system follows these models the maximum expected μ_{eff}, is usually not higher than the value of the paramagnetic ions (Neel 1962; López et al. 1997; Lázaro et al. 2005), which is around 6 μ_B for iron. In contrast, the effective moment per iron ion of an assembly of ferromagnetic or ferrimagnetic particles will be higher than the single ion one.

At lower temperatures, the parameter Kv/kT is no longer negligible and more involved theories of the dynamic susceptibility must be taken into account (Garcia-Palacios 2000). In this temperature range the net magnetic moment of the particle, in order to rotate by the action of the external field, must surmount its anisotropy energy barrier $E_a = Kv$. In the simplest model of uniaxial anisotropy and for moderate AC frequencies (ω), this process is assumed to take place immediately in the case of intra-well rotations, but it takes a time of the order of the relaxation time (τ) to rotate from one anisotropy potential well to the other. For decreasing temperature this relaxation time increases exponentially and, as soon as τ becomes comparable to the characteristic time of the experiment ($1/\omega$), alterations from the equilibrium susceptibility start to appear. In this context, for an assembly of non-interacting particles with randomly oriented easy axes, the complex susceptibility can be written as

$$\chi = \frac{\mu_0 \varepsilon}{kT} \int_0^\infty dD.n(D).m(D)^2 \left[\frac{1}{3} \frac{R'}{R} \frac{1}{1 + i\omega\tau} + \frac{2}{3} \frac{R - R'}{2R} \right] \quad \text{Eq. 8}$$

where R and R' are σ dependent integral functions, $n(D)dD$ is the number of particles with diameters in the (D, D+dD) interval, $m(D)$ the magnetic moment of particles of diameter D and ε the fraction of the total sample volume occupied by magnetic particles (Garcia-Palacios 2000; Lázaro et al. 2005). In the limit of high temperature, this equation results in the Curie law, while in the limit of low temperature represents the behaviour of a fully blocked assembly of magnetic moments. For intermediate temperatures it predicts a $\chi'(T)$ maximum, which in fact results from the antagonism of the Curie law and the magnetic relaxation, which for lowering temperatures makes to increase and decrease respectively the in-phase susceptibility, and a $\chi''(T)$ maximum which represents magnetic energy absorption. This behaviour is the typical one for magnetic nanoparticle assemblies (Garcia-Palacios 2000).

The shape and location in temperature of the χ''(T) maximum depends on the single particle anisotropy, being related to the crystalline structure and the particle size (Garcia-Palacios 2000). This means that the out-of-phase susceptibility profile may act as a fingerprint of a compound containing iron oxides or oxyhydroxides nanoparticles.

In conclusion, the AC magnetic susceptibility of an assembly of superparamagnetic nanoparticles will show a departure of χ'(T) from its Curie law behaviour and an appreciable contribution to χ". The χ"(T) temperature profile, under the assumption of negligible interparticle interactions, will reflect the distribution of particle sizes (see (Garcia-Palacios 2000) and references therein).

1.4.2.4. Diamagnetism: iron-containing species and matrix

The in-phase susceptibility of diamagnetic species is a temperature-independent negative value and there are no contributions to the out-of-phase susceptibility component (Fig. 19).

When measuring samples of low iron content, as it is the case of biological systems, the diamagnetic contributions can be of the same order of magnitude as the rest of the iron-containing species. For example, in tissue samples, there will be a diamagnetic contribution coming from the sample holder, the organic matrix and maybe some diamagnetic iron-containing species (e.g. oxyhaemoglobin) that will explain the negative values of the in-phase susceptibility.

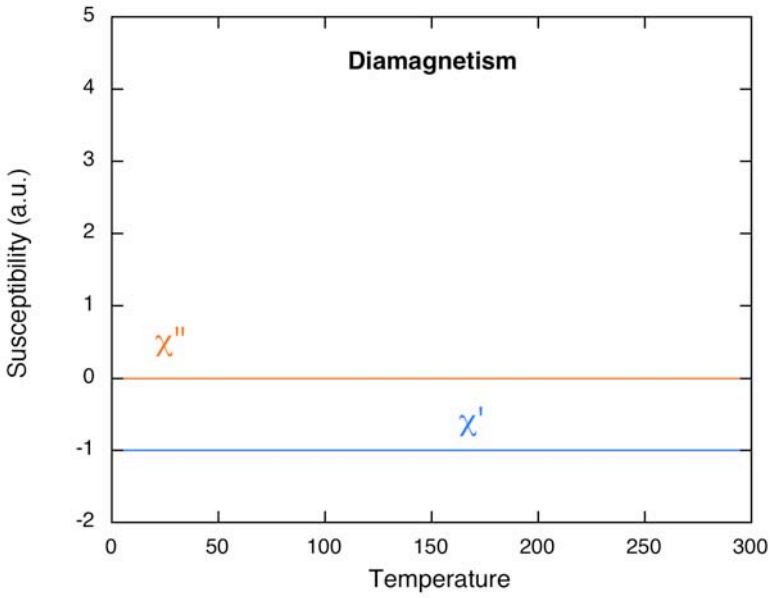

Fig. 19. Scheme of temperature dependence of the in phase and out-of-phase components of the AC susceptibility of a diamagnetic substance.

1.4.2.5. AC susceptibility of tissues

To interpret the magnetic susceptibility results of the tissues samples it has to be taken into account that some of the contributions that have been explained before may form part of the tissue total susceptibility.

First, it has to be noted that there will be a diamagnetic contribution coming from the matrix and the sample holder. Some of the iron-containing proteins are also diamagnetic, and although their diamagnetic contribution can be negligible in comparison with the diamagnetism of the organic matter, they have to be taken into account when interpreting the total magnetic moment of the sample. Anyway, the most important contributions to the susceptibility will correspond to the most abundant iron-containing species present in the tissues, which are usually paramagnetic species or biomineralised iron in the form of iron oxides or oxyhydroxides nanoparticles. Therefore, the total tissue susceptibility can be expressed as

$$\chi = \chi_{Fe-PARAMAGNETIC} + \chi_{Fe-PARTICLES} + \chi_{dia} \qquad \text{Eq. 9}$$

where $\chi_{Fe\text{-}PARAMAGNETIC}$ is the susceptibility of the paramagnetic iron-containing species, as e.g. deoxyhaemoglobin, χ_D the total diamagnetic susceptibility, (including the contribution of the sample holder, the tissue matrix and iron-containing diamagnetic-species) and $\chi_{Fe\text{-}PARTICLES}$ the susceptibility of the iron-containing particles. In the case of the endogenous particles present in the tissues that are inside the ferritin protein shell, $\chi_{Fe\text{-}PARTICLES}$ will include a high temperature

superparamagnetic contribution (χ_{SP}), a low temperature relaxational contribution (χ_R) and a small antiferromagnetic contribution (χ_{AF}) that in this case will be considered positive and temperature independent.

While all the iron-containing species present in the tissues contribute to the in-phase susceptibility signal, just the relaxational part of $\chi_{Fe\text{-}PARTICLES}$ will present a substantial contribution to the out-of-phase component. This fact is important, as it would allow the selective identification and quantification of superparamagnetic nanoparticles independently of the presence of other iron-containing species.

The in-phase component of the susceptibility will be a sum of all the contributions. As in the temperature range where $\chi'' \approx 0$, the susceptibility contributions from $\chi_{Fe\text{-}PARAMAGNETIC}$ and also $\chi_{Fe\text{-}PARTICLES}$ will follow a Curie law (assuming negligible thermal variations of χ_{AF}) the total high temperature susceptibility will be still proportional to $1/T$ allowing μ_{eff} to be calculated from the $\chi'(T)$ data. However, it has to be taken into account that in this case, the calculated effective moment would be an average value of the different iron-containing species in the tissue allowing us to now a little bit more about the iron speciation in the sample. For example, in a system that contains paramagnetic species and superparamagnetic particles composed of an antiferromagnetic material, the effective moment would be lower than or of the same order of the single ion value, depending on the size of the particles, on the type of spin uncompensation (Neel 1962) and on the relative amount of each species. On the contrary, if the particles were composed of a ferro- or ferrimagnetic material, whose intraparticle exchange interactions enhance the orientation of the ion spins towards the applied field, then the tissue effective moment would result higher than the single ion magnetic

moment, also depending on the relative amount of each species. If we add the presence of a third kind of species to these examples: Iron-containing diamagnetic species (that account for the total iron content but whose magnetic moment is zero), the value of the tissue effective moment per iron ion will decrease.

1.4.2.6. Interparticle interactions: calculation of τ_0 and T_{dip}

As a general rule, most of the samples characterised in this thesis will contain magnetic particles surrounded by an organic shell therefore potential interparticle interactions, if having any importance, would just be due to dipolar mechanisms. Dipole-dipole interactions may affect the shape and location in temperature of the χ' and χ'' maxima (Berkov et al. 2001), so its existence should be checked in order to use the susceptibility profile as an indication of the particle size distribution.

The importance of the interparticle interactions, and especially in what may affect the magnetic dynamics of the system, can be studied by the calculation of τ_0, which is the pre-exponential factor that appears in the Arrhenius expression for the relaxation time,

$$\tau = \tau_0 \exp(E_a / kT) \qquad \text{Eq. 10}$$

being k the Boltzmann constant and E_a the single particle anisotropy energy barrier. It is known that if the net particle magnetic moments reverse independently of each other following intraparticle coherent reversal of the atomic spins, τ_0 is usually in the range between 10^{-9}–10^{-12} s (Garcia-Palacios 2000).

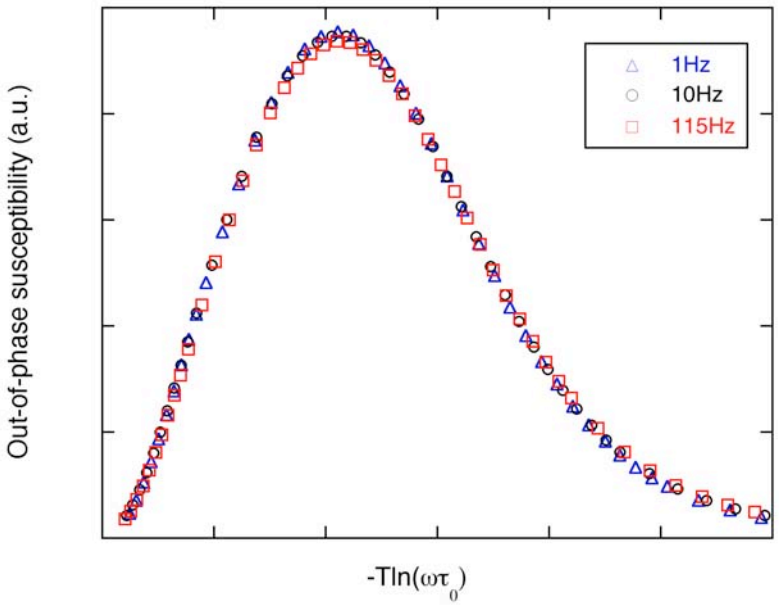

Fig. 20. Example of the scaling plot of the out-of-phase susceptibility for the determination of τ_0. The measured sample is iron sucrose, an iron supplement that will be described in the next chapter.

In what follows, the two different methods that have been employed in this thesis for the calculation of the preexponential factor are described.

The first method consist on the use of a scaling plot (Fig. 20) where χ" is represented as a function of $-T\ln(\omega\tau_0)$, ω being the AC angular frequency. In this representation, in the case of *negligible interparticle interactions*, the dynamics of the magnetic moments follows the Arrhenius model, in such a way that the χ" vs. $-T\ln(\omega\tau_0)$ data, measured at different frequencies, must superpose on a single master curve if a preexponential factor in the range mentioned before is used (Garcia-Palacios 2000).

The disadvantages of this method to obtain τ_0 are that it requires the sample to be measured at several frequencies and with a low noise level. If one of the previous conditions are unattainable, the method cannot be used.

The alternative method for the determination of τ_0 is based on the fact that the information that χ' and χ'' contain about the dynamical behaviour of particles is not the same. For non-interacting particle assemblies, χ''(T) and the derivative d(Tχ')/dT are theoretically related according to

$$\frac{\partial T\chi'_{\exp}}{\partial T} = -\frac{2}{\pi}\chi''\ln(\omega\tau_0) + \frac{\mu_0 M_s^2}{3K}\int_{D_b}^{\infty} dDf(D) + \chi'_{dia} \qquad \text{Eq. 11}$$

where M_S is the spontaneous magnetisation, $f(D)dD$ the volume fraction occupied by particles with diameters between D and $D + dD$ and the lower limit of the integral term, D_b, the so-called blocking diameter. For low and high enough temperatures [For a deeper description see (López et al. 2007)], equation 11 gives respectively:

$$\left.\frac{\partial T\chi'_{\exp}}{\partial T}\right|_{T\to 0} = -\frac{2}{\pi}\chi''\ln(\omega\tau_0) + \frac{\mu_0 M_s^2}{3K} + \chi'_{dia} \qquad \text{Eq. 12}$$

$$\left.\frac{\partial T\chi'_{\exp}}{\partial T}\right|_{T\to\infty} = -\frac{2}{\pi}\chi''\ln(\omega\tau_0) + \chi'_{dia} \qquad \text{Eq. 13}$$

According to these equations, the plotting of d(Tχ')/dT versus χ'' will be a way to obtain τ_0 (Fig. 21). This second method for the

determination of τ_0 is especially interesting when the measurements are rather noisy and the superposition of the curves is difficult to achieve.

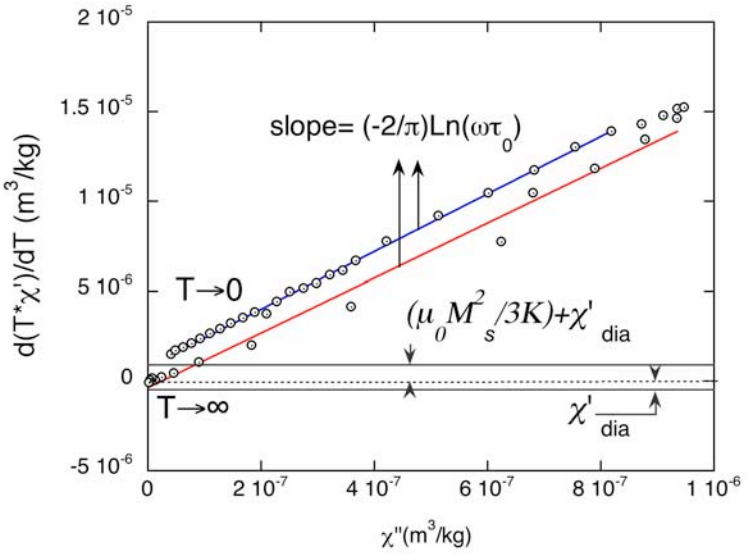

Fig. 21. Alternative method for the calculation of τ_0 based on equations 12 and 13. The data correspond to the iron sucrose sample that will be described in the next Chapter.

When working with biological tissues, the calculation of τ_0 from any of the two methods described above will provide information about the degree of interaction of the particles. In the case of the antiferromagnetic particles, it is not usual to observe this kind of interactions, however, in the case of tissues containing ferrimagnetic particles, this parameter will inform if the particles are homogeneously distributed in the tissue or if they present some degree of local aggregation.

The calculation of the temperature parameter T_{dip}, is also another way to assess the importance of dipole–dipole interparticle interactions (López et al. 1997). T_{dip} is defined in equation 14 as:

$$T_{dip} = \frac{3C\rho}{4\pi} \qquad \text{Eq. 14}$$

where C is the Curie constant in mass susceptibility representation and ρ is the iron mass per unit volume in the sample.

T_{dip} values lower than the temperature range used for the measurements may justify the use of a non-interaction model in the interpretation of the susceptibility results.

1.4.2.7. Anisotropy constant and particle volume

In the previous section, in Fig. 21, it has been detailed how the plotting of d(Tχ')/dT versus χ'' will allow the determination of a value for M_s^2/K from the intercept of the extrapolated experimental curve. If knowing the value of the spontaneous magnetisation (M_s) of the material, the effective anisotropy constant can be calculated. According to equation 15, it will be possible to obtain a value of the diameter of the particle from these data.

$$D_B = -\left[\frac{6k_BT/\pi K}{\ln(\omega\tau_0)}\right]^{1/3} \qquad \text{Eq. 15}$$

This type of relative granulometry is independent of the TEM results, as it is based on different phenomena, and, unlike the microscopical observations, informs simultaneously about the whole sample.

Alternatively, if the size of the particle is known, e.g. from TEM observations, the effective anisotropy constant can be estimated from the next equation

$$K = \left(\frac{kT}{v}\right)\ln\left(\frac{1}{\omega\tau_0}\right) \qquad \text{Eq. 16}$$

where v is the average particle volume and T is the temperature of the χ'' maximum, in order to check its agreement with previously reported data on the same material.

1.4.2.8. Optimization of the measurements

In biological samples the iron content is usually low and, besides, the endogenous iron-containing species are usually paramagnetic, diamagnetic or superparamagnetic particles of antiferromagnetic iron oxyhydroxides, which correspond to low efficient magnetic states. For these reasons, the magnetic signal of biological samples is sometimes near the detection limits of the technique and special protocols to reduce the noise of the measurement and to avoid the presence of oxygen, which may contribute to the magnetic signal, have to be carried out. All of these special issues have been described in this section.

Presence of oxygen

In low temperature experiments, adsorbed oxygen is known to be possibly present in the samples.

This spurious oxygen contributes to the susceptibility either with a paramagnetic low temperature tail and/or with an antiferromagnetic ordering anomaly at around 50 K (Kanoh et al. 1996). These contributions, that depend on the specific form of the adsorbed species, are known to disappear after forced oxygen desorption, heating the sample to high temperatures (QuantumDesign 1997). The result is that if

a second temperature run is made the obtained data do not reproduce those of the first run (Fig. 22).

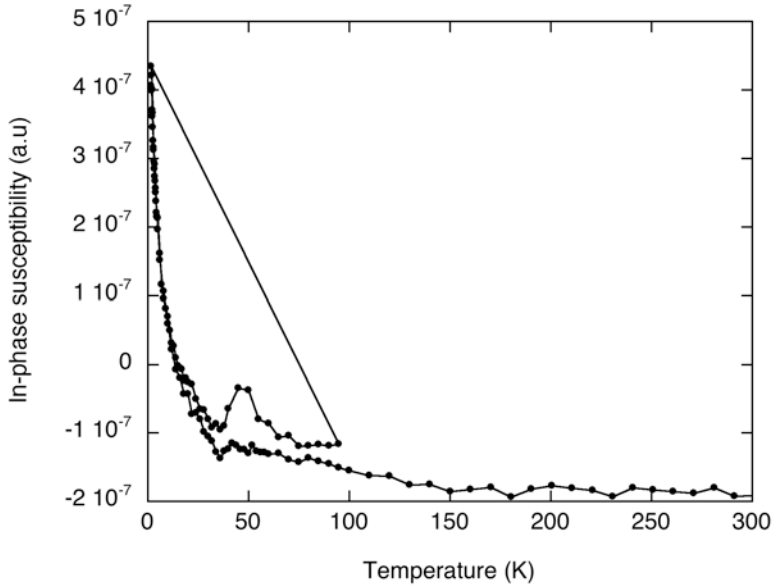

Fig. 22. Detection of the presence of oxygen in a sample. The measurements start at 5 K and continue up to 70K when the sample was heated up to 200 K for 10 min. Then, the measurement was performed again from 5 to 300 K. See that the data of the second measurement do not reproduce the first one.

In what concerns to the measurements presented in this thesis, it has to be specified that the data presented were fully reproducible after a first run up to 200 K, so the importance of the paramagnetic tails will not be due to residual oxygen.

Measurements at different frequencies

The AC susceptibility measurements can be performed at different frequencies of the AC field. When working with samples with a very low magnetic signal, near the detection limits, frequency-dependent contributions to the susceptibility, associated not with the sample but with the equipment, that will not be observed when working with samples with higher magnetic signal start to be appreciable.

This is the case of a temperature independent background signal that appears in the out-of-phase susceptibility when increasing the frequency of the AC field. This background signal is related with induced currents in the transport rod of the SQUID magnetometer.

To study the contribution produced by these currents, measurements of the out-of-phase susceptibility at the 3 different frequencies of a very little amount of a paramagnetic salt (Potassium chromium(III) sulphate dodecahydrate, $CrK(SO_4)_2 \cdot 12H_2O$), which has zero out-of-phase susceptibility were performed (Fig. 23).

It was observed that when increasing the frequency, although it makes the experiment shorter (e.g. for the same sequence it changes from 10 h to 13 h when measuring at 10 Hz and 1 Hz respectively), a bigger background signal was obtained in the out-of-phase susceptibility. To reach a compromise between these two factors, at the beginning of the studies presented here the samples were measured using a frequency of 10Hz.

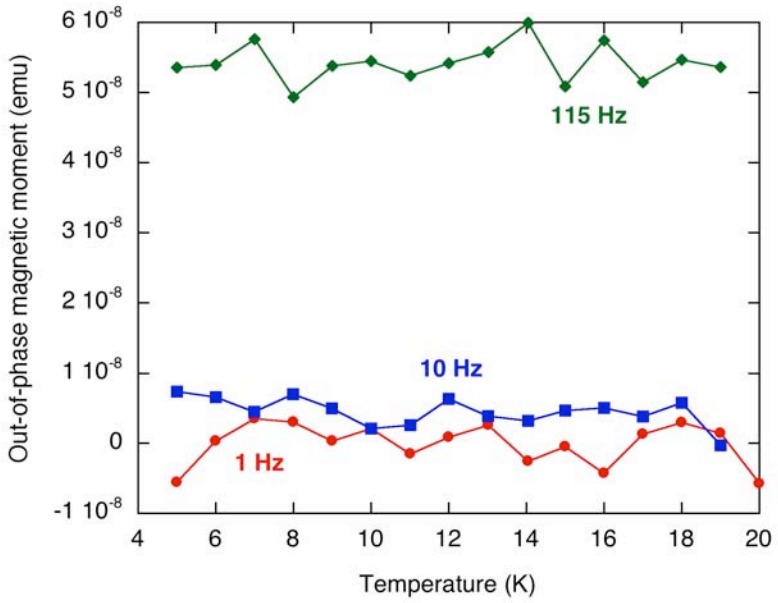

Fig. 23. Temperature dependence of the out-of-phase susceptibility of $CrK(SO_4)_2 \cdot 12H_2O$, a paramagnetic salt, measured at different frequencies in order to observe the contribution of the induced currents.

At one point of the magnetic characterisation of samples with a very weak magnetic signal, it was observed that a special reduction of the noise was obtained for a given combination of parameters in the measurement. For this reason, a study was performed in order to optimize the noise reduction. A sample with a very low magnetic signal was measured by two AC susceptometers (Quantum Design MPMS-5S and MPMS-XL) in the temperature range between 5 and 10K at three different frequencies (1, 10 and 120 Hz) varying one of the installation parameters (number of blocks to average in the measurement). The results can be observed in Fig. 24 and Fig. 25

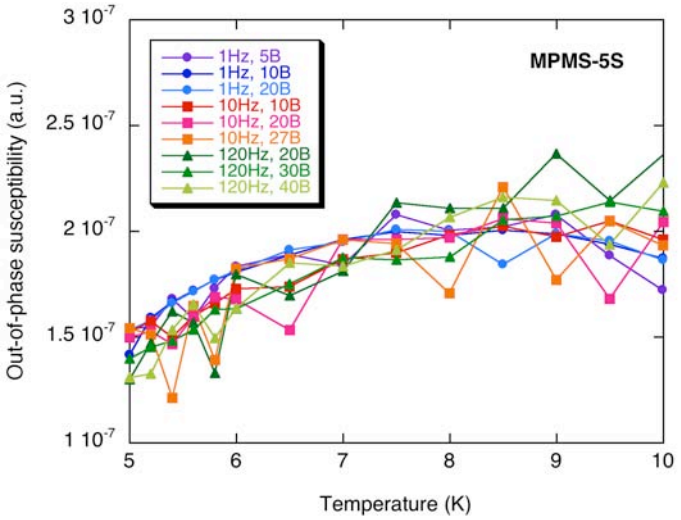

Fig. 24. Evaluation of the influence of the frequency of the AC magnetic field and the number of blocks to average in the noise of the measurement of the AC susceptibility in a MPMS-5S SQUID magnetometer.

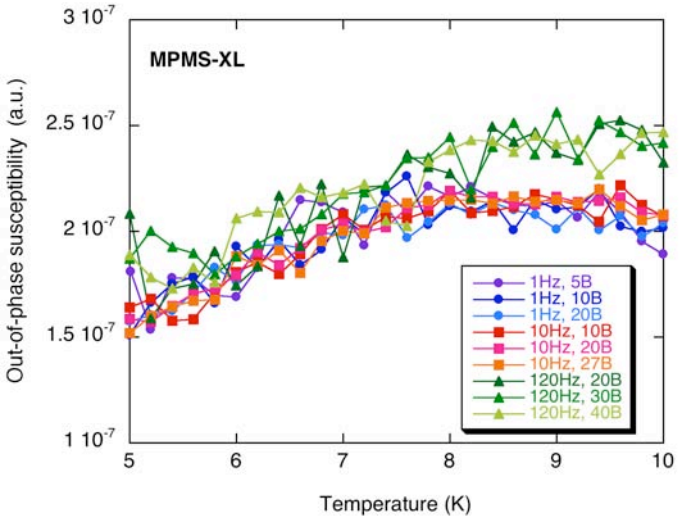

Fig. 25. Evaluation of the influence of the frequency of the AC magnetic field and the number of blocks to average in the noise of the measurement of the AC susceptibility in a MPMS-XL SQUID magnetometer

It was observed that the measurements performed in the MPMS-5S susceptometer at 1Hz and with 10 blocks to average were substantially less noisy than the rest of the combinations, so from the time of this observation, the rest of the measurements were performed in these conditions.

1.5. Transmission Electron Microscopy

The TEM characterisation performed in the studies presented in the following chapters has provided useful information about the size and microcrystalline structure of the iron-containing nanoparticles present in the different samples. Besides, when characterising tissues of biological origin, TEM analysis informs about the localization of the particles within the tissue and about the tissue histology.

As this is a commonly used technique for the study of biological samples, conventional protocols for the preparation of the samples have been used (Robards et al.). Only a special issue, related with the sample staining has to be taken into account.

When studying tissues by TEM, the protocols used for the samples preparations usually include a staining step, which enhances the contrast in the image and highlights the structures in the tissues. However, this typical staining process is counterproductive for the study of the iron deposits. The staining may difficult the study of the ferritin cores and other iron deposits that are usually identified by their electron density. For this reason, in order to facilitate the study of the iron deposits, a crucial issue is the use of unstained or lightly stained sections, that allows the identification of the ferritin molecules because of the typical size of the

electron-dense cores that besides appear mutually separated by the non electron-dense protein shells.

The study of tissue samples by transmission electron microscopy has only been performed in given samples selected after the magnetic characterisation. The specific protocol used in the study of rat and mice tissues presented in the following chapters has been detailed in each of them.

1.6. Elemental analysis

The elemental analysis has two main objectives: (i) to determine the total elemental iron content in the samples and (ii) to discard the presence of other magnetogenic elements as Co, Ni, Mn or Cu in order to interpret the magnetic results as only due to iron.

Although there are different techniques in order to characterise the elemental composition of a given sample, in this thesis, it has been performed by Inductively Couple Plasma - Atomic Emission Spectroscopy (ICP-AES). A different technique, Inductively Coupled Plasma- Mass Spectrometry (ICP-MS), usually has lower detection limits than ICP-AES. However, the formation of $^{40}Ar^{16}O^{+}$ and $^{40}Ar^{16}OH^{+}$ at m/z 56 and 57 interfere with iron determination by ICP-MS. So, although the use of ICP-MS seemed better for the quantification of Co, Ni, Mn or Cu, it has been preferred to use a technique that provides better results in the iron determination.

In order to perform the elemental analysis by ICP-AES, a liquid solution is needed. Tissue samples have been diluted by microwave acid

digestion with a solution 4:1 (v/v) of HNO_3 (65%) and H_2O_2 (30%). The program used in the digestion (Caroli et al. 2000) is detailed in Table 3.

Step	Time (min)	Power (W)
1	10	600
2	6	0
3	10	300

Table 3. Program of the three different steps of power and time of the microwave acid digestion.

2. Iron supplements

2.1. Introduction and main aims

As it has been previously stated, iron is an element of key importance in every form of life and participates in very important biological processes. Thus, the deficiency of iron constitutes a pathological situation in humans as we depend on iron for our growth and development. In fact, iron deficiency is the most common and widespread nutritional disorder in the world. According to the World Health Organization (www.who.int), 2 billion people (over 30% of the world's population) are anaemic mainly due to iron deficiency. As expected, this deficiency affects a large number of children and women in developing

countries due to the iron-poor diets, but it is also the only nutrient deficiency that is significantly prevalent in industrialized countries.

The treatment of mild to moderate iron-deficiency anaemia consists in iron supplementation that can be administered orally or parenterally (Hudson et al. 2001). Oral iron supplements are extensively used because of the similarity of their assimilation mechanism with the natural one, although a repeated oral administration can produce adverse effects due to gastroduodenal toxicity. In contrast, parenteral iron preparations are only used with patients who cannot tolerate oral forms or those who steadily loose large amounts of blood. These last treatments have higher efficacy but require clinical supervision.

A wide variety of formulations are nowadays used as haematinics although most of them contain either iron oxyhydroxide nanoparticles surrounded by a carbohydrate shell or iron salts. The iron speciation in these drugs is a key factor with respect to its absorption. It appears that ferrous iron is better absorbed than ferric iron (Atanasova et al. 2005). Besides, in those compounds that contain iron oxyhydroxide particles, their crystalline structure and size may also determine the solubility and diffusion coefficient of the drugs, eventually affecting degradation kinetics and biodistribution (Funk et al. 2001; Danielson 2004). As an example, smaller particle sizes and poorer crystallinity are expected to improve bioavailability. For this reason, the characterisation of the physicochemical properties of the different drugs is of great relevance.

In this context, as these drugs are nanodisperse systems in which iron is the only magnetogenic element, they constitute a good system to use the magnetic characterisation to study the iron speciation, which is directly related to their absorption kinetics. Furthermore, besides obtaining information about the iron speciation in this kind of drugs, their

magnetic characterisation is the necessary first step in pharmacological studies by magnetic means of iron metabolism in real tissues after drug administration (Lázaro et al. 2005), as the one described in the following chapter.

This chapter has been divided into two parts. First, the results of the characterisation of each of the most commonly used haematinics are presented. The second part of the chapter aims at comparing the dynamic susceptibility of those haematinics that contain nanoparticles of iron oxyhydroxides with especial emphasis on the correlation between the magnetic properties and the microstructure, as these drugs are currently used examples of nanostructured materials.

This work is the continuation of an already existing research line in which two drugs were previously analysed (iron sorbitol and iron dextran). Although a brief description of these two compounds will also be provided, a more detailed characterisation of these samples can be consulted in Refs. (Lázaro et al. 2002) and (Lázaro et al. 2003). As a rule, all the studied haematinics have been characterised by AC susceptibility measurements and atomic emission spectrometry, and those of them that showed a magnetic behaviour typical of magnetic particles were also studied by field dependent magnetisation, Transmission Electron Microscopy and Selected Area Electron Diffraction.

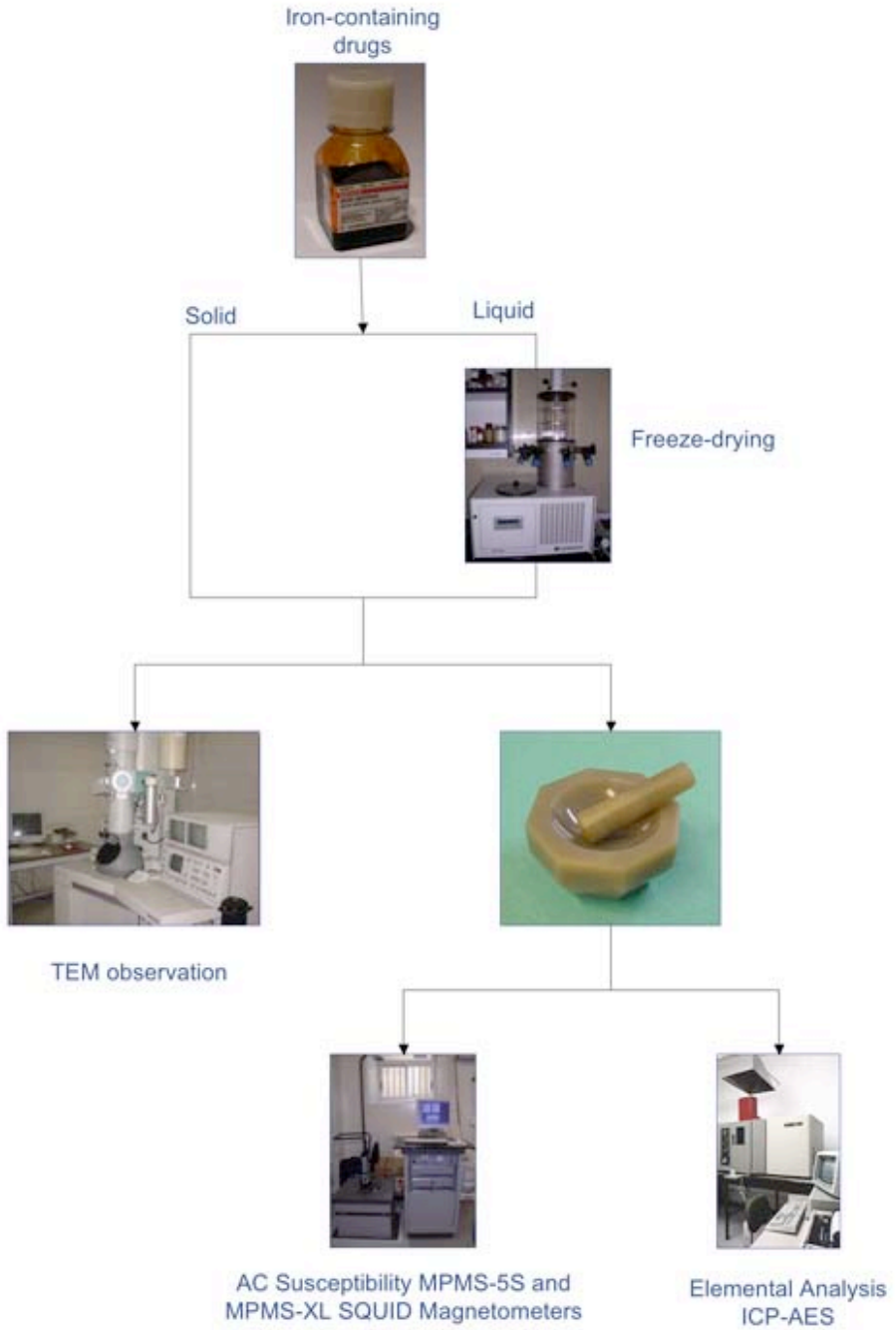

Fig. 26. Work protocol scheme including all the steps described in this section..

2.2. Studied compounds and analytical methods

In what follows, a description of the compounds that have been characterised together with the specific parameters of the used techniques is given. A schematic representation of the different steps carried out in the work presented in this chapter is provided in Fig. 26.

2.2.1. Studied drugs

Samples were obtained from different commercial pharmaceuticals whose formulations are listed in Table 4. Iron sorbitol, iron dextran and iron sucrose are parenterally administered while the rest of the drugs are used in oral treatments.

Formulation	Trade name	Supplier	Form
Iron sorbitol	Yectofer®	Astra España	Liquid
Iron dextran	Iron dextran	Sigma-Aldrich	Liquid
Iron sucrose	Venofer®,	Vifor	Liquid
Hydrated ferrous sulphate	Tardyferon®	Pierre Fabre Ibérica	Tablets
Hydrated ferrous sulphate	Ferogradumet®	Ross, Abott Científica	Tablets
Ferrimannitol-ovalbumin	Profer®	Tedec-Meiji Farma	Powder
Ferric protein	Ferroprotina®	FAES	Powder
Ferrous lactate	CromatonbicFerro®	Menarini	Powder

Table 4. List of the iron-containing haematinics included in this study. The formulations correspond to what the suppliers indicate about their composition.

2.2.2. Freeze-drying and milling

In order to get a solid sample for the magnetic characterisation, the liquid commercial compounds (see Table 4) were lyophilised during

48 h in a Telstar-Cryodos freeze-dryer. The resulting product was ground to powder in a mortar to get a homogeneous sample for the elemental analysis and the magnetic measurements. The drugs that are commercialised as tablets or powder were also milled in a mortar for better homogeneity.

2.2.3. Elemental analysis

The elemental analysis of all the powders, a part of which were magnetically characterised, was performed after acid digestion by inductively coupled plasma-atomic emission spectrometry (ICP-AES) with a Perkin Elmer P-40.

Obviously, the elemental analysis was performed with especial focus on the determination of iron, nevertheless, the presence of other magnetogenic elements as Co, Ni, Mn and Cu that might also contribute to the magnetic signal was also checked.

2.2.4. Magnetic measurements

The magnetic characterisation was carried out in Quantum Design MPMS-5S and MPMS-XL SQUID magnetometers, both equipped with an AC option (AC amplitude of 0.45 mT and 0.41 mT respectively). The AC susceptibility measurements of all the drugs were performed at 10 Hz in the temperature range between 1.8 K and 300 K. Field and temperature dependence magnetisation and dynamic magnetic measurements at different frequencies were also performed in selected samples.

For these measurements the powders of the different drugs were placed in gelatine capsules.

2.2.5. TEM observations

TEM analysis of iron sucrose and ferrimannitol-ovalbumin (FMOA) was performed in a JEOL 2000 FXII microscope operated at 200 kV. Electron diffraction was carried out on selected areas and the maxima were identified using a thallous chloride diffraction standard to calculate accurately the camera length.

The preparation of the samples for the TEM observation consisted in a dispersion of the drug in acetone in an ultrasonic bath for some minutes. Then, a drop of this liquid was placed on a carbon-coated copper grid and allowed to dry.

2.2.6. X-ray diffraction

X-ray diffraction analysis was performed in the iron sucrose sample for a structural characterisation. The freeze-dried iron sucrose was milled in a mortar and the powder was used to record the X-ray diffraction patterns between 5º and 90º (2θ) at 0.5º/min in a Phillips PW1710 diffractometer with Cu K_α radiation.

2.3. Results

2.3.1. Ferrous lactate

The iron content determined by ICP-AES of ferrous lactate is 197.4 mg Fe/g sample, while the concentration of other magnetogenic elements was negligible ([Co]= 0.013 mg/g, [Mn]= 0.029 mg/g, [Ni]= 0.057mg/g).

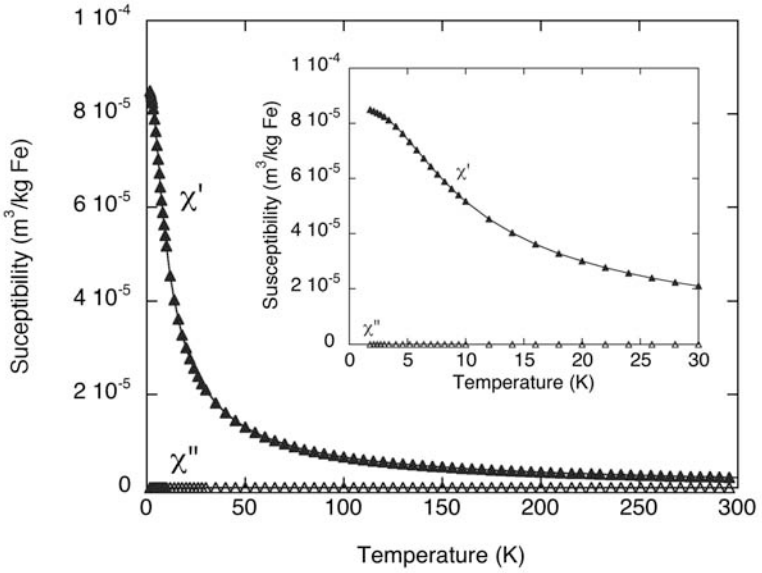

Fig. 27. Temperature dependence of the AC mass susceptibility per iron amount of ferrous lactate at 10 Hz. Note the absence of relaxation in all the temperature range. The inset shows the slight bending of χ' at the lowest temperatures.

The temperature dependence of the AC susceptibility of ferrous lactate is shown in Fig. 27. It can be observed that the in-phase susceptibility presents a Curie-type behaviour accompanied by a negligible out-of-phase susceptibility, χ", in nearly all the measured temperature range. However, a slight departure from the Curie-type behaviour, observed in the bending of $\chi'(T)$, has been detected at the lowest temperatures (see inset of Fig. 27).

The $\chi'(T)$ data can be fitted with a Curie-Weiss equation (Eq. 7) in nearly all the temperature range. Supposing the diamagnetic contributions to be negligible, the obtained value for θ is 3.2 K, whose positive sign indicates the presence of antiferromagnetism. Although the complete peak in $\chi'(T)$, as the described in the previous chapter for

antiferromagnetic compounds, cannot be observed in the measured temperature range, the slight bending of $\chi'(T)$ at the lowest temperatures may be an indication of the expected peak at lower temperatures.

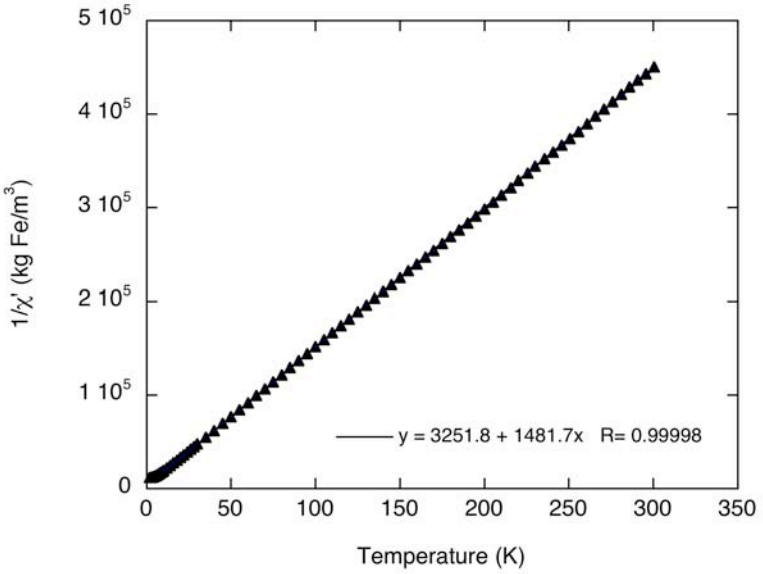

Fig. 28. Temperature dependence of the inverse of the in-phase susceptibility per iron amount of ferrous lactate at 10 Hz.

The value of the Curie constant, obtained from the slope of the curve in the $1/\chi'$ vs T representation (Fig. 28), has been used to determine the effective moment per iron ion, μ_{eff} by use of Eq. 6. The obtained μ_{eff} value is 4.91 μ_B, which is slightly lower than the values reported for Fe^{2+}.

2.3.2. Ferrous sulphate

The two compounds containing $FeSO_4$ also show negligible χ'', within the accuracy of the experiments, in all the temperature range although a peak can be clearly observed in $\chi'(T)$ at around 30 K (Fig. 29). Both $FeSO_4$ samples, although coming from different commercial

compounds and with slightly different formulations have an extremely similar magnetic behaviour typical of an antiferromagnetic material.

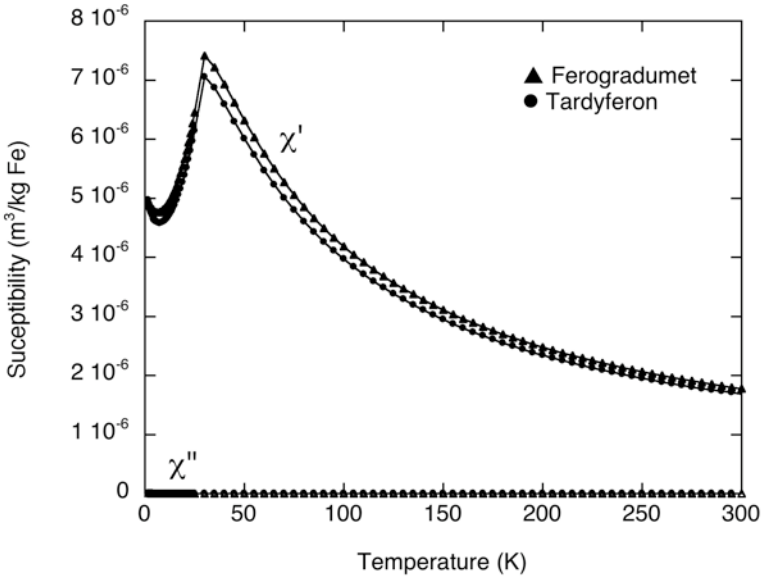

Fig. 29. Temperature dependence of the AC mass susceptibility per iron amount of ferrous sulphate samples at 10 Hz. Triangles correspond to Ferogradumet® while circles correspond to Tardyferon®. Note the absence of relaxation in all the temperature range.

Above ≈30K, the two $\chi'(T)$ data can be fitted with a Curie-Weiss equation (Eq. 7). Supposing the diamagnetic contributions to be negligible, the obtained values for θ are 46.9 K and 46.5 K for Ferogradumet® and Tardyferon® respectively, whose positive sign indicates antiferromagnetic behaviour.

The value of the Curie constant of both compounds has been obtained from the slope of the curve in the $1/\chi'$ vs T representation (Fig. 30). By use of Eq. 6, the effective moment per iron ion, μ_{eff} has been calculated to be 4.67 μ_B and 4.54 μ_B for Ferogradumet® and Tardyferon®

respectively. These values are slightly lower than the values reported for Fe^{2+} (Cornell et al. 1996).

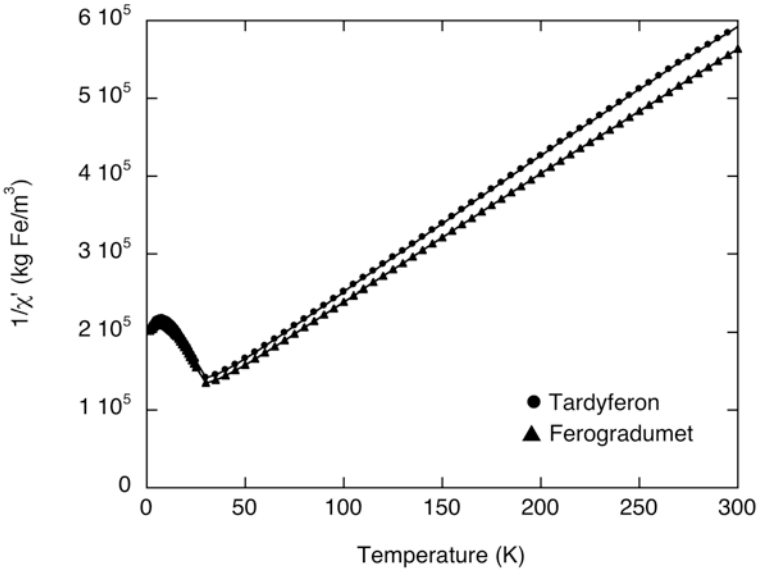

Fig. 30. Temperature dependence of the inverse of the in-phase susceptibility per iron amount of the two drugs containing ferrous sulphate at 10 Hz.

2.3.3. Ferrimannitol-ovalbumin (FMOA)

The iron concentration in the FMOA powder sample was 12.7 mg Fe/g sample, while the content of the other analysed magnetogenic elements (Co, Cu, Mn and Ni) was less than 0.09 mg/g.

The in-phase susceptibility of the FMOA shows a maximum in the vicinity of 8 K, for measurements at 10Hz, accompanied by an out-of-phase susceptibility maximum at slightly lower temperatures (Fig. 31), which evidences a magnetic relaxation phenomenon. As this is typical of magnetic particles, TEM and SAED observations together with a more detailed magnetic study was performed on this drug.

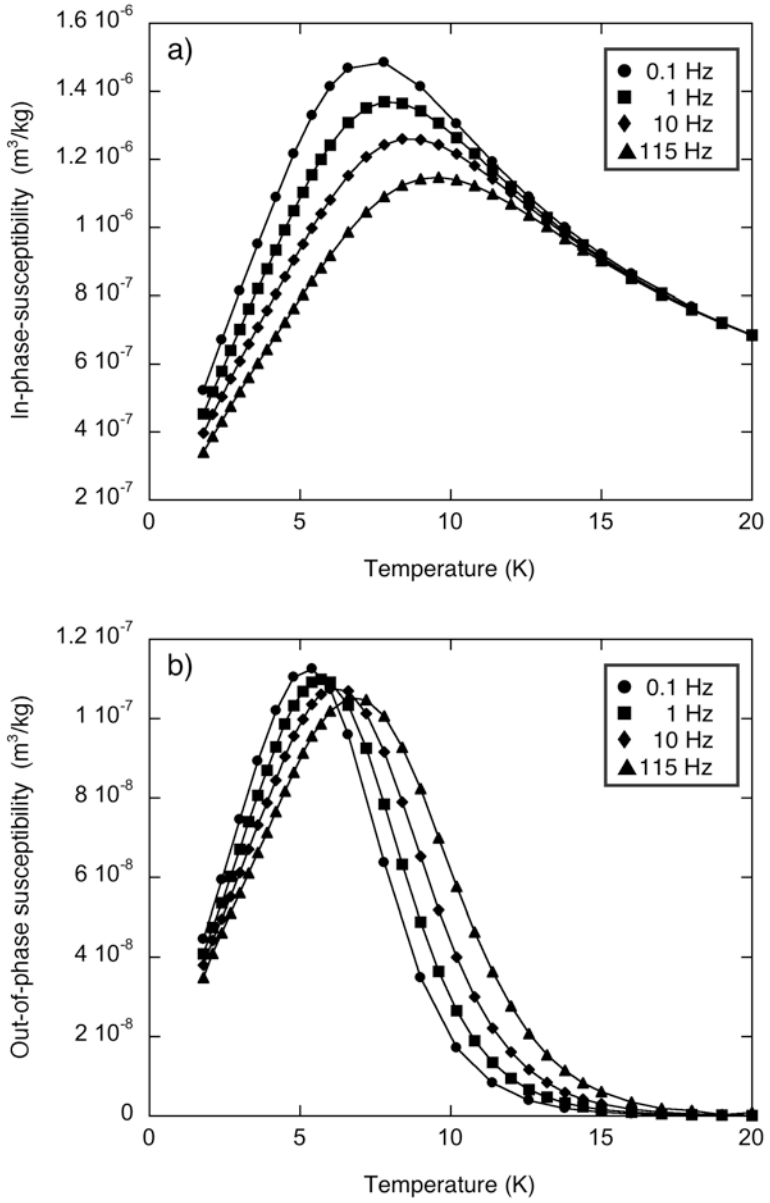

Fig. 31. Temperature dependence of the AC mass susceptibility of FMOA at four different frequencies. a) In-phase component, b) Out-of-phase component. Note the absence of relaxation above approximately 20 K.

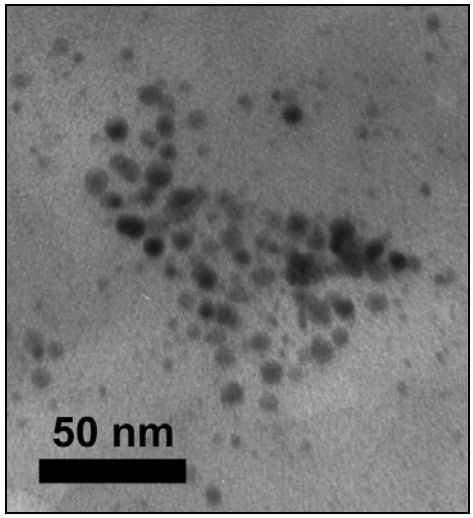

Fig. 32. Transmission electron micrograph of the FMOA sample. The electrodense particles most likely correspond to the iron oxyhydroxide ferrihydrite.

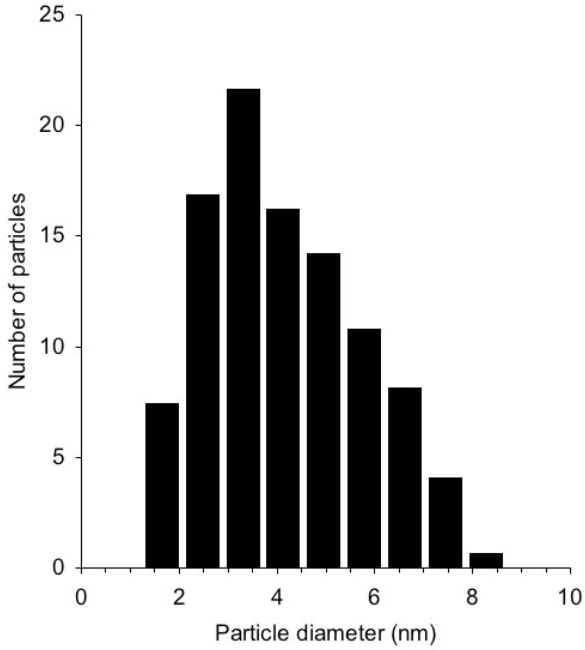

Fig. 33. Particle size distribution histogram corresponding to the species shown in Fig. 32.

A transmission electron micrograph of a representative zone of the FMOA sample is shown in Fig. 32. Electrodense particles typically smaller than 10 nm can be distinguished in a less electrodense matrix that most likely corresponds to the excipient matter. Their size distribution is represented in the histogram of Fig. 33, which contains data from the measurement of 150 particles. The results indicate that the mean particle size is 4.2±1.6 nm.

Selected area electron diffraction (SAED) patterns were obtained from different zones of the sample. The SAED intensity profiles present two intense diffraction peaks corresponding to interplanar spacings of d = 0.25 nm and 0.15 nm (Fig. 34), that are typical of two-line ferrihydrite (Janney et al. 2000).

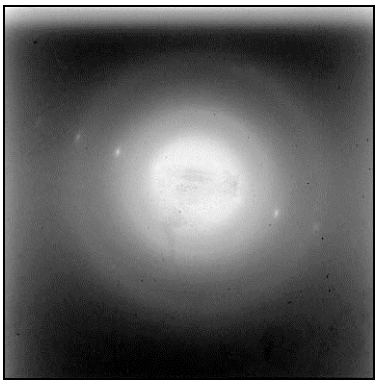

Fig. 34. SAED pattern of the FMOA sample.

Coming back to the magnetic characterisation, as above approximately 20 K χ'' is zero, within the accuracy of the experiments, in this temperature range $\chi' = \chi_{SP} + \chi_{AF} + \chi_{dia}$, where χ_{SP}= C/T . The value of the Curie constant, as well as the corresponding to $\chi_{AF} + \chi_{dia}$, have been obtained from the χ' vs $1/T$ representation, assuming, as a first

approximation, the thermal variations of χ_{AF} to be negligible. The χ_{AF} + χ_{dia} value obtained for FMOA is -1.4x10-6 0.5x10-6 m3/kg Fe, whose negative sign indicates that the diamagnetic susceptibility is greater than the antiferromagnetic one. The obtained value for the Curie constant has been used to determine the effective moment per iron ion (Eq. 6). The calculated μ_{eff} value for FMOA is 6.1± 0.2 μ_B per iron ion, which is not significantly different from the single ion magnetic moment. This result indicates that the intraparticle spin configuration is close to the expectations of the volume uncompensation model, which in fact predicts an effective moment similar to the paramagnetic ion (López et al. 1997).

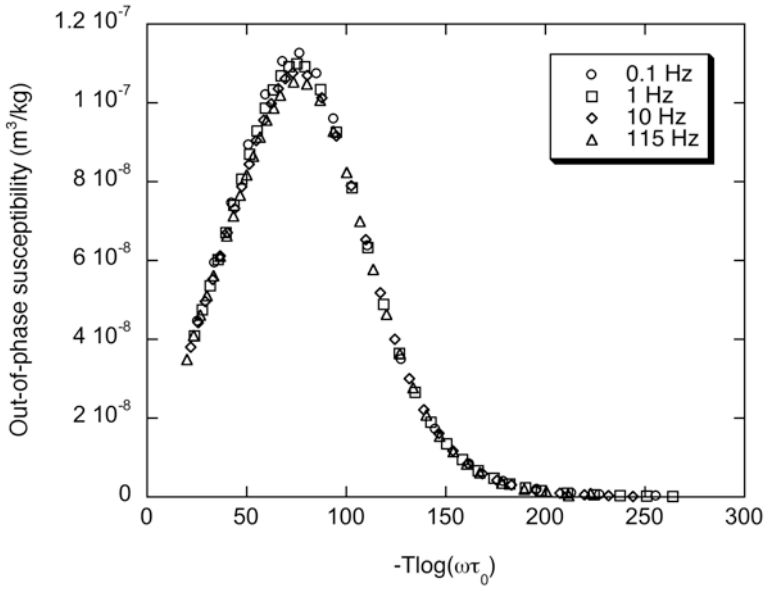

Fig. 35. Scaling plot of the out-of-phase mass susceptibility of FMOA measured at four different frequencies. The best superposition is obtained with with $\tau_0 = 10^{-15}$ s .

The magnetic dynamics of FMOA have been studied to assess the validity of the superparamagnetic model of non-interacting particles. The

χ''(T) data measured at 0.1, 1, 10 and 115 Hz have been plotted (Fig. 35) as a function of $-T\log(\omega\tau_0)$ and the best superposition has been obtained using a τ_0 value of 10^{-15} s. This value is rather close, but lower, than the values reported for other ferrihydrite nanoparticles systems showing non-interacting particle dynamics (López et al. 1997; Lázaro et al. 2002).

The value of the effective anisotropy constant K has been estimated from Eq.16, using the mean particle size determined with TEM. The obtained effective anisotropy constant yields $7.3\text{x}10^4$ J/m^3, which is close to previous results for ferrihydrite (Cornell et al. 1996) and for different compounds that contain similar ferrihydrite nanoparticles (López et al. 1997; Luis et al. 1999).

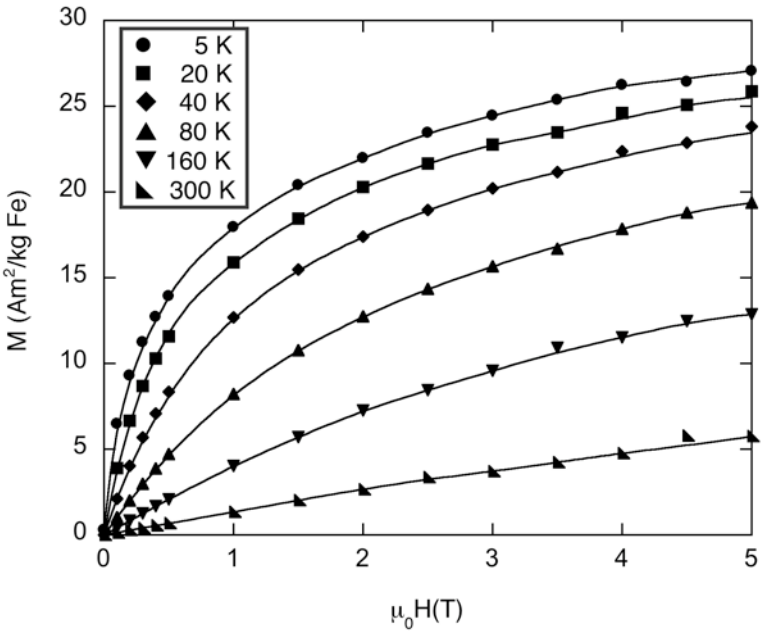

Fig. 36. Field dependence of the magnetisation of FMOA at the indicated temperatures. Solid lines are just a guide for the eye.

The field dependent magnetisation measured at 5, 20, 40, 80, 160 and 300 K under increasing field up to 5 T, are shown in Fig. 36. In additional experiments performed for decreasing field, sizeable hysteresis is only observed at 5 K, with a remanence value of 1.41 Am^2/kg Fe, although this hysteresis obviously results from the single particle relaxation process. The field dependent magnetisation results agree with the AC susceptibility as remanence is only observed at temperatures in the range where χ'' is different from zero.

The magnetisation can be interpreted with the expression

$$M = M_{SP} + (\chi_{AF} + \chi_D)H \qquad \text{Eq. 17}$$

where M_{SP} is the superparamagnetic magnetisation of the iron oxides or oxyhydroxide particles, which would follow a Langevin-type law, and H is the applied field. To check the validity of this interpretation, in Fig. 37 it has been plotted M as a function of H/T (Bean et al. 1956). A good superposition has been obtained at low fields by considering the value of $\chi_{AF} + \chi_D$ equal to -1.4×10^{-6} m^3/Kg Fe, determined from the $\chi'(T)$ data. The observed discrepancy at high fields can be easily explained as follows. In previous theoretical calculations of M(H) for magnetic nanoparticle assemblies, with consideration of single particle anisotropy, and making use of the parameter $\sigma = KV/kT$, it was predicted that at medium fields M(H) exhibits a departure from the zero anisotropy curve which increases for increasing σ (Hylton 1993; Garcia-Palacios 2000). Although our system contains a distribution of particle sizes, by consideration of the average particle size and our previously determined K value, we obtain σ = 10.7, 5.2, 2.6, 1.3, and 0.7 for T = 20, 40, 80, 160 and 300 K respectively. In Fig. 37, it is clearly seen that not only the M(H) curves follow the predicted sequence but also that the departures

from the zero anisotropy case are of the same order as those theoretically expected (Hylton 1993; Garcia-Palacios 2000).

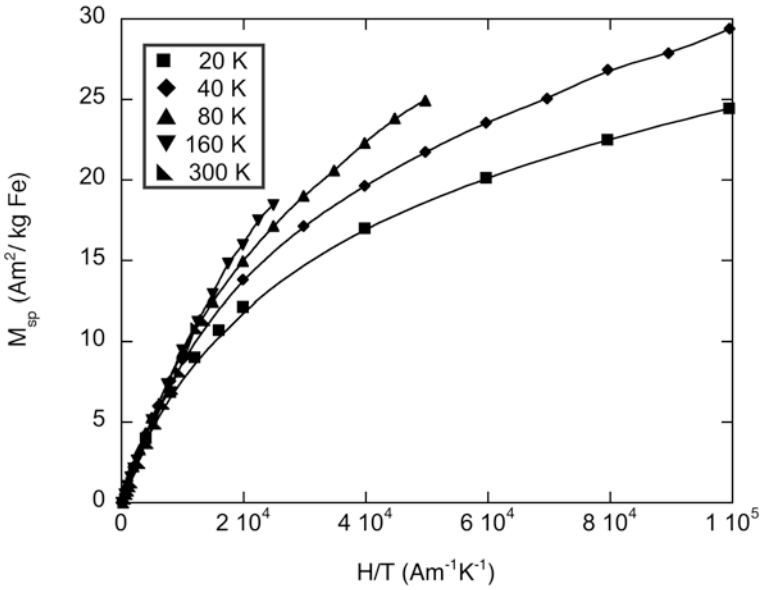

Fig. 37. Scaling plot of the superparamagnetic magnetisation of FMOA measured at different temperatures. The solid lines are just a guide for the eye

2.3.4. Iron sucrose

For the study of this compound, the solid powder obtained after freeze-drying the content of one ampoule (5 ml) was used for all the measurements. The iron concentration in the freeze-dried sample was determined to be 47.11 mg Fe/g.

The temperature dependence of the AC susceptibility is shown in Fig. 38. The out-of-phase susceptibility χ" is zero above 50 K, within the accuracy of the experiments. χ' shows a maximum at around 25 K, for 10 Hz, accompanied by a χ" maximum at slightly lower temperatures which evidences a magnetic relaxation phenomenon.

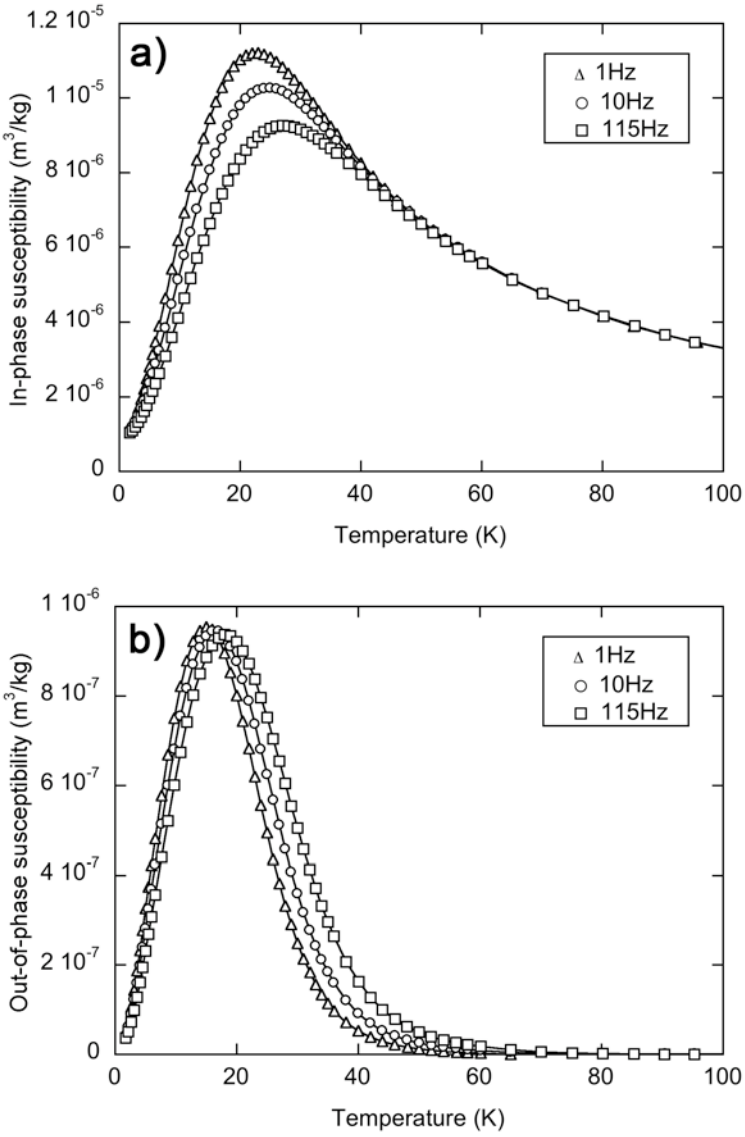

Fig. 38. Temperature dependence of the a) In -phase and b) Out-of-phase AC mass susceptibility of freeze-dried iron sucrose at three different frequencies. See the clean absence of relaxation above approximately 50K.

As it has been shown with the FMOA sample, TEM, SAED observations and a more detailed magnetic study were performed on this drug to study the presence of the iron-containing particles. Furthermore, an X-ray diffraction analysis was also carried out with this sample.

A representative zone of the iron sucrose sample is shown in Fig. 39. Two components can be distinguished: Disperse electrodense particles, most likely due to the iron-containing inorganic part of the sample, with an average diameter of 5 nm and a less electrodense matrix, expectedly corresponding to the sucrose where the particles are dispersed.

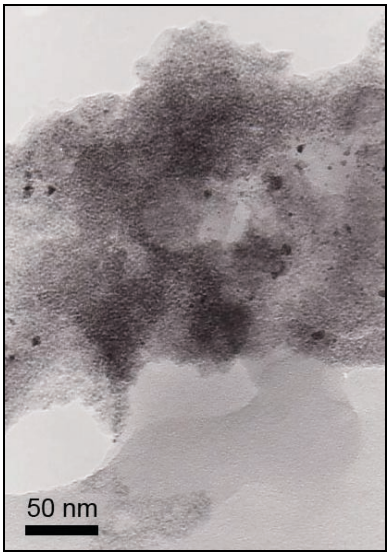

Fig. 39. Transmission electron micrograph of freeze-dried iron sucrose. The electrodense particles likely correspond to the iron oxyhydroxide.

Selected area electron diffraction (SAED) patterns were obtained from different zones of the sample. The SAED corresponding to the micrograph of Fig. 39 is shown in Fig. 40. The SAED intensity profile is shown in Fig. 41. The two most intense diffraction peaks correspond to interplanar spacings of d = 0.25 and 0.15 nm, typical of two-line

ferrihydrite (Janney et al. 2000) and the weak peaks corresponding to *d* values of 0.32, 0.21 and 0.12 nm were assigned to the carbon coating the TEM grid. Additional, still identifiable, very small peaks, at 0.22, 0.19 and 0.17 nm may correspond to a small amount of six-line ferrihydrite.

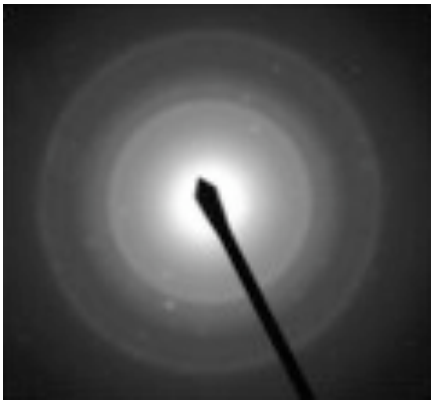

Fig. 40. SAED pattern of the same region shown in Fig. 39 for iron sucrose.

The X-ray diffractogram of iron sucrose is shown in Fig. 42. The spectrum corroborates the presence of sucrose, in particular from the peaks corresponding to d = 0.41 and 0.67nm (JCPDS 1974). Within the accuracy of the experiment, ferrihydrite peaks are seen at d = 0.25 and 0.15 nm corresponding to the (110) and (300) planes, respectively (Cornell et al. 1996). The average ferrihydrite crystallite size has been obtained by using the full-width at half-maximum of the (110) reflection using the Scherrer equation (Azároff 1968), resulting in a diameter of 5 ±1 nm.

The X-ray diffraction and the TEM/SAED results are absolutely coincident from the structural and the particle size point of view. Therefore, the analysed iron sucrose consists of nanometric particles of about 5 nm diameter, most likely composed of two-line ferrihydrite, dispersed in a sucrose matrix.

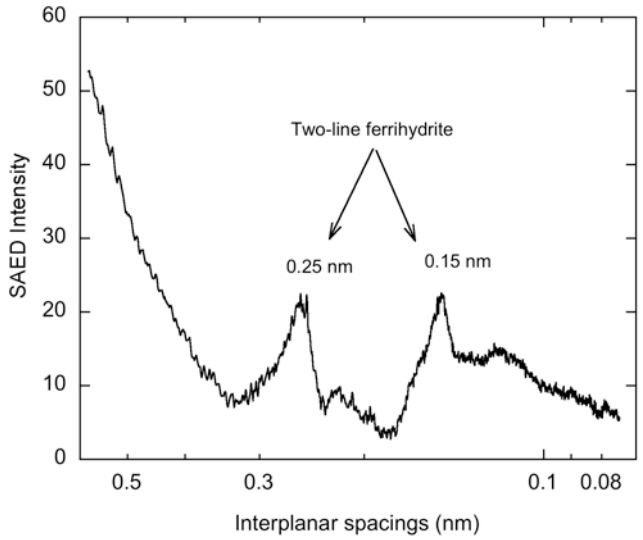

Fig. 41. Radial distribution of diffraction rings intensity corresponding to the SAED in Fig. 40. The shown spectrum results after subtraction of a Gaussian background.

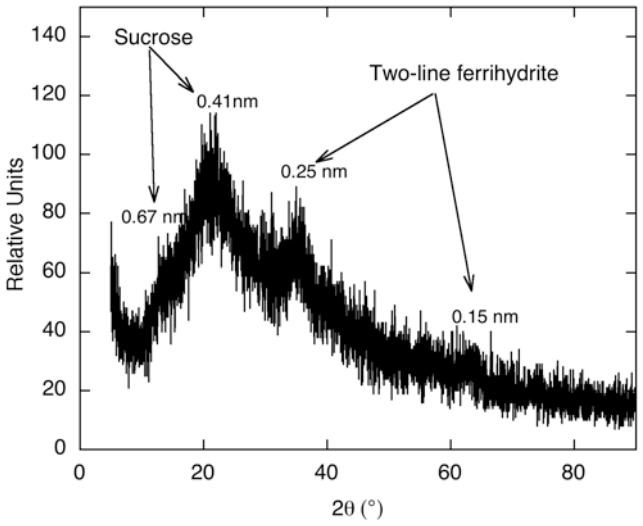

Fig. 42. X-ray diffractogram of the freeze-dried iron sucrose powder. The interplanar distances are shown in nm.

Coming back again to the results of the AC susceptibility measurements of iron sucrose, at temperatures above 50 K, that is, where $\chi'' \approx 0$; $\chi'(T)$ can be expressed as $\chi' = \chi_{SP} + \chi_{AF} + \chi_{dia}$. In order to obtain the Curie constant, χ' has been represented vs. 1/T. In this representation, the data ideally must form a straight line with slope C and intercept with the χ-axis equal to $\chi_{AF} + \chi_{dia}$. In our case we have obtained a rather linear result resulting in a ($\chi_{AF}+\chi_{dia}$) intercept value between -2.3 x10^{-7}m^3/kg and -6.3 x 10^{-7} m^3/kg. The negative sign of these values indicates that the diamagnetic susceptibility is indeed greater than the antiferromagnetic one. The μ_{eff} has been calculated form the Curie constant by using Eq. 6 to be 16.5 ± 0.7 μ_B per iron ion, where the error value responds to the slight difference in the high- and low-temperature slope determination. It has been observed experimentally that for antiferromagnetic oxide nanoparticles it is almost a general rule that the mass magnetic susceptibility increases for decreasing particle size (Cohen et al. 1962). This result indicates that the particle magnetic moment is not proportional to the particle volume and, in this respect, several models to explain the net magnetic moment per particle as result of spin uncompensation have been proposed (Neel 1962). The experimentally determined μ_{eff} value, definitely higher than the single ion magnetic moment which is typically near 5 μ_B for iron ions, cannot be explained with the volume uncompensation model which predicts a number of uncompensated spins in the particle proportional to square root of its number of spins, and less by other models which restrict the spin uncompensation only to the particle surface. If any of the models is considered, the maximum expected effective moment per ion never results higher than the one corresponding to the paramagnetic ion (López et al. 1997). We should,

however, indicate that effective moments also of the order of 15 Bohr magnetons have previously been obtained for assemblies of two-line ferrihydrite nanoparticles in zeolitic matrices (López et al. 1997).

To assess the importance of dipole–dipole interparticle interactions, the temperature parameter T_{dip} (Eq. 15) has been estimated (López et al. 1997). The iron mass per unit volume in the sample has been calculated to be ρ = 71.9 kgFe/m^3. T_{dip} for freeze-dried iron sucrose results in 0.13 K. This low value justifies the use of non-interaction models in the interpretation of the susceptibility results in the temperature ranges that we have studied.

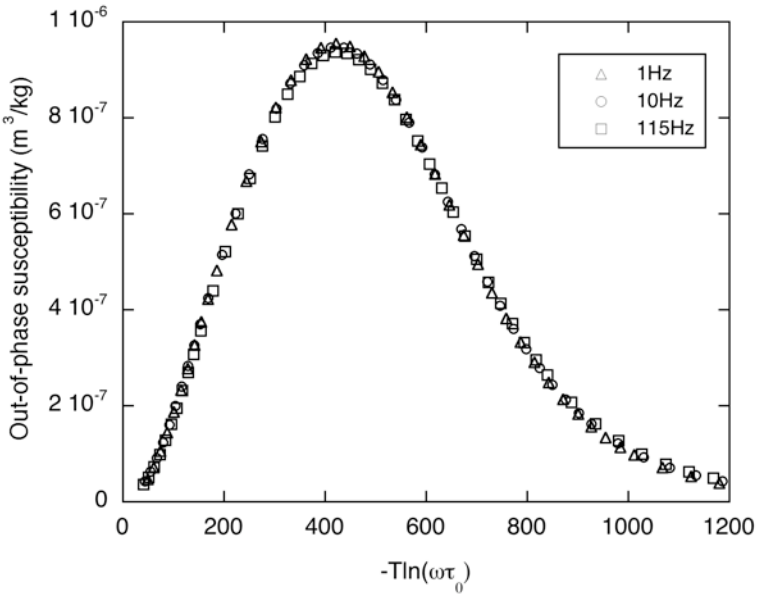

Fig. 43. Scaling plot of the out-of-phase susceptibility of freeze-dried iron sucrose measured at three different frequencies. The best fit is obtained with a preexponential factor of $\tau_0 = 10^{-14}$

The calculation of τ_0 has been performed as an alternative way of estimating the importance of the interparticle interactions, and especially in what may affect the magnetic dynamics of the system. In Fig. 43, the χ" data measured at 1, 10 and 115 Hz are represented vs. -Tln($\omega\tau_0$) having an optimum superposition at $\tau_0 = 10^{-14}$ s. This value is close to the expected one in a non-interacting model (10^{-9} –10^{-12} s).

The field-dependent magnetisation results on the same sample are shown in Fig. 44. The temperatures of the experiments have been selected in the range where the out-of-phase AC susceptibility is negligible. The data shown were taken under decreasing field, confirming the expected zero remanent magnetisation.

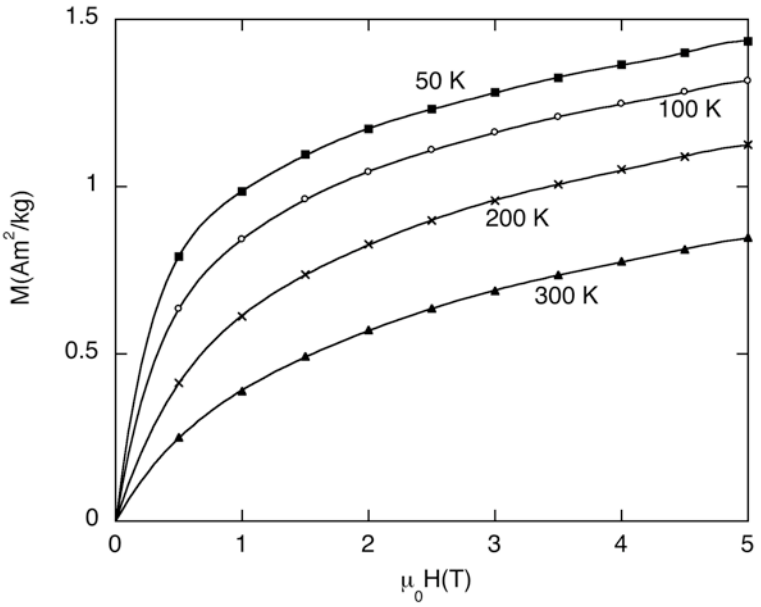

Fig. 44. Field dependence of the magnetisation of freeze-dried iron sucrose at the temperatures indicated. Zero remanence has been obtained in this temperature range. The continuous lines are just guides for the eye.

In this case, the magnetisation will follow Eq. 17. As it usually occurs for assemblies of antiferromagnetic particles, the customary representation M vs. H/T does not result in a good superposition of the data unless the (χ_{AF} + χ_{dia}) term is considered, as it also happened for the FMOA sample. However, it is known that χ_{AF} is typically temperature dependent (Makhlouf *et al.*, 1997), complicating the analysis. The best superposition in our case has been obtained by considering (χ_{AF} + χ_{dia}) values of the order of the susceptibility intercepts given above.

The mean particle size determined by TEM measurements has been used to estimate the anisotropy constant by use of Eq.16. *K* has been estimated to be around $1x10^5$ J/m^3, which is in agreement with previously reported values for this material (Cornell et al. 1996).

2.3.5. Ferric protein

The elemental analysis of this drug has provided a value for the iron concentration of 12.85 mg Fe/g sample. The content of other magnetogenic elements was negligible in comparison with the amount of iron ([Co] = 0.001 mg/g; [Cu] = 0.010 mg/g; [Mn] = 0.042 mg/g; [Ni] = 0.009 mg/g).

The in-phase susceptibility of this drug shows a maximum around 5 K for the measurement at 10 Hz (Fig. 45). The out-of-phase susceptibility also shows a maximum at low temperature, at around 2.7 K, although the complete profile is not observable as it do not enters into the accessible experimental temperature window (Fig. 45). However, this behaviour evidences a magnetic relaxation phenomenon that indicates the presence of magnetic particles.

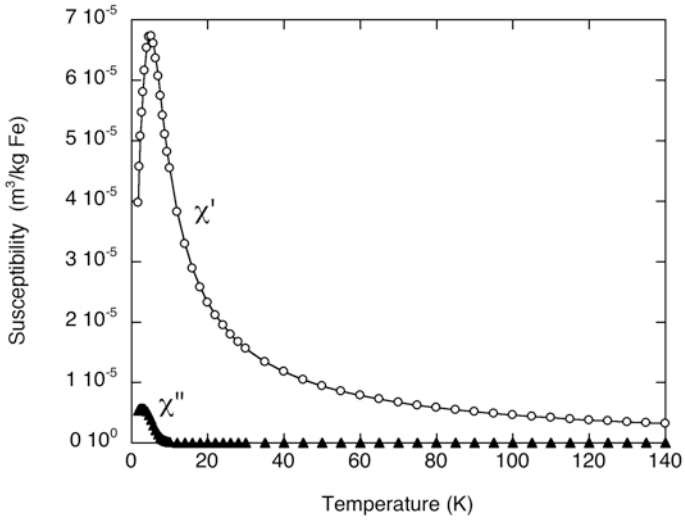

Fig. 45. Temperature dependence of the AC mass susceptibility of Ferric protein at 10Hz. Note the absence of relaxation above approximately 12 K.

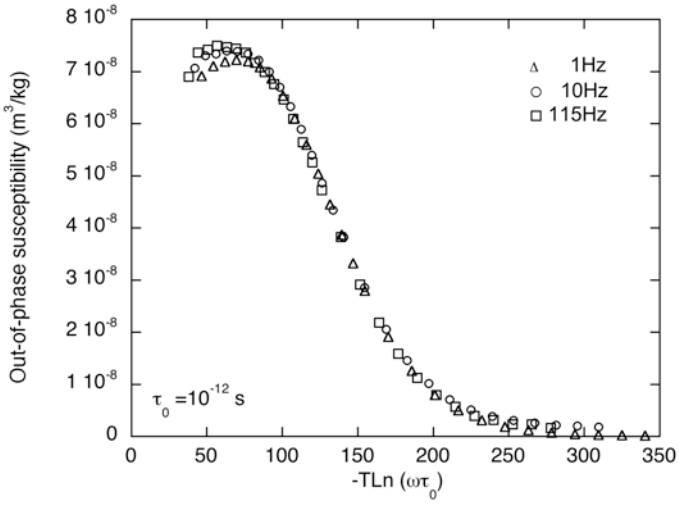

Fig. 46. Scaling plot of the out-of-phase mass susceptibility of Ferric protein measured at three different frequencies. The best superposition is obtained with a pre-exponential factor $\tau_0 = 10^{-12}$ s .

The magnetic dynamics of this compound have been studied by the measurements at different frequencies (1, 10, and 115 Hz). In order to study the importance of the interparticle interactions, the scaling plot of the $\chi''(T)$ data measured at different frequencies as a function of $-T\log(\omega\tau_0)$ has been plotted and is is shown in Fig. 46. The best superposition has been obtained using a τ_0 value of 10^{-12} s, which is in the range of a non-interacting model (10^{-9} - 10^{-12} s).

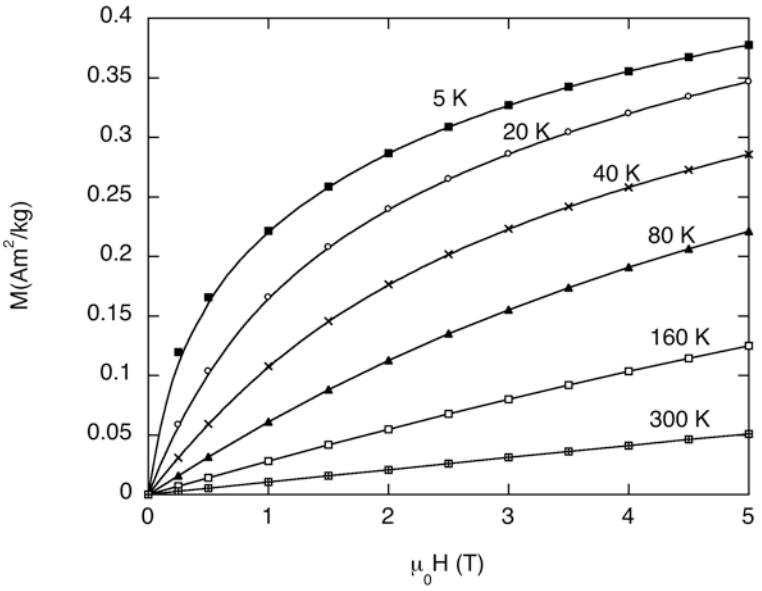

Fig. 47. Field dependence of the magnetisation of ferric protein at the indicated temperatures. Solid lines are just a guide for the eye.

Although no TEM observations have been performed on this drug, if a composition of the particles similar to most of the studied drugs is assumed (spherical ferrihydrite nanoparticles), the diameter of the particles of the ferric protein can be calculated by using a K value similar to the obtained for the FMOA, iron sucrose and iron sorbitol. Using the K

values obtained for those compounds, the diameter of the ferric protein particles results between 2.8 and 4.0 nm.

The field dependent magnetisation results are plotted in Fig. 47. Although, only the values obtained under increasing field are shown in the graph, weak remanence can only be observed in the measurement at 5 K, in agreement with the susceptibility results.

2.3.6. Iron sorbitol and Iron dextran

Both compounds have previously been characterised and the results can be consulted in published papers (Lázaro et al. 2002; Lázaro et al. 2003). However, as some of the magnetic results and the TEM characterisation will be used in the comparison with the previously described drugs, a brief summary of the most relevant properties of these drugs is provided ahead.

Iron sorbitol contains spherical nanoparticles with an average diameter of 3 nm whose composition is close to two-line ferrihydrite while iron dextran contains nanometric spindle shape nanoparticles whose electron diffraction pattern corresponds to that of the iron oxyhydroxide akaganéite (β-FeOOH) of an approximate size of 4 x 20 nm.

Compound	Oxyhydroxide	Size (nm)	$T_{(\chi'' max)}$ (K)	m_{eff} (μ_B)	τ_0 (s)	K ($10^4 J/m^3$)	T_{dip} (K)
Iron sorbitol	Ferrihydrite	< 3	<1.8	2.85	10^{-11}	3.6	
Iron dextran	Akaganéite	4×20	≈20	1.5	10^{-20}	-	0.004

Table 5. Summary of the magnetic parameters of iron sucrose and iron sorbitol previously characterised (Lázaro et al. 2002; Lázaro et al. 2003)

The AC susceptibility measurements of both compounds indicate superparamagnetic behaviour with magnetic blocking starting at low temperatures (see Table 5 for details).

The τ_0 value ($10^{-11\pm1}$ s) obtained for iron sorbitol indicates that there are no interparticle interactions. In contrast, a τ_0 value (10^{-20} s) outside the range of a non-interacting regime was obtained for iron dextran. However, the calculation of T_{dip} for iron dextran (0.004 K) indicated that the dipolar interaction were actually very weak and most likely not the reason for the anomalous magnetic dynamics of the system (see (Lázaro et al. 2003) for a deeper discussion on it).

The rest of the magnetic parameters of interest for the comparison with the results of the rest of the drugs, as the effective moment, K and the location in temperature of the χ'' maxima have been summarised in Table 5.

2.4. Comparative discussion on the particulated compounds

The AC susceptibility temperature dependence of the iron supplements that contain iron oxyhydroxide nanoparticles has been plotted together for their comparison (Fig. 48 and Fig. 49). All of these compounds (iron sorbitol, iron dextran, ferrimannitol-ovalbumin, ferric protein and iron sucrose) present a maximum in $\chi'(T)$ accompanied by a $\chi''(T)$ maximum at slightly lower temperatures which evidences a relaxation phenomenon of magnetic blocking of superparamagnetic particles (Fig. 48 and Fig. 49). In the figures, the maxima corresponding to the iron dextran sample is hardly visible due to the used scale.

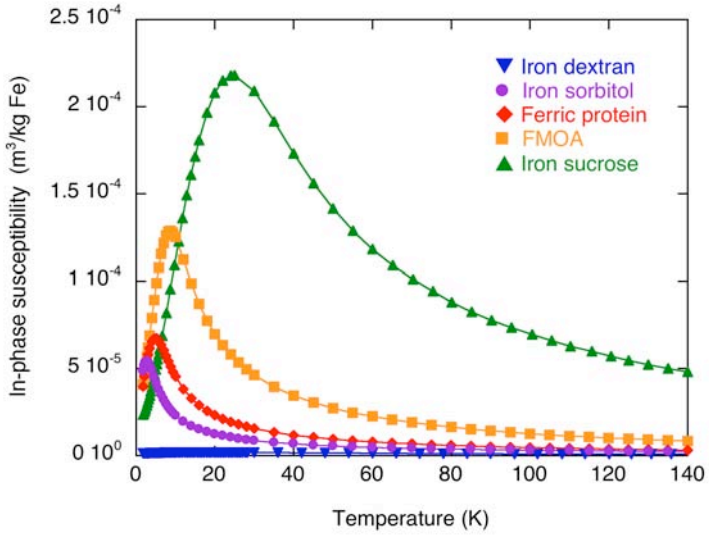

Fig. 48. Temperature dependence of the in-phase AC mass susceptibility per iron amount of iron sorbitol, ferric protein, FMOA, iron sucrose and iron dextran at 10 Hz.

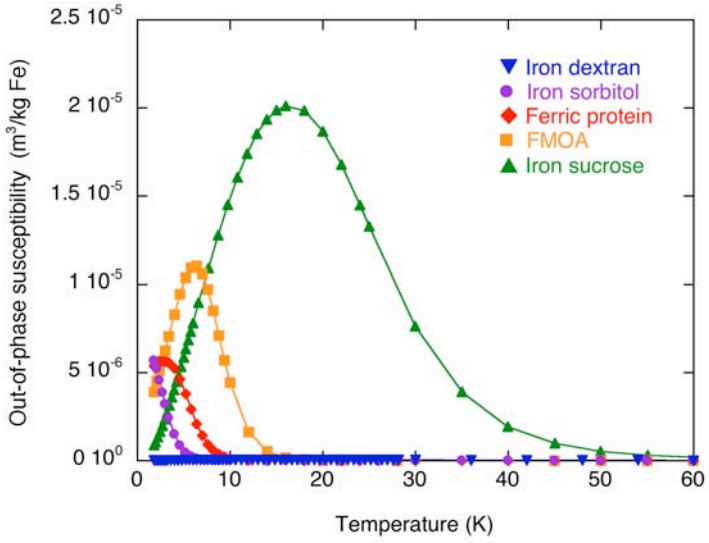

Fig. 49. Temperature dependence of the out-of-phase AC mass susceptibility per iron amount of iron sorbitol, ferric protein, FMOA, iron sucrose and iron dextran at 10 Hz.

Compound	Oxyhydroxide	Shape	Size (nm)	$T_{\chi'' max}$ (K)	μ_{eff} (μ_B)	K ($10^4 J/m^3$)
Iron sucrose	Ferrihydrite	Spherical	5	16	16.5	7.3
FMOA	Ferrihydrite	Spherical	4.2	6.4	6.1	10
Ferric protein	-	-	*2.8-4.0*	2.7	4.09	*3.6-10*
Iron sorbitol	Ferrihydrite	Spherical	< 3	<1.8	2.85	3.6
Iron dextran	Akaganéite	Spindle	4×20	≈20	1.5	-

Table 6. Effective moment per iron ion, composition and size of the particles and effective anisotropy constant, K of the studied iron-containing drugs. *The values of the diameter of the ferric protein have been obtained assuming the K of the compounds that contain spherical ferrihydrite nanoparticles.

It is of clear interest to compare the $\chi''(T)$ profiles of these compounds as it represents the activation energy distribution and can be interpreted as a measure of the particle size distribution in the case of assemblies of non-interacting particles.

The importance of the interparticle interactions was studied through the calculation of τ_0. Preexponential values of 10^{-11}, 10^{-15}, 10^{-14} and 10^{-20} s were obtained for iron sorbitol, FMOA, iron sucrose and iron dextran respectively. Although, especially the last τ_0 value is not within the typical range expected for non-interacting particles, the low values of the temperature parameter T_{dip} indicate non dipole-dipole interparticle interactions in the studied temperature range (see previous sections for further details).

However, the $\chi''(T)$ results can only be compared to obtain information about the particle size distribution if the compounds present the same effective anisotropy constant, K, which may occur in particles of the same iron oxyhydroxide. The K values (Table 6), obtained from Eq. 16, of the drugs containing spherical two-line ferrihydrite nanoparticles are similar to the value previously reported for ferrihydrite of 10^5 J/m^3

(Cornell et al. 1996), also supporting the interpretation of the χ"*(T)* data as a measure of the particle size distribution.

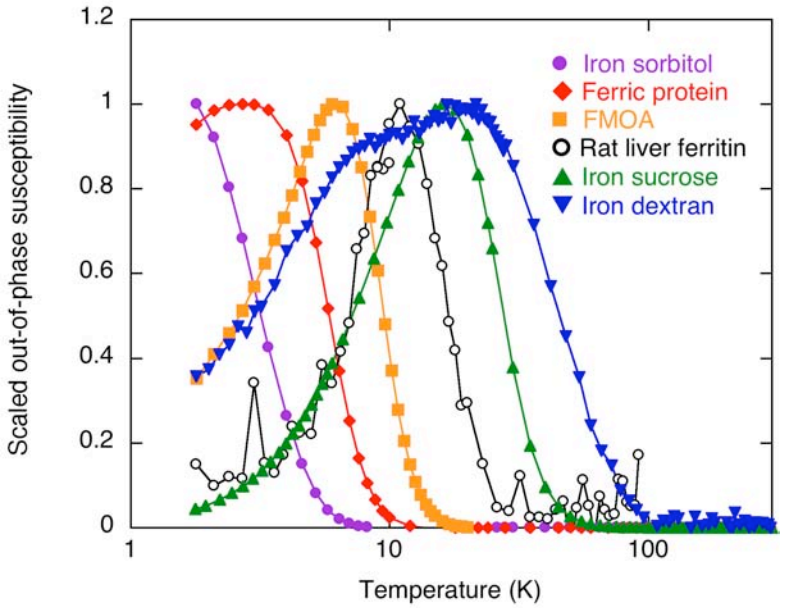

Fig. 50. Comparison of the scaled temperature dependence of the out-of-phase susceptibility of iron sorbitol, ferric protein, FMOA, rat liver ferritin, iron sucrose and iron dextran.

The order of the mean particle size (Table 6), obtained by transmission electron microscopy (TEM) measurements of iron sorbitol, FMOA and iron sucrose coincides with the order of the location in temperature of their χ" *(T)* maximum (Fig. 50), suggesting that the χ" *(T)* data may be a not too bad estimate of its actual particle size distribution. The influence of the particle size distributions in the temperatures of the χ"*(T)* maximum in similar systems of six-line ferrihydrite nanoparticles has been observed previously (Guyodo et al. 2006).

As iron dextran contains particles of a different iron oxyhydroxide it has not been included in the discussion above. However,

as its particle size, observed by TEM (Table 6), is larger than the rest of the samples and its χ'' maximum is wider and located at higher temperatures (Fig. 50), it may indicate a K value similar to the ferrihydrite samples.

Another interesting parameter to compare these drugs is the μ_{eff} value, listed in Table 6. In assemblies of antiferromagnetic particles, in the volume or surface spin uncompensation models, μ_{eff} either increases or stays constant converging to the single ion moment μ for decreasing particle size (López et al. 1997). The μ_{eff} values of the samples containing two-line ferrihydrite nanoparticles increase with increasing size, meaning that these compounds do not fulfil the required premises of these models. The sequence of increasing μ_{eff} values of all the compounds agrees with the increasing height of the $\chi''(T)$ maxima observed in Fig. 49, which is not influenced by diamagnetic or paramagnetic contributions, and only depends on the size of the fluctuating moments.

In Fig. 50 it has also been plotted the $\chi''(T)$ of rat liver ferritin (whose magnetic behaviour is deeply detailed in the next chapter). The different location in temperature of the out-of-phase susceptibility of ferritin in comparison with the drugs allows its distinction when studying the degradation of these drugs in biological tissues.

2.5. Conclusions

In this chapter, the magnetic and structural characterisation of eight of the most commonly used iron supplements for the treatment of iron deficiency anaemia has been described.

A distinctive $\chi'(T)$ and $\chi''(T)$ profiles of each compound has been obtained, meaning that this kind of characterisation may act as a fingerprint of these drugs. These differences are of special interest for monitoring this kind of drugs in biological tissues in pharmacological studies, as they would be distinguished from the biogenic iron.

Furthermore, the magnetic characterisation of these iron supplements has allowed the detection of the presence of iron-containing nanoparticles in some of them, in which a TEM characterisation has provided information about their crystalline structure and particle size. This information is of great relevance as the absorption kinetics and bioavailability of the drugs depend on their particle size and crystalline structure.

The comparison of the magnetic behaviour and the TEM results of the drugs composed of iron oxyhydroxide particles has revealed a good correlation between both techniques, in a way that it has been evidenced the high sensitivity of the magnetic measurements to small differences in particle size that can be sharply discerned from the AC susceptibility measurements. As a result, these compounds can be used as new examples in the study of the dependence of the magnetic properties of nanodispersed materials on particle size and crystallinity.

Finally, as most of the characterised drugs contain two-line ferrihydrite nanoparticles, whose magnetic behaviour has been much less explored than other iron oxides/oxyhydroxides, this study gives a new example of the influence of the particle size in the magnetic properties of two-line ferrihydrite nanoparticles.

3. Animal models of iron overload I: Iron dextran-injected rats

3.1. Introduction and main aims

As stated in the previous chapter, due to the important role of iron for life, iron deficiency results in a pathological situation. Nevertheless, not only the iron deficiency is a cause of disease, the iron excess is also synonym of pathology. In fact, iron overload diseases affect a great percentage of the world population (Steinberg et al. 2001; Lucotte et al. 2003; Adams et al. 2005).

Iron overload disorders may have different origins: genetic or acquired. Genetic iron overload includes HFE haemochromatosis, hereditary aceruloplasminemia, etc. while acquired iron overload includes

diseases as thalassemia, chronic liver disease, etc (Deugnier et al. 2008). Anyhow, what all of these diseases have in common is that the amount of iron present in the tissues is increased with respect to the normal values. This "extra iron" is usually found in the form of iron oxyhydroxides nanoparticles. As the iron biomineralisation may be related with its toxicity, an intense effort has been done in its characterisation, using also techniques typical of material science as Mössbauer spectroscopy (St Pierre et al. 1987; Andrews et al. 1988; St Pierre et al. 1992; Ward et al. 1994; Webb et al. 1996; St Pierre et al. 1998; St Pierre et al. 2000; Hackett et al. 2007), Transmission Electron Microscopy (Richter 1959; Richter 1984; Iancu 1992; Iancu et al. 1997), infrared spectroscopy (Chua-anusorn et al. 2000) and AC susceptibility measurements (Allen et al. 2000).

The inherent difficulties of a systematic characterisation of human tissues favour the use of animal models of iron overload. Although different animal models can be used for this purpose (Iancu 1993), the simplest ones are those in which the iron accumulation is generated by an iron-loaded diet or an iron injection (Richter 1959; Chua-anusorn et al. 1999).

The work presented in this chapter is primarily devoted to the dynamic magnetic characterisation of freeze-dried tissues in a rat model of iron overload, constructed by a single administration of iron dextran. Apart from analysing the biomineralisation of the iron deposits generated in the tissues, this study, that includes Transmission Electron Microscopy observations, aims also at a better understanding of the iron metabolism, pharmacokinetics and biodistribution of the injected drug.

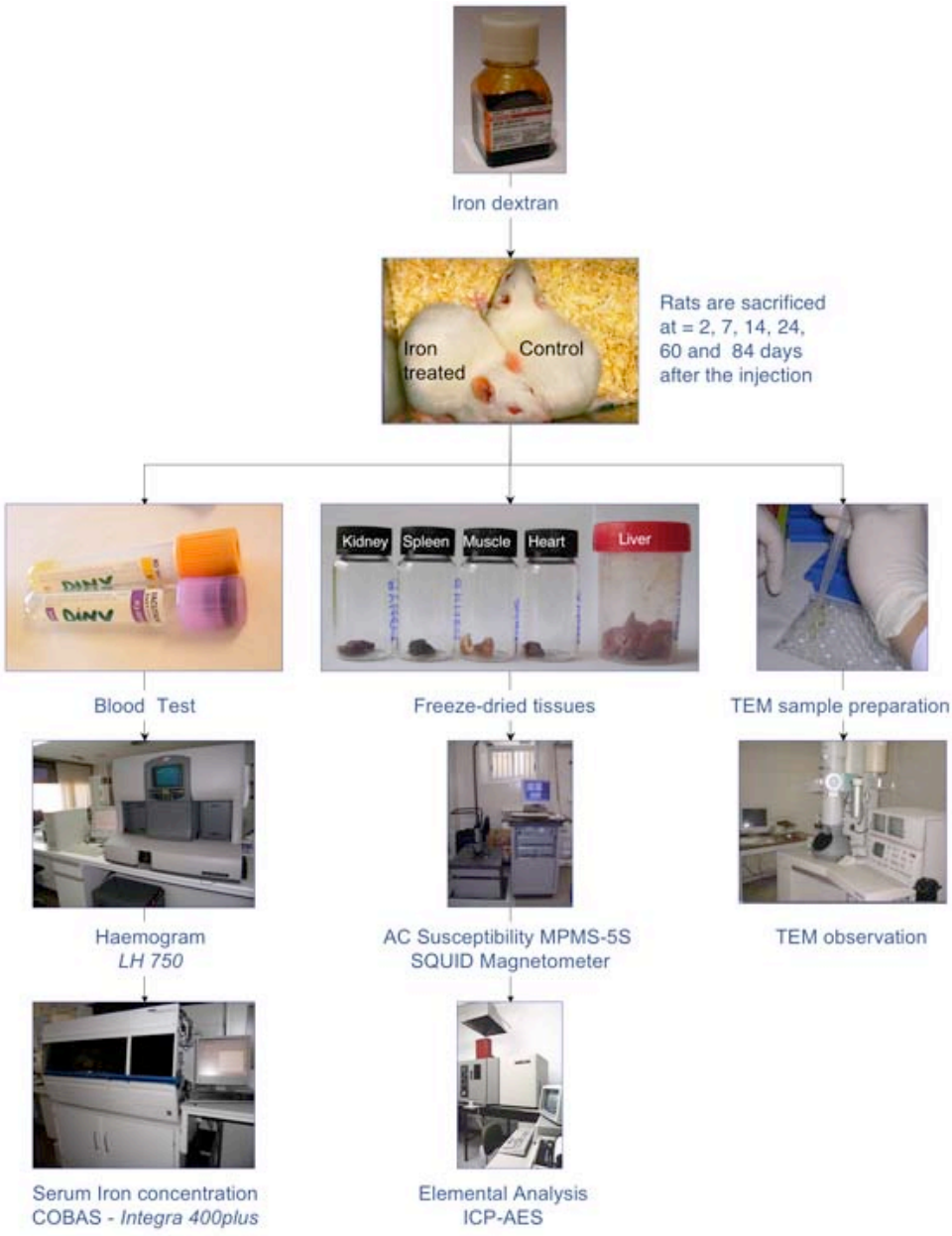

Fig. 51. Work protocol scheme

3.2. Materials and methods

3.2.1. General considerations

In physiological conditions, iron is in minute amounts in the tissues and moreover, the species in which it is taking part are weakly magnetic. For these reasons, special care has to be taken to avoid sample contamination during all the acquisition and treatments of the tissues, specially refraining from using metallic instruments as blades, tweezers, scissors and using instead plastic or ceramic ones.

Moreover as one of the main objectives of this work is to study the variations on the iron speciation, it has been tried to minimize the treatments of the sample until the magnetic characterisation, to avoid undesirable speciation changes. For this reason, whole tissues were analysed instead of isolating the different iron-containing species.

In Fig. 51, a schematic representation of the different steps carried out in the work presented in this chapter is provided.

3.2.2. Animal model

A total of 50 male Wistar rats (WI-SIMA075Z, purchased from Charles River Laboratories, Spain), all of them six weeks old at the moment of the drug administration, were used in the experiment.

Animals were acclimatised for 7 days before the administration of the drug and kept one or two per cage, placed in racks at 12 hours of light and 12 hours of darkness, and controlled temperature and ventilation. The experiments were performed with the approval of the Ethical Committee for Animal Experiments of the Universidad de Zaragoza. All animals were allowed *ad libitum* access to both food and water.

Following the iron overload animal model proposed by Carthew (Carthew et al. 1991), some of the animals (n = 36) were treated with a single dose (1 mg Fe per gram of body weight) of iron dextran (Sigma) by subcutaneous injection in the rat back. These animals were sacrificed at times t = 2, 7, 14, 24, 60 and 84 days after the drug administration. The rest of the animals (n = 14) were used as controls and sacrificed at t = 0, 24, 60 and 84 days.

All animals were weighted immediately prior to sacrifice. Following the protocol approved by the Ethical Committee, animals were sedated under a single dose of sodium pentobarbital anaesthesia (25 mg/ml/kg). Once the animals were insensible, about 4 ml of blood were taken out of each animal by heart puncture. Then, the spleen, kidneys, heart, liver and muscle from the lumbar back, located in the vicinity of the iron dextran injection, of each animal were removed, using ceramic blades and plastic tweezers, rinsed with isotonic saline solution (0.9% NaCl) to eliminate excess blood and stored at -20 ºC.

3.2.3. Blood test

From the extracted blood of each animal, 2 ml were dispensed into BD Vacutainer® K3E tubes, that contain EDTA (ethylenediaminetetraacetic acid), and the remainder into BD Vacutainer® SST tubes (silicone-coated serum separation tubes). The haematological tests were assessed from anticoagulated blood samples (EDTA) immediately after blood extraction using standardised COULTER® LH 750 Haematology Analyzer with VCS (volume, conductivity, scatter) technology. The quantitative determination of serum iron concentration,

on centrifuged serum samples, was based on a colorimetric technique using the Guanidine/Ferrocine® method (COBAS-Integra 400 Plus, Roche® Diagnostic GmbH). The quantitative determination of serum ferritin concentration was turbidimetrically performed in the same equipment.

3.2.4. TEM observations

Portions of the livers of selected animals were prepared for TEM observations immediately after the liver removal. Fragments of the liver were fixed for 2 h at room temperature and overnight at 4 ºC in a solution of 2% glutaraldehyde in 0.4 M Hepes buffer (pH 7.2). Some of the fragments of the fixed samples were postfixed with 1% OsO_4 during 1h at 4 ºC while other fragments stayed in a Hepes buffer solution for the same time. All samples were later dehydrated in graded series of acetone, embedded in Epon resin at room temperature and polymerised at 60 ºC during 48 h. Ultra-thin sections of osmicated and non-osmicated blocks of about 40-60 nm thick were directly collected on Formvar-covered gold grids. The sections were observed unstained or lightly stained with 2% uranyl acetate in water for 30-60 s. In addition, some observations were performed on conventional uranyl acetate and lead citrate stained sections for rapid identification of the structures.

The TEM characterisation was carried out in a Jeol 1200 EXII microscope operated at 100 kV and in a Philips CM 200 FEG equipped with an energy dispersive X-ray spectrometer (EDS). Occasionally, selected area electron diffraction (SAED) was performed in the same

equipments. The samples analysed by TEM corresponded to the same animal livers that were magnetically analysed.

3.2.5. Freeze-drying

The tissue samples were stored at -20 ºC until being freeze-dried. To facilitate the complete freeze-drying of the livers, which are the biggest of all the dissected tissues, they were cut into small pieces with ceramic blades, making easier the sublimation of water.

All the tissues were freeze-dried during 48 h in a Telstar-Cryodos equipment. The complete freeze drying was verified by making sure that the samples have lost around 70% of its original weight and also by observation of the tissues texture, using the plastic tweezers to check the dryness. The freeze-dried tissues were then ground to powder in a mortar to get a homogeneous sample to be used in the elemental analysis and the magnetic measurements. The freeze-dried samples were stored at room temperature.

3.2.6. Elemental analysis

The freeze-dried samples, a part of which were magnetically characterised, were submitted to elemental analysis by inductively coupled plasma atomic emission spectrometry (ICP-AES).

The elemental analysis was performed after acid digestion (method described in Chapter 1), with especial focus on the determination of Fe. The presence of other magnetogenic elements as Co, Ni, Mn and Cu was also studied as its presence may affect the magnetic results.

3.2.7. Magnetic measurements

The magnetic characterisation has been carried out in a Quantum Design MPMS-5S SQUID magnetometer with an AC susceptibility option. The measurements have always been performed with an AC amplitude of 0.45 mT, in the temperature range 1.8-300 K and at a frequency of 10 Hz. Selected samples were also measured at different frequencies to investigate the magnetisation dynamics. The measurements on the freeze-dried tissues were performed by directly placing the powders into gelatine capsules.

In order to assure the absence of any magnetic contribution coming from adsorbed oxygen in the samples, repeated runs above and below its boiling temperature were used in the measurements of each sample (Kanoh et al. 1996).

As the duration of the magnetic experiment is around 10 hours per sample, in a first attempt, only one liver or muscle sample for each *t* value was magnetically characterised, although additional samples of these tissues were occasionally measured to have an estimate of reproducibility. Heart, kidneys and spleen tissues from selected animals have also been magnetically characterised.

3.2.8. Reference materials

In previous studies on iron dextran administration to mice (Richter 1959) and to rats (Andrews et al. 1988), together with ferritin and other iron deposits, rests of the drug were still detected in the liver

and spleen tissues at least until 3 weeks after the injection. For this reason, it is necessary to know the individual structural and magnetic properties of iron dextran and ferritin prior to the interpretation of the results in tissues.

A commercial glycerol suspension of rat liver ferritin (1.55 mg/ml) (Sigma) has been used in this study as a reference material. For the magnetic measurements, the liquid suspension of ferritin was introduced into ESR (Electron Spin Resonance)-grade quartz tubes.

The magnetic and structural properties the administered drug, iron dextran, data from (Lázaro et al. 2003), will also be summarized.

3.3. Characterisation of rat liver ferritin and iron dextran

The magnetostructural properties of the injected drug, iron dextran, and the iron storage protein, ferritin, are described in this section as these data constitute an indispensable element for the monitorisation of these two species in the tissues.

As it has been detailed in chapter 2, the injected drug, iron dextran, contains spindle shape particles of about 4×20 nm in size, whose structure corresponds to the iron oxyhydroxide akaganéite (β-FeOOH), surrounded by dextran. This drug exhibit superparamagnetism above approximately 100 K, with $\mu_{eff} = 1.5 \pm 0.1\ \mu_B$. The blocking of the particle magnetic moments gives rise to a $\chi'(T)$ maximum near 20 K (Fig. 52) accompanied by a $\chi''(T)$ flattened maximum at slightly lower temperatures (for more details see (Lázaro et al. 2003)).

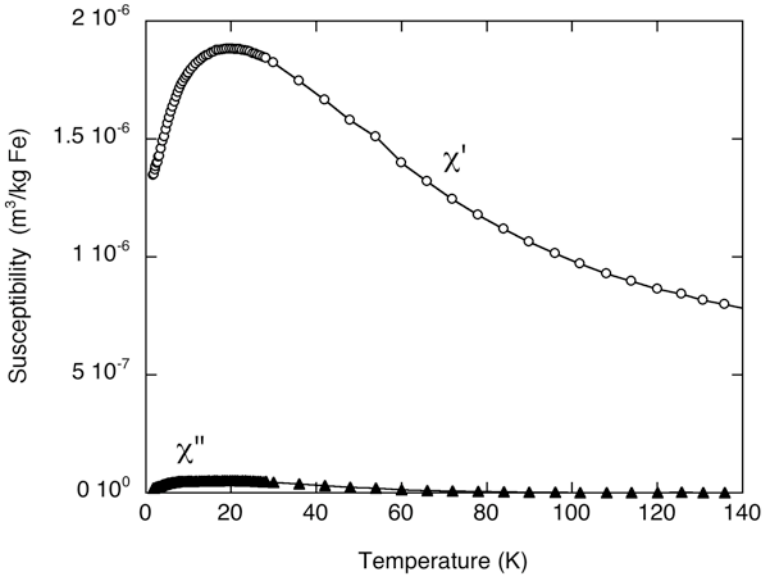

Fig. 52. Temperature dependence of the AC mass susceptibility of freeze-dried iron dextran at 10Hz. See the clean absence of relaxation above approximately 100 K.

The ferritin protein contains nanocrystals in its core whose size is limited by the protein shell to maximum diameter of 8 nm. In physiological conditions, the crystalline structure of the particles is usually described as the iron oxyhydroxide ferrihydrite (see chapter 1).

The temperature dependence of the AC susceptibility per mass of iron of rat liver ferritin is shown in Fig. 53. A maximum in $\chi'(T)$ can be observed at around 16 K accompanied by a non-zero $\chi''(T)$ at slightly lower temperatures which evidences a magnetic relaxation phenomenon. Also there is a small χ' tail at the lowest temperatures. The negative values of χ' in nearly the whole temperature range are due to a large diamagnetic contribution that, in this case, must correspond to the sample holder and the glycerol solution in which the commercial rat liver ferritin

is suspended. The out-of-phase susceptibility is negligible, within the accuracy of the experiments, above 35 K.

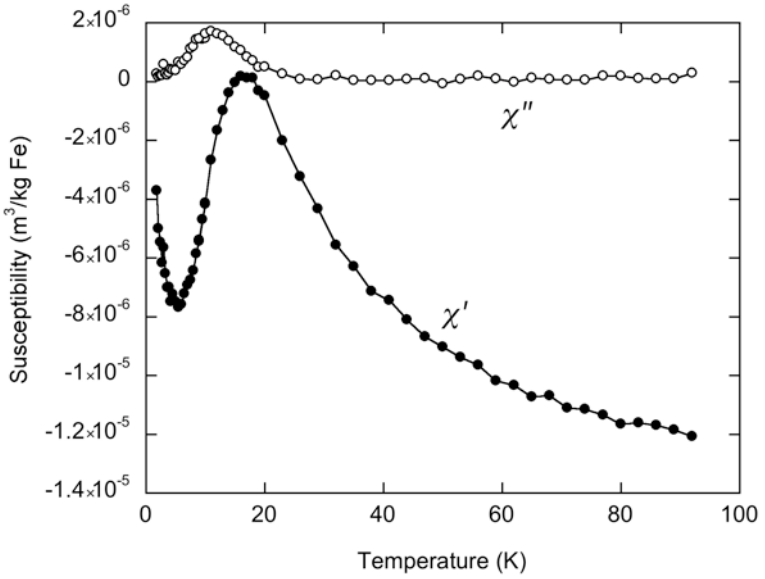

Fig. 53. Temperature dependence of the mass AC susceptibility per iron ion for rat liver ferritin measured at 10 Hz.

The relaxation anomaly, resulting from blocking of the mineral cores magnetic moment, takes place, for rat liver ferritin, in a very similar temperature range as for other ferritins (horse spleen (Luis et al. 1999), human spleen (Allen et al. 2000)), meaning that there are no big differences between the iron biomineralisation inside this protein in mammals. The only difference observed between this result and the previously reported ones on ferritins from different animals is the low temperature χ' tail that can be observed in Fig. 53, typical of paramagnetism. This tail may be explained by the presence of isolated iron atoms in the sample different from those of the ferritin cores.

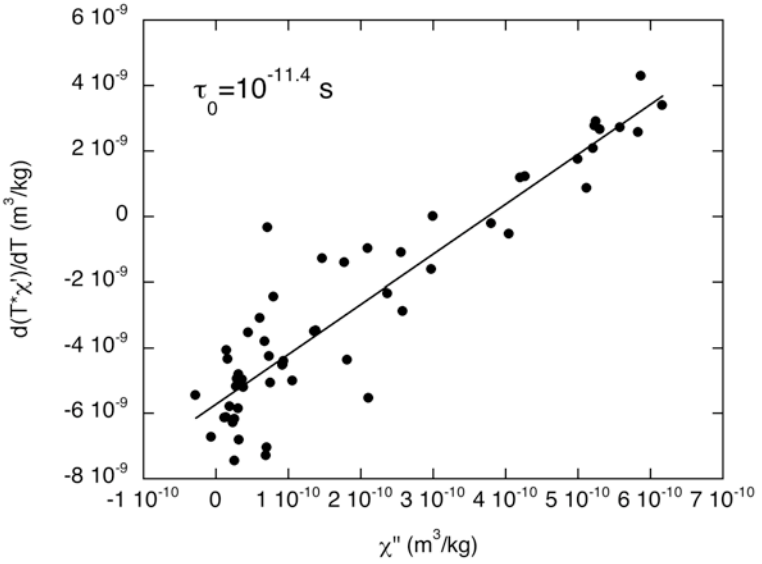

Fig. 54. Determination of τ_0 of rat liver ferritin by using the method described in Chapter 1.

The importance of the interparticle interactions has been studied by the determination of τ_0. From the scaling measurements at different frequencies a value of the preexponential factor of $10^{-10\pm1}$ s, has been obtained indicating that the particle magnetic moments fluctuate independently. However as the measurements at different frequencies were a bit noisy, the alternative method for the calculation of τ_0 has been performed and is shown in Fig. 54, the τ_0 value obtained by this method also agrees with a non-interaction regime. Additionally, the parameter T_{dip} has been calculated resulting in $9 \cdot 10^{-6}$ K, which fully confirms the negligible interparticle interactions assumption, at least of dipolar origin.

The effective moment per iron ion has been calculated to be μ_{eff} = 3.4 ± 0.1 μ_B, similar to previously obtained values (Michaelis et al. 1943).

The iron content of rat liver ferritin was also determined resulting in 0.36 milligrams of iron per gram of liquid suspension.

3.4. Blood test results

The data resulting from the blood tests of the animals treated with iron dextran as well as the control rats are shown in Table 7 and Fig. 55.

	t (days)	n	Serum iron (μg/dl)	Serum ferritin (ng/ml)	Haemoglobin (g/dl)	Haematocrit (%)
Iron-loaded	2	5	7766 (304)	27 (7)	12.3 (0.6)	33.4 (1.2)
	7	6	251 (115)	208 (55)	11.7 (0.4)	33.3 (1.1)
	14	5	200 (49)	165 (15)	12.6 (0.6)	35.5 (1.7)
	24	7	274 (80)	267 (116)	13.3 (0.4)	38.1 (1.9)
	60	6	342 (105)	218 (194)	14.8 (0.9)	35.6 (3.6)
	90	7	308 (72)	203 (130)	15.0 (0.6)	40.2 (1.3)
Control	0	3	241 (44)	13 (3)	11.4 (0.6)	32.7 (1.2)
	24	4	169 (57)	15 (2)	13.1 (0.2)	37.8 (3.0)
	60	4	239 (46)	19 (4)	14.2 (0.4)	40.2 (1.7)
	84	3	177 (10)	43 (13)	14.1 (0.5)	38.5 (1.5)

Table 7. Haematological data of all the individuals included in this study. Values in brackets correspond to standard deviations; *t* indicates the number of days after the iron administration and n the number of individuals.

The serum iron exhibits a huge increase (up to 7766 μg/dl) just after the iron dextran administration (t = 2 days). This value indicates the existence of a quick input of iron in the bloodstream during the first two days after the iron dextran administration followed by a subsequent sudden decrease, returning to values only slightly higher than the normal ones after 7 days. At t = 60 and 84 days the serum iron levels in the

treated rats are higher than in the control rats suggesting that the iron absorption still continues even at 84 days after administration.

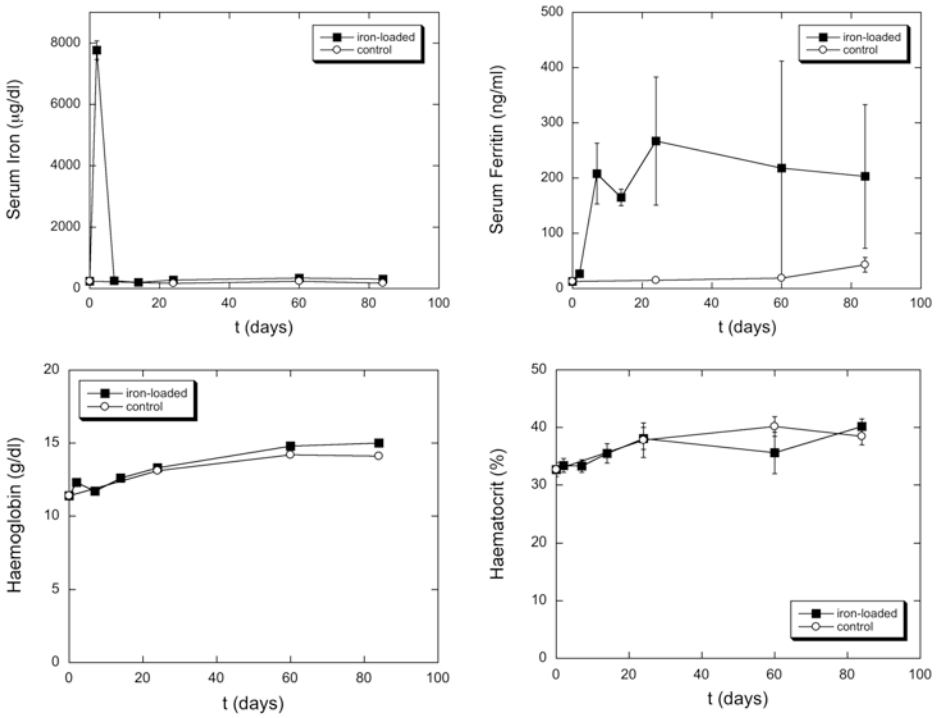

Fig. 55. Haematological data (serum iron, serum ferritin, haemoglobin and haematocrit) of rat blood samples as a function of the time *t* after the single-dose iron dextran administration.

Serum ferritin reaches a mean value of 208 ng/ml at t = 7 days and remains on the mean range 165-267 ng/ml until the end of the experiment, values that are always higher than the corresponding control rat values (mean range 13-43 ng/ml). This parameter most likely indicates that the administration of a single dose of iron dextran induces a high synthesis of ferritin with the aim of detoxifying the administered iron.

Haemoglobin and haematocrit levels of the treated rats do not show a substantial change compared with those of the control rats, but it

must be taken into account that the rats included in the study did not have previous iron deficiency.

3.5. Liver tissues

In this animal model, the injected iron is expected to be accumulated mainly in the liver. In this section the results from the elemental analysis, transmission electron microscopy and AC susceptibility measurements of liver tissues from the iron overload animal model described previously are presented.

The main aim is to monitor the accumulation of iron in the liver and the transformations of the iron speciation in this tissue with time after the injection of iron dextran.

3.5.1. Elemental analysis

The results of the elemental analysis (Table 8) indicate that the iron content of the iron-loaded liver tissues is, as expected, higher than that of the control ones and shows a decreasing trend for increasing *t* which may result from the different mechanisms of iron excretion.

The content of the other analysed magnetogenic elements (Co, Ni, Cu and Mn) resulted always less than about 0.005 wt.% of the freeze-dried tissue. The very low content of these magnetogenic transition metal elements, different from iron, makes it safe to interpret the tissue magnetic properties as only due to iron.

The order of magnitude of the determined iron contents is similar to other studies on liver tissues of different iron overload animal models

(Ward et al. 1991; Chua-anusorn et al. 1999), confirming the validity of our model to study the iron speciation in iron overload situations.

Sample	t (days)	mg Fe/g dry tissue
D *	2	18.26
D *	7	14.56
D *	14	11.65
D	24	11.74
D *	24	6.17
D	60	7.59
D *	60	5.54
D	84	13.70
D *	83	5.86
C *	24	0.36
C	84	0.42

Table 8. Iron content in the liver determined by ICP-AES. Tissues from iron dextran-loaded rats and controls are labelled as "D" and "C" respectively. All the samples correspond to different rat individuals. * samples whose magnetic behaviour is shown in the plots.

3.5.2. Transmission Electron Microscopy - Ultrastructural observations

In Fig. 56, it is shown a low magnification TEM image of conventionally stained section of a control liver tissue for the comparison with an iron-loaded one in the same conditions, shown in Fig. 57. Both animals had the same age at the moment of the sacrifice, 24 days after the injection of the iron dextran, and the histological differences are only due to the iron excess. Contrarily to what can be observed in the control tissue, damaged hepatocytes with very deteriorated cytoplasm are observed in the iron-loaded one.

Moreover, in the iron-loaded tissues intracellular large electron-dense bodies can also be observed in some of the cells, similar to what is shown in Fig. 57 a. Unstained or lightly stained sections of these types of cells (Fig. 57b) show the typical appearance of Kupffer cells. These cells contain a variety of cytoplasmic electron-dense bodies with different shape, size and contrast. In particular, bodies with two distinguishable electron densities, indicated in the figure with one and two asterisks, apparently coexist.

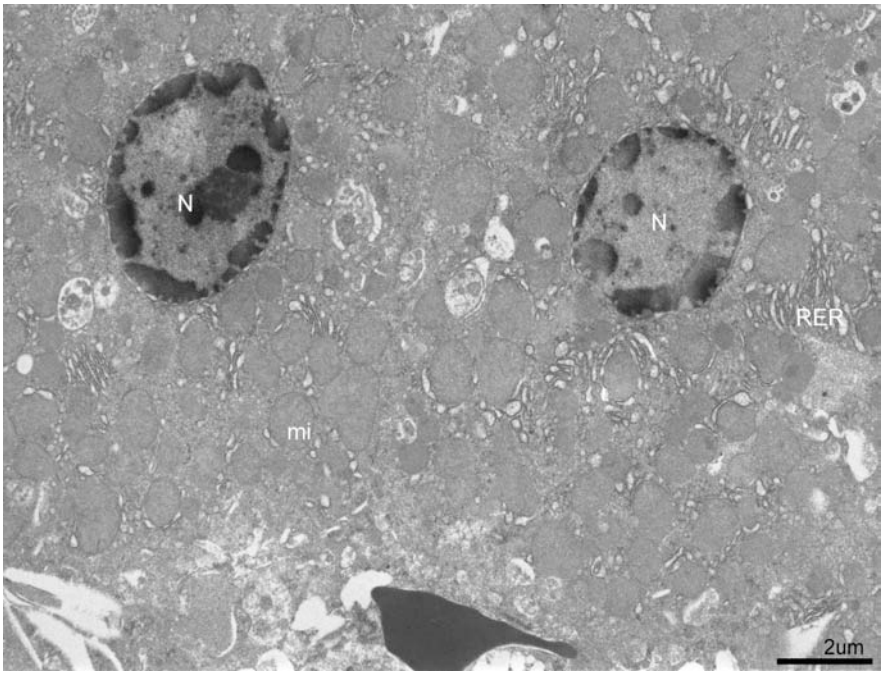

Fig. 56. Liver tissue TEM micrograph from a control rat sacrificed at t = 24 days. The nuclei (N) of two hepatocytes can be observed at low magnification together with the typical cytoplasmatic organelles as mitochondria (mi) and the rough endoplasmic reticulum (RER).

When studying with more detail the ultrastructure of the cytoplasmic electron-dense species, (Fig. 58), it is possible to resolve:

(F) Isolated spherical particles most of them of a size around 5 nm, typical of ferritin, scattered throughout the cytoplasm.

(A) Scattered acicular particles never longer than about 17 nm and around 4 nm wide that remind the akaganeite particles present in iron dextran.

(#) Spherical and electron-dense particles of 5-7 nm in diameter, apparently some of them in mutual contact, forming membrane-encapsulated clusters similar to what has been described in some cases as secondary lysosomes, containing partially degraded iron-rich ferritin molecules (Iancu 1992; Harrison et al. 1996).

(*) Clusters of elongated particles, never longer than about 17 nm and 3-4 nm wide.

(**) Very electron-dense clusters containing, in a very compact manner, particles of different morphologies, in some cases difficult to resolve, similar to the siderosomes observed in severe states of iron overload (Iancu 1992).

These different types of electron-dense objects just mentioned above have been analysed by EDS showing in all the cases the presence of iron.

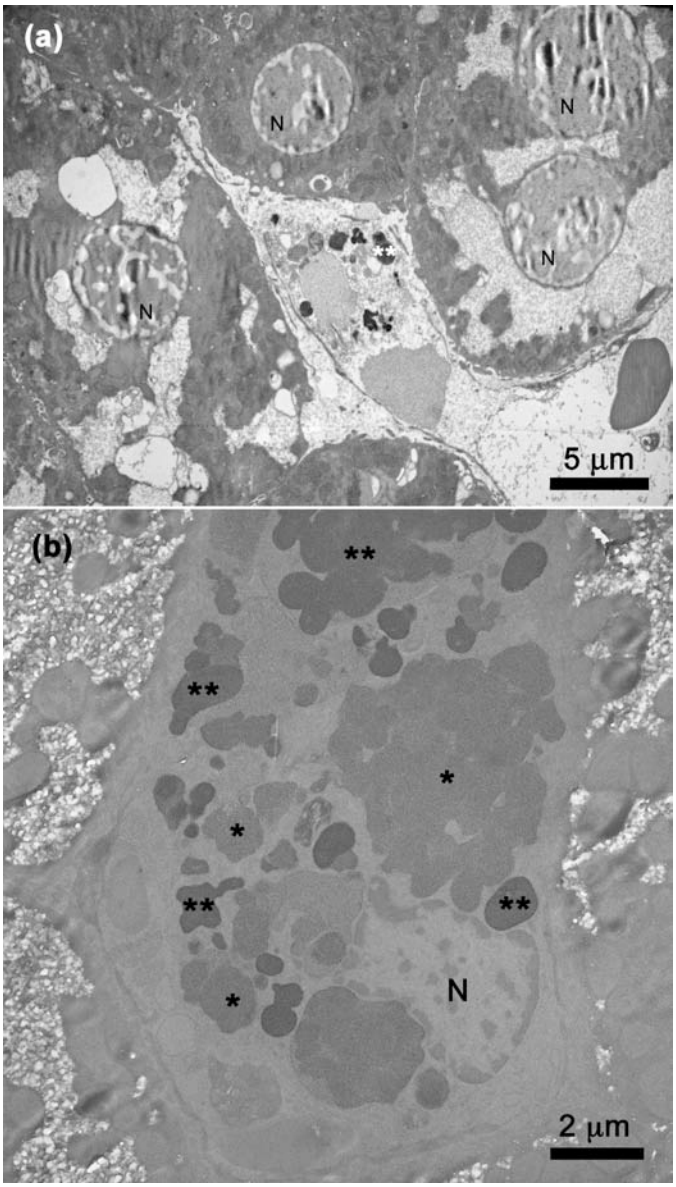

Fig. 57. Liver tissue TEM micrographs from an iron-loaded rat sacrificed at t = 24 days. (a) Damaged hepatocytes with very deteriorated nuclei (N) and a cell with electrodense aggregates (**) observed at low magnification; (b) Kupffer cell containing particle clusters with low and higher electron density, indicated as (*) and (**), respectively.

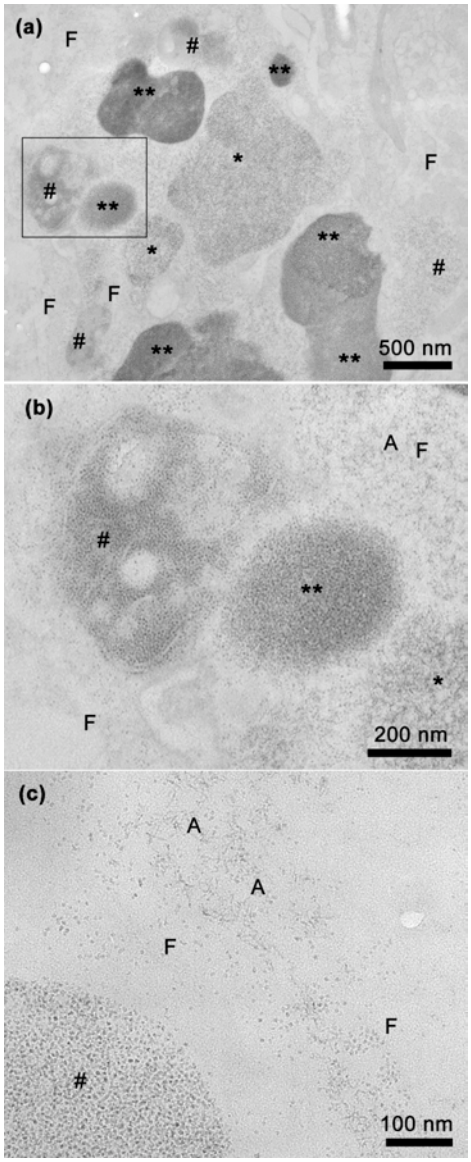

Fig. 58. Liver tissue TEM micrographs from a rat sacrificed at t = 24 days at different magnifications. The different items in the figure are labelled as follows: (F) isolated spherical particles typical of ferritin; (A) scattered acicular particles; (#) spherical electron-dense particles forming membrane- encapsulated clusters; (*) clusters of elongated particles; and (**) very electron-dense clusters.

Although no further details on the protein shell can be obtained from the TEM observations when studying unstained or lightly stained sections (Richter 1984), the ferritin molecules can be identified because of the shape (spherical) and size (no longer than 8 nm) of the electron-dense cores that besides appear mutually separated by the non electron-dense protein shells. The particles that have been termed as F fulfil these characteristics. However, we cannot distinguish if the ferritin molecules have been transported to the liver trough the bloodstream (see high serum ferritin values obtained in the haematological analysis) or if it has been synthesised in the liver. When looking with the same detail at the livers of control rats just a few sparsely distributed cytoplasmic spherical electron-dense particles, similar to the "F" particles observed in Fig. 58, can be observed (results not shown).

The electron-dense particles inside the clusters termed as (#), that also present the typical size and shape of the ferritin cores, are in mutual contact and this fact may indicate the degradation of the protein shell. These divested cores have been previously described (Hoy et al. 1981; Richter 1984) in the degradation sequence of ferritin in the lysosomes to form haemosiderin (see discussion of the unclearness of this word in chapter 1). Some authors (St Pierre et al. 1987) have also named these clusters of divested cores as "prehaemosiderin" as for "relatively short periods of the iron overload condition, the nature of the mineral cores would not be altered"(sic). Independently, of the term used to describe these clusters, it is clear that they contain a big percentage of the iron accumulated in the liver.

The observed elongated particles, scattered (A) or inside clusters (*), have a size and shape that clearly reminds the observed akaganéite particles of the injected drug. From the TEM micrographs, it can be

concluded that the iron dextran particles have been transported to the liver. Furthermore, the presence of the drug, or its degradation products is still observed at least until 24 days after the injection. Due to the high electron density of the clusters termed as (**) no further details can be obtained from the particles inside them.

Besides the morphological differences observed in the micrographs, the electron-dense particles present a different crystalline structure that has been observed in the SAED analysis. The diffraction patterns of the spherical electron-dense nanoparticles (ferritin-like) (Fig. 59b), isolated or forming clusters, are clearly different to those of the iron dextran-like electron-dense particles (Fig. 59a).

When analysing a cluster of only spherical nanoparticles, similar to what has been called "#" and that may correspond to rat prehaemosiderin, its SAED pattern intensity maxima (lower profile in Fig. 59c) are consistent with those of 2-line ferrihydrite (Cornell et al. 1996), as expected from the iron-containing cores inside ferritin. Although differences in the crystalline structure between ferritin and haemosiderin have been observed in human tissues with iron overload (Dickson et al. 1988b; Mann et al. 1988; St Pierre et al. 1992), the studies on rat haemosiderin have provided similar crystalline structures to the analogous ferritin (Andrews et al. 1988), as it has been observed in this case.

The SAED patterns obtained from regions of the same tissue that contain clusters of elongated particles show striking similarity to that of the administered iron dextran (Fig. 59a) (Lázaro et al. 2003). The corresponding locations of the akaganéite diffraction maxima have been plotted together with the radial diffraction intensities obtained from the pattern of the tissue (Fig. 59a) in Fig. 59c (upper curve).

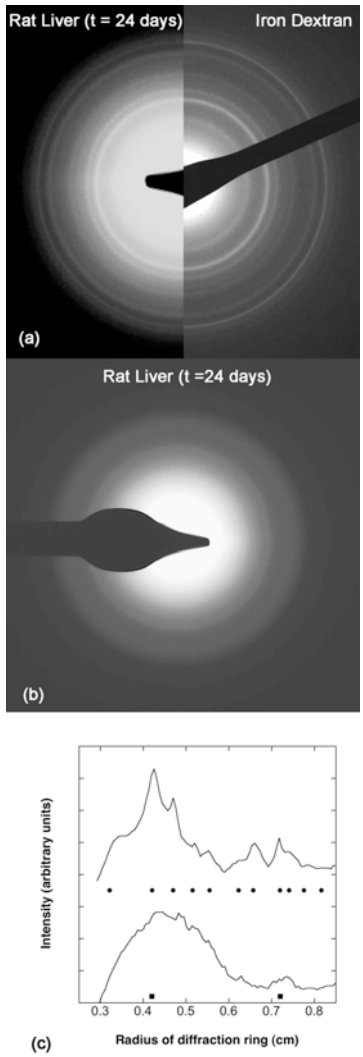

Fig. 59. Selected area electron diffraction results corresponding to the liver tissue from a rat sacrificed at t = 24 days. (a) Diffraction pattern of electron-dense aggregates as those labelled as (*) and (**) in the previous figure are compared to that of iron dextran (Lázaro et al. 2003). (b) Diffraction pattern from a region of the same type as those labelled with (#) in the previous figure. (c) Radial diffraction intensities corresponding to the (a) (upper profile) and (b) (lower profile) patterns. Black circles and black squares correspond to the diffraction maxima of iron dextran and two-line ferrihydrite.

The SAED pattern corresponding to ferrihydrite in the case of aggregates of spherical particles (Fig. 59b) and the pattern obtained from the electron-dense aggregates similar to akaganéite (Fig. 59a) confirm, together with the morphological observations, the presence of, at least, these two kinds of different iron-containing nanoparticles in the tissues in agreement with previous studies (Richter 1959; Andrews et al. 1988). It may indicate that in a case of a fast iron overload, as it happens in this model, the tissues are not capable of synthesising enough ferritin to accumulate the administered iron and that is why the excess is directly accumulated in lysosomes given place to different forms of iron deposits. Richter (Richter 1959) previously observed this fact, as he studied the evolution of the iron deposits by TEM in mice after the administration of iron dextran. That study followed the evolution of the iron deposits with time concluding that at the first stages after the iron dextran administration, the drug was quickly transported to the tissues and then enclosed by membranes. It was 48 hours after the injection when ferritin micelles started to be observed together with the iron dextran aggregates.

Following the definition by Testa (Testa 2002), if the term haemosiderin corresponds to "a poorly defined iron-protein complex that forms an insoluble iron storage system thought to be derived from the lysosomal degradation of the ferritin protein shell", the divested cores observed in the siderosomes (#) may correspond with the concept of a haemosiderin or pre-haemosiderin (St Pierre et al. 1987) coming from degraded ferritins however, the other observed iron deposits containing elongated particles (coming from the injected drug (*)) and also particles with an heterogeneous morphology (**) may not be termed as haemosiderin. The term haemosiderin may be ambiguous in this study as there coexists in the tissues iron deposits with different morphology and

crystalline structure, so for the rest of the discussion the particles will be termed as iron-dextran-like or ferritin-like species referring to the different kinds of electron-dense particles.

From the TEM characterisation, it is not clear whether the deposits containing iron-dextran-like particles may still be degraded and used to fill new apoferritins. In order to study the disappearance of iron dextran from the livers, the magnetic measurements of tissues at different times after the injection was performed and is described ahead.

3.5.3. AC magnetic susceptibility

In what follows the AC susceptibility results of liver tissues are presented. Although more than one sample has been measured for selected times after the injection, just one representative curve for each t is shown in the plots for the sake of clarity.

The temperature dependence of χ', per mass of sample, of freeze-dried liver tissues as a function of time (t) is shown in Fig. 60 only up to 100 K. In the high temperature region all the $\chi'(T)$ curves show Curie-type behaviour, which is typical of a paramagnet, a superparamagnet or a mixture of both.

The low temperature tail observed in $\chi'(T)$ is related to the presence of paramagnetic iron-containing species that, in the case of the control sample, may be associated to rests of blood (haemoglobins, transferrin) or other iron-containing species present in the tissues in physiological conditions. Nevertheless, the low temperature tail of samples t = 2 and 7 days is greater than the control one, which may indicate the progressive travelling of paramagnetic iron towards the liver,

although no more detailed information on its chemical speciation can be extracted from the magnetic experiments. The importance of the tails in the iron-loaded animals decreases for increasing *t*, indicating the diminution of these paramagnetic species generated in the days immediately after the injection.

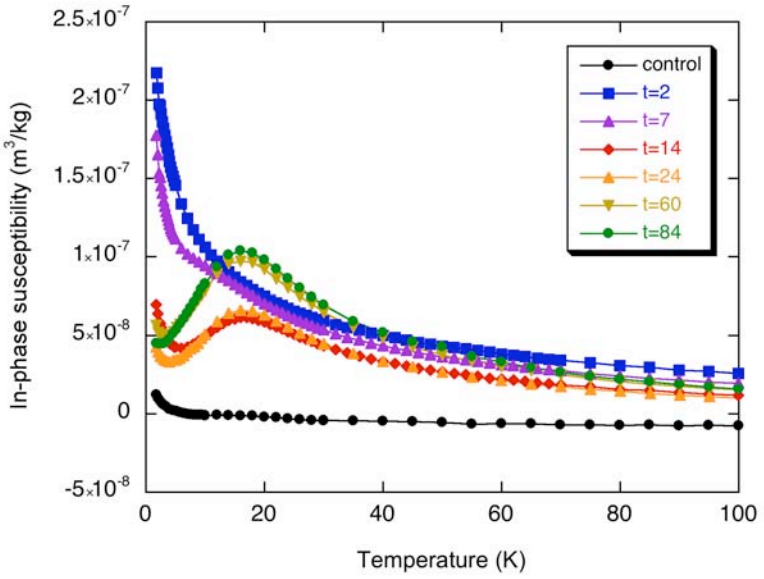

Fig. 60. Temperature dependence of the in-phase susceptibility, at 10 Hz, per mass of freeze-dried liver tissue corresponding to rats sacrificed at different times t (expressed in days) after iron dextran administration.

In addition, except for the control sample, the susceptibility of samples for $t > 7$ days, present a rounded maximum slightly below 20 K. The importance of this maximum increases with increasing *t*, and is hardly visible in the control sample and in sample $t = 2$ days. Due to the large paramagnetic contribution, only a small shoulder can be observed in the sample $t = 7$ days. This maximum is related to a maximum observed

in the out-of-phase susceptibility at slightly lower temperatures (see Fig. 61) and corresponds to the relaxation phenomenon of magnetic blocking of superparamagnetic particles which resembles the rat liver ferritin standard (see previous sections). The increase of the importance of the $\chi'(T)$ maximum with time after the injection indicates an accumulation of ferritin-like iron in the tissues. It must be said that the term *ferritin-like iron* makes reference to isolated ferritins but also to the observed pre-haemosiderin that shows the typical morphological and crystalline structure of the ferritin cores.

All the liver samples have a small diamagnetic contribution, mainly due to the tissue matrix, that in these samples can only be observed in the control one as it is the one with the lowest iron content.

As it has previously been explained, both the $\chi_{Fe\text{-}PARAMAGNETIC}$ and χ_{SP} contributions at high temperature are mixed up in a Curie-law susceptibility whose properties can be condensed in the μ_{eff} value. From the data of Table 9 it can be observed that μ_{eff} departs from a value not much higher than that of iron dextran for t = 2 days and presents an almost steady increase, for increasing t, eventually approaching the value for the ferritin standard. This variation indicates the presence of low-μ_{eff} species at short times after the injection, and their progressive disappearance, consistent with the degradation of the iron dextran akaganéite particles, together with an increase of the amount of higher-μ_{eff} species, most likely associated to the presence of paramagnetic iron or to the synthesis of ferritin-like iron-containing particles.

In Fig. 61, the $\chi''(T)$ curves corresponding to the in-phase susceptibility results of Fig. 60 are plotted. In all the cases there is a single maximum around 10 K whose height systematically increases with

t. From the data analysis of all the samples magnetically characterised (n = 11) slight variations in the temperature and height of the χ" maximum between samples corresponding to the same *t* value have been detected. However, in all the cases, the χ" maxima are located within the interval 7.5 - 12 K and its height tends to increase for increasing *t*.

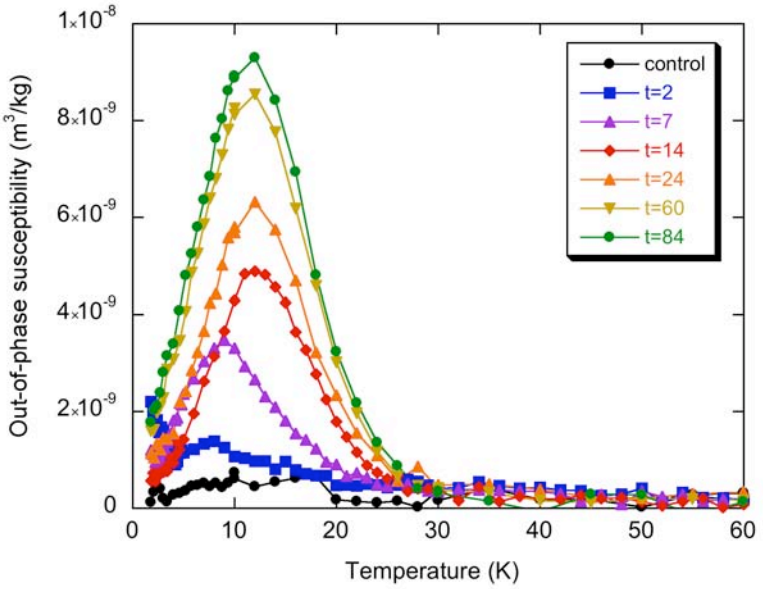

Fig. 61. Temperature dependence of the out-of-phase susceptibility, at 10 Hz, per mass of freeze-dried liver tissue corresponding to rats sacrificed at different times *t* (expressed in days) after iron dextran administration.

Although for the ferritin standards it has been verified the non-interaction model between the particles, as in the tissues the local concentration of ferritin cores can be higher in some of the cells, and also the degradation of the ferritin shell in the observed clusters may influence the distances between the cores, the tissue's τ_0 values have been calculated to assess the validity of the superparamagnetic model of non-interacting particles.

In Fig. 62, the scaling plot of the out-of-phase susceptibility data measured at different frequencies for the sample of t = 84 days is represented. The τ_0 value that leads to optimum scaling results $10^{-12\pm1}$ s, which is typical for a non-interacting assembly of small particles. The same calculation has been done for the sample of t = 60 days resulting in identical pre-exponential factor. These results strongly indicate that the $\chi''(T)$ main maximum for these samples correspond to single particle activation modes, which is the first requirement to associate the $\chi''(T)$ profiles to distribution of particle sizes. As it has been observed in the SAED analysis (Fig. 59) that both the ferritin cores and the divested ferritin cores have identical crystalline structure, the same effective anisotropy constant, K, can be assumed for both species.

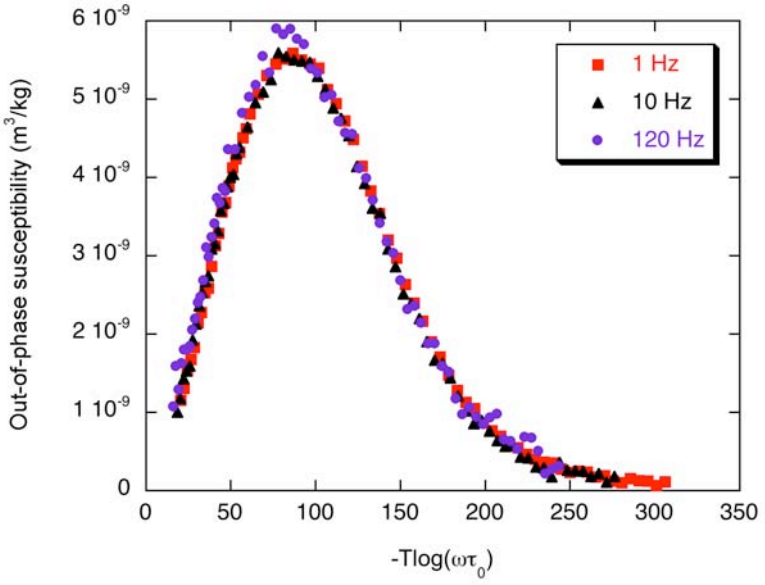

Fig. 62. Scaling plot of the out-of-phase susceptibility from the simple sacrificed at t = 84 days. Best superposition is obtained with a pre-exponential factor $\tau_0 = 10^{-12\pm1}$ s.

Since the involved particles are antiferromagnetic, the interparticle dipole-dipole interactions are expected to be very weak. This fact has been confirmed by calculating the T_{dip} value, resulting for all the studied liver tissues in values never exceeding $5 \cdot 10^{-4}$ K, which lies much below than the temperature range of the measurements.

Sample	t (days)	μ_{eff} (μ_B)
Iron dextran		1.58
*D	2	2.12 ± 0.16
*D	7	2.21 ± 0.07
*D	14	2.21 ± 0.10
D	24	2.38 ± 0.10
*D	24	3.11 ± 0.10
D	60	2.72 ± 0.07
*D	60	3.85 ± 0.11
D	84	2.73 ± 0.13
*D	83	3.91 ± 0.12
*C	24	3.10 ± 0.26
C	84	4.59 ± 0.90
Ferritin		3.39 ± 0.01

Table 9. Effective moment per iron ion of the liver tissue samples together with data for iron dextran and rat liver ferritin. Tissues from rats that received the iron dextran injection and controls are labelled as "D" and "C" respectively. All the samples correspond to different rat individuals.

Although originated from the same raw data as in Fig. 61, two different representations of the $\chi''(T)$ curves are presented below as they allow a better understanding of the biotransformation of iron dextran after its administration to the rats.

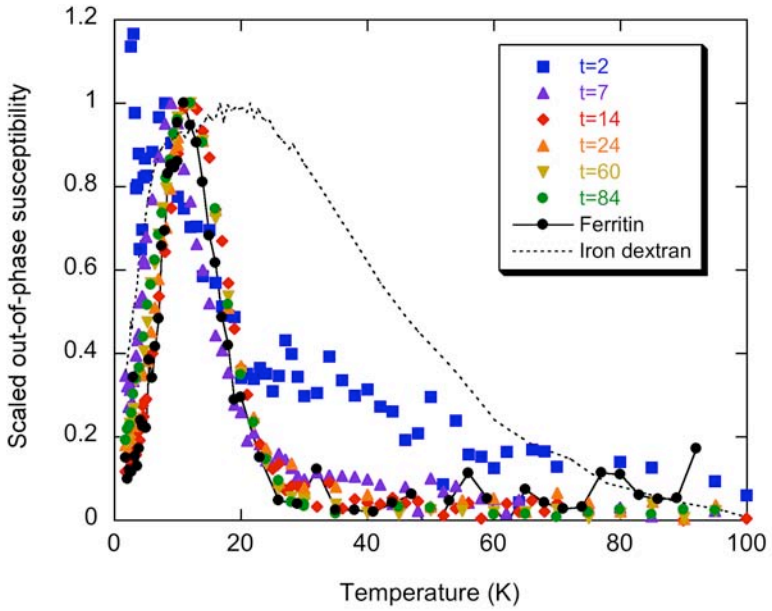

Fig. 63. Comparative plot of the $\chi''(T)$ profiles for ferritin, iron dextran and liver tissues as scaled to their respective maxima. The times t after the administration are indicated in days.

In Fig. 63, the $\chi''(T)$ curves are shown scaled to their maxima allowing the comparison of the shape and width of the profiles. This kind of representation facilitates the study of differences in the particle size, assuming that the samples contain particles of the same iron oxyhydroxide.

From this representation it can be concluded that, except for the sample obtained 2 days after the iron dextran injection, $\chi''(T)$ of liver tissues seems to be similar to that of the ferritin standard in terms of peak temperature and peak width. The shoulder that can be observed at the right hand side of the $\chi''(T)$ peak for the sample of t = 2 days, due to its temperature location and shape, may very probably be caused by the

presence of akaganéite particles coming from iron dextran, since they were still detected by TEM and electron diffraction at t = 24 days. These results are also in agreement with the low μ_{eff} values observed for these samples.

However, when looking with more detail at the profiles shown in Fig. 63, it can also be observed that the location in temperature of the maximum of the t = 7 sample is situated at slightly lower temperatures than the ferritin standard. Moreover, there is also a marked difference in the shape of the maximum that instead of superposing with the ferritin standard profile, seems to be, in general, located at lower temperatures. These facts, that inform about the presence of smaller particle sizes at short times after the iron dextran injection may be associated with the synthesis of ferritin, resulting in not-fully loaded ferritin molecules.

Although all of the samples of $t > 7$ seem to have a $\chi''(T)$ profile very similar to that of the ferritin standard, in fact, some small differences can also be observed. Samples t = 60 and 84 days show a wider maxima in the low temperature side of the peak. One possible explanation to this fact is that at longer times after the injection there will be a greater amount of pre-haemosiderin, which has been reported to be formed by smaller cores than the ferritin. As both ferritin and pre-haemosiderin will contribute to the $\chi''(T)$ peak, the wider maxima could be associated with the presence of a greater amount of smaller particles associated to the presence of more haemosiderin at longer times after the injection.

The out-of-phase susceptibility *per mass of iron* in each liver sample is represented in Fig. 64 together with the data for rat liver ferritin and iron dextran. There is a systematic increase of the $\chi''(T)$ maximum

height corresponding to liver samples for increasing *t*, departing from that of iron dextran towards that of ferritin.

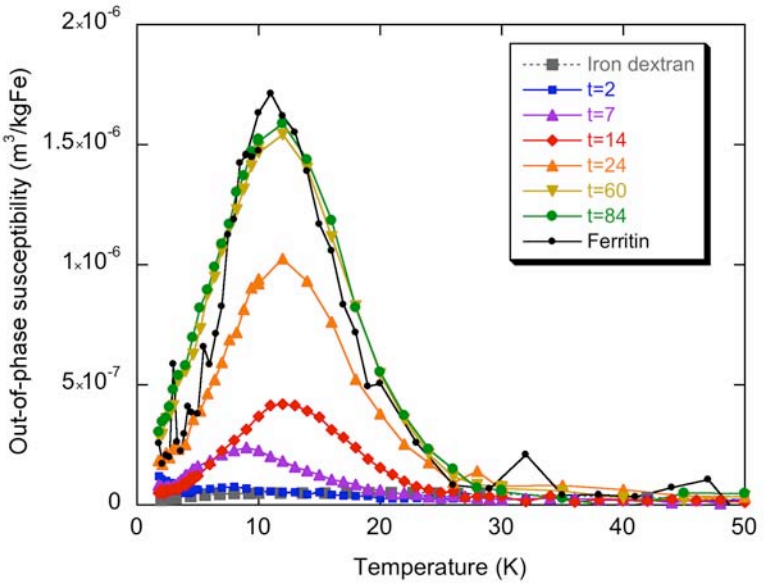

Fig. 64. Temperature dependence of the out-of-phase susceptibility relative to the iron content for rat liver ferritin, iron dextran and liver tissues. The times *t* after the administration are indicated in days. It is remarkable the low $\chi''(T)$ per iron ion of iron dextran (dashed line), whose temperature profile (very close to the $t = 2$ liver curve) is in this representation hardly visible.

The iron dextran out-of-phase susceptibility per mass of iron is *much lower* than that of the ferritin standard, in agreement with the lower effective moments per iron ion that have been obtained from the $\chi'(T)$ data. This result also explains the very low magnetic contribution of the remaining iron dextran for samples with $t > 7$ days in the curves of Fig. 63, in a way that, although rests of the drug have been detected by TEM at least 24 days after the injection, its contribution is not observed in the out-of-phase susceptibility curves due to its low effective moment.

In this type of representation (Fig. 64), if all of the iron atoms in the liver tissues were in the same form, the corresponding $\chi''(T)$ profile per mass of iron would coincide, as it approximately occurs for samples of t = 60, 84 days and ferritin. The nearly overlap of these curves indicates that at times longer than one month after the injection most of the iron in the liver tissues is in the form of ferritin or ferritin-like particles (pre-haemosiderin).

It can be observed that for t values lower than 24 days, the $\chi''(T)$ maximum height is smaller than that of ferritin, although with the same shape and location in temperature (Fig. 63). This indicates that for short post-administration times a substantial iron fraction is still in a non-ferritin form, as for example paramagnetic or diamagnetic species, that have no contribution to $\chi''(T)$, or as iron dextran or its degradation products. The presence of paramagnetic species in these short post-administration times samples is observed in their corresponding low temperature $\chi'(T)$ tails (Fig. 60). However, since for low t the μ_{eff} values resulted lower than that of ferritin, the largest non-ferritin fraction of iron in this case may very likely correspond to iron dextran or other diamagnetic iron-containing species. This fact is again coherent with the TEM and SAED results that show rests of akaganéite in the liver cells still at t = 24 days.

From all the previous data it appears that for increasing t the transformation of the iron species consist in a progressive degradation and elimination of iron dextran particles together with an increase of the number of ferritin or ferritin-like iron-containing species. No considerable differences have been observed in the magnetic behaviour between the ferritin cores and the divested cores at these stages of the iron overload.

3.6. Muscle tissues

As, in this animal model of iron overload, iron has been administered subcutaneously near the rat back, the muscle tissues near the place of injection have been magnetically characterised in order to monitor the transformations of the iron speciation with time.

This section describes the obtained results from the elemental analysis and the AC susceptibility measurements of muscle tissues from the animal model previously described.

3.6.1. Elemental analysis

The elemental iron content in the samples systematically decreases for increasing t (Table 10). This fact can be understood from the progressive diffusion of iron to other parts of the rat body or by any other mechanism of iron excretion.

Sample	t (days)	mg Fe/g dry tissue
D	2	7.18
D	7	5.61
D	14	3.52
D	24	5.20
D	60	2.01
D	84	1.15
C	84	0.03

Table 10. Dependence of the iron content with time after the iron dextran administration. Tissues from rats that received the iron dextran injection and controls are labelled as "D" and "C" respectively. Data correspond to the muscle tissue samples whose magnetic behaviour is presented below.

Since the content of the other analysed magnetogenic elements is less than about 0.003 wt% freeze-dried tissue, much lower than the iron content, it is safe to interpret the tissue magnetic properties as only due to iron.

3.6.2. AC magnetic susceptibility

Due to the time needed for the magnetic characterisation, as a first attempt only one muscle sample for each t value was measured. Additional samples of muscle tissues at t = 2, 7 and 24 days were also measured providing good reproducibility, so only one result for each t has been included in the magnetic susceptibility plots for the sake of clarity.

The temperature dependence of the in-phase susceptibility per mass of freeze-dried tissue is shown in Fig. 65, only up to 100K. As it happened in the livers, different contributions can be observed in the $\chi'(T)$ plot: A low temperature paramagnetic tail, a rounded maximum somehow below 20 K, a negative contribution to the susceptibility, and a high-temperature Curie-type behaviour.

The negative susceptibility values observed in the control sample, but also in samples of t = 84 and 60 days, corresponds to the presence of a diamagnetic contribution from the tissue matrix and the gelatine capsule. Although this contribution is present in all the samples, only negative values of the in-phase susceptibility are observed in the tissues with the lowest iron content (see Table 10).

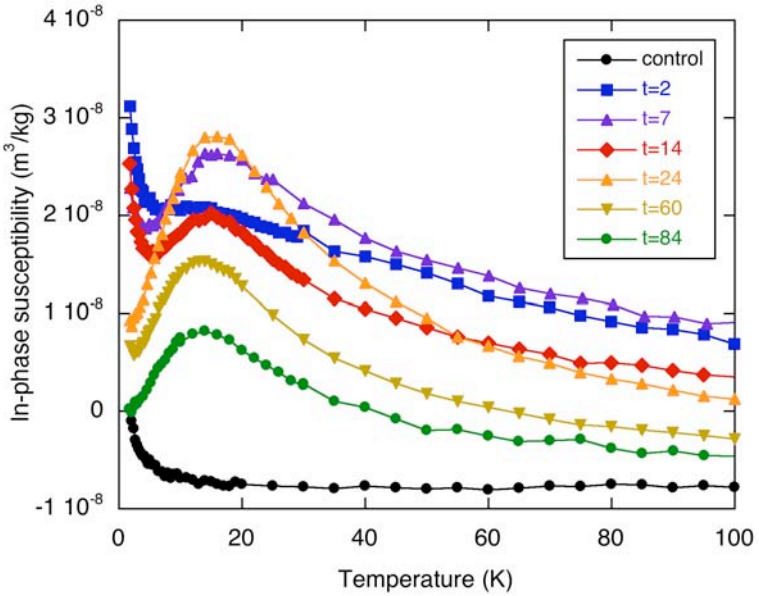

Fig. 65. Temperature dependence of the in-phase susceptibility per mass of freeze-dried muscle tissue corresponding to rats sacrificed at different times t after iron dextran administration. Values of t are indicated in days. The continuous lines are just guides for the eye.

The low temperature paramagnetic tail of the control sample can be associated to iron-containing paramagnetic species coming from rests of blood or present in the tissue cells. This tail is also observed in tissues up to 14 days after the injection and nearly disappears at $t \geq 24$ days. Although the paramagnetic iron seems to decrease for increasing t, this fact does not have yet a clear interpretation as at least the same amount of paramagnetic species as in the control sample should be expected in all of the muscle tissues.

The rounded maximum that can be observed below 20 K in all the samples except in the control one (Fig. 66) resembles the observed in the rat liver ferritin standard and the liver tissues previously characterised.

The amounts of ferritin in the muscle tissues seem to first increase and then decrease with time after the injection. In fact, at short times after the injection, t = 2 days, only a small shoulder can be observed, due to the big paramagnetic contribution and the small maximum. Then, the maximum height of the peak corresponding to the presence of ferritin is observed 24 days after the injection, and finally the amount of ferritin seems to be reduced.

The in-phase susceptibility at temperatures higher than 60 K is free from relaxational contributions ($\chi''(T) \approx 0$) in all the samples and shows a Curie-type behaviour. The calculation of the effective moment of each tissue provide values (Table 11) that departs from a value very similar to that of the original iron dextran compound for the rat sacrificed at t=2 days and presents a steady increase for increasing t eventually approaching a value similar to the one obtained for the rat liver ferritin standard, in the iron-loaded rats. The observed variation with t indicates a relative decrease of the number of low μ_{eff} species, as iron dextran (μ_{eff} = 1.58 μ_B), and an increase of higher μ_{eff} species, as iron-containing nanoparticles inside ferritin (μ_{eff} = 3.4 μ_B), or divested cores as the observed in the livers, or paramagnetic ions ($\mu_{eff} \approx$ 5-6 μ_B). As it was also observed in the liver tissues, this result indicates the progressive degradation or elimination of iron dextran in the muscle tissue and the apparition of ferritin or ferritin-like iron. The control rat muscle tissue presents the highest effective moment in agreement with the obvious absence of large antiferromagnetic particles coming from the drug. As the effective moment obtained for the control rat is higher than that of rat liver ferritin although not surpasses the moment of the paramagnetic iron ions, the value is in agreement with the fact that the main iron-containing

species expected to be in the control muscle are ferritin and other iron-containing paramagnetic species.

Sample	t (days)	μ_{eff} (μ_B)
Iron dextran	-	1.58
D	2	1.88
D	7	2.32
D	14	2.35
D	24	2.50
D	60	2.82
D	84	3.43
C	84	4.21
Ferritin	-	3.40

Table 11. Dependence of the iron content and effective moment μ_{eff} with time (t) after the iron dextran administration. Tissues from iron dextran-loaded rats and controls are labelled as "D" and "C" respectively. Data correspond to the muscle tissue samples whose iron content is shown in Table 10.

The temperature dependence of the out-of-phase susceptibility $\chi''(T)$ per mass of freeze-dried tissue is shown in Fig. 66. All the samples, except the control one, present a maximum located always at slightly lower temperatures than its $\chi'(T)$ maximum counterpart indicating a magnetic blocking.

In this case, the out-of-phase susceptibility is only related to the presence of superparamagnetic particles, and there are no more contributions from the rest of the iron-containing species. As the only superparamagnetic species that may be present in the tissues are the particles inside the ferritin shell (or similar particles as the divested cores) and the administered iron dextran, the out-of-phase susceptibility can be explained by the relative amount of these species.

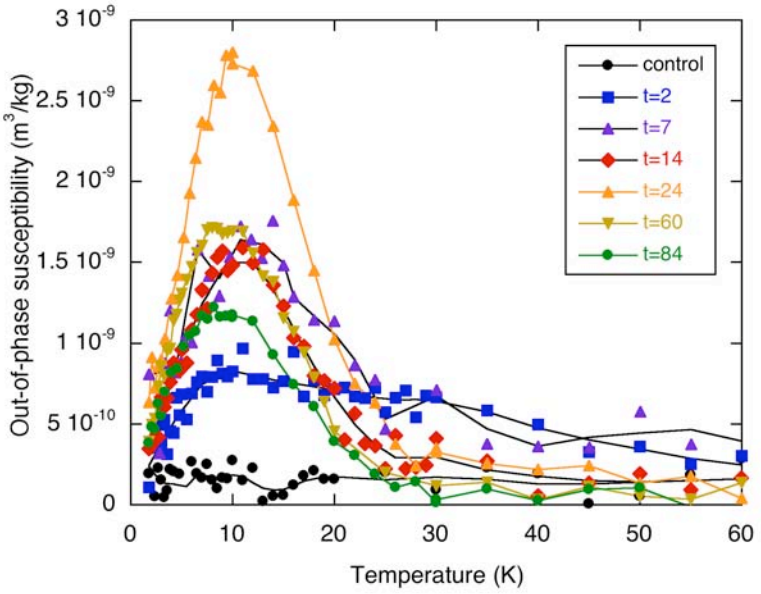

Fig. 66. Temperature dependence of the out-of-phase susceptibility per mass of freeze-dried muscle tissue corresponding to rats sacrificed at different times t after iron dextran administration. Values of t are indicated in days. The continuous lines are just guides for the eye.

In Fig. 66 it can be observed that the maximum height increases systematically with t up to t = 24 days and then it decreases again. However, the width of the maxima changes with time after the iron dextran administration.

In order to assure the particles behave within the non-interaction regime, which allows the interpretation of the $\chi''(T)$ profile as an approach the distribution of particle sizes, the value of τ_0 has been calculated. The preexponential factor has been calculated from the measurements at different frequencies of samples of t = 24 and 84 days.

The results (shown in Fig. 67 for t = 24 days) yield prefactors of the order of 10^{-13} s which are very close to the usually determined values for non-interacting assemblies of small particles.

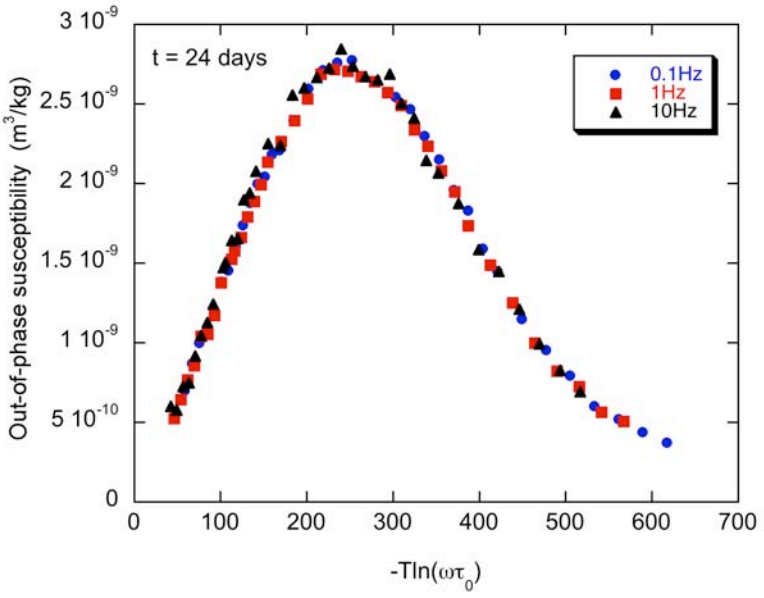

Fig. 67. Representative scaling plot of the out-of-phase susceptibility (in this case for a t=24 days sample). Best superposition of the data correspond to a preexponential factor $\tau_0=10^{-13}$ s.

In order to study the differences between the out-of-phase susceptibility profiles of the different animals it is adequate to scale the $\chi''(T)$ curves to their maxima (Fig. 68), to compare their shape, width and location in temperature. The shape of the $\chi''(T)$ maximum from the sample of t = 2 days is wider than the rest of the samples and resembles that of iron dextran. The sample of t = 7 days presents a maximum similar to the ferritin one but it also can be observed a shoulder in the right flank which may indicate the presence of a considerable amount of

iron dextran in the tissue still one week after its injection. The rest of the samples with iron overload, present a bell-shaped $\chi''(T)$ maximum located around 10 K, whose shape and location in temperature resembles that of rat liver ferritin, expected to be formed also in the muscle to accumulate the iron excess.

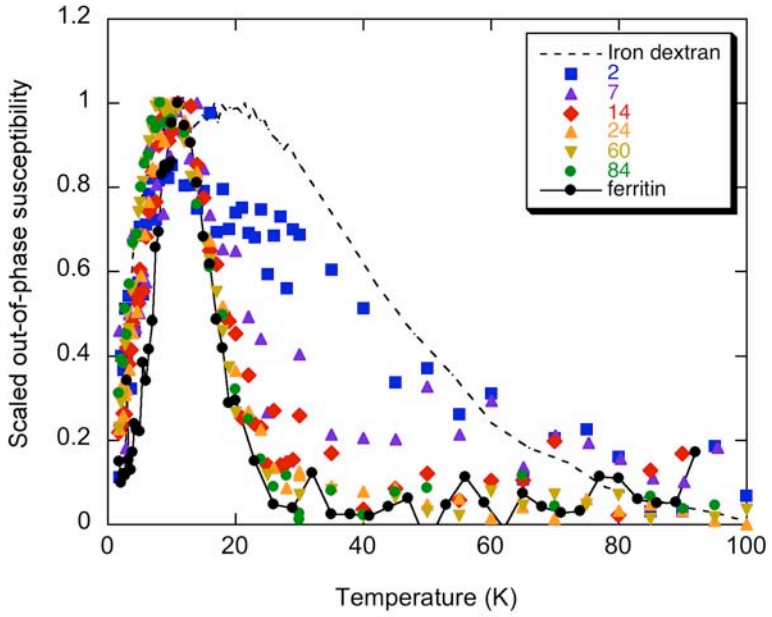

Fig. 68. Comparative plot of the out-of-phase susceptibility profiles, for tissues at different t values and for the injected iron dextran (dashed line), scaled to their respective maxima. Values of t are indicated in days. The continuous line, which corresponds to data of t=84 days, is just a guide for the eye.

The evolution of the shape of the $\chi''(T)$ maximum with time indicates the degradation of iron dextran in favour of the accumulation of iron in the form of ferritin-like iron. These changes in the $\chi''(T)$ profile are in agreement with the effective moments in a way that the degradation

of iron dextran and the generation of ferritin-like particles is observed by the two methods.

Slight differences can be observed in the low-temperature flank of the out-of-phase susceptibility maxima between the rat liver ferritin and the muscle tissues. More specifically, muscle tissues show a wider maximum at the lower temperatures, which may indicate a slight different biomineralisation or particle size between the ferritins from different tissues. However, it may also be related with the presence of pre-haemosiderin, as it has been observed in the livers, whose iron-containing cores have previously been reported to be smaller than ferritin.

In Fig. 69 is presented the out-of-phase susceptibility per mass of iron in each of the iron-loaded muscle samples and also for the two standards: Iron dextran and rat liver ferritin. It is clear from the figure that the iron dextran out-of-phase susceptibility per mass of iron is *much lower* than that of the ferritin standard, in agreement with the lower effective moments per iron ion that have been obtained from the $\chi'(T)$ data (see Table 11). Also, there is a systematic increase of the $\chi''(T)$ maximum height corresponding to muscle samples for increasing t, departing from that of iron dextran towards that of the ferritin standard. As explained also for the liver tissues, in this type of representation, if the iron speciation was the same in all the samples, the corresponding $\chi''(T)$ profile per mass of iron would have coincided. Nevertheless, it can be observed in the figure that, except for the sample of t = 2 days, the $\chi''(T)$ maximum shape and location in temperature of the rest of the samples is similar to that of ferritin, although with smaller height. This indicates that in these samples a substantial iron fraction is still in non-ferritin form, as for example iron dextran or its degradation products, or as paramagnetic

or diamagnetic species, that have no contribution to $\chi''(T)$, in agreement also with the observed μ_{eff} values.

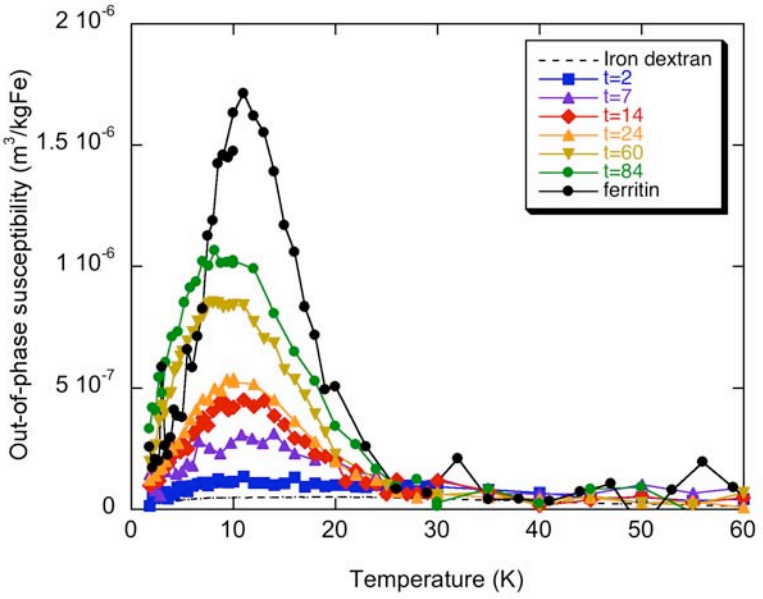

Fig. 69. Temperature dependence of the out-of-phase susceptibility relative to the iron content in the tissue of freeze-dried muscle samples of rats sacrificed at different t times. Values of t are indicated in days. The dashed line corresponds to data of iron dextran.

As the height of the $\chi''(T)$ maximum represented per mass of iron increases for increasing t it appears that the transformation of the iron species consist in a progressive degradation and elimination of iron dextran particles (which have a low effective moment per iron ion and also have a very low effect on χ'') together with an increase of the number of iron-loaded ferritin molecules or the divested cores previously observed in the livers (which have a higher effective moment per iron ion and much larger effect on χ'').

In this representation, as it is relative to the iron content in the sample, it is evidenced that the magnetic signal of a given concentration

of iron atoms, totally or partially aggregated into particles, depends dramatically on their size and nature.

3.7. Other tissues: Spleen, heart and kidneys

When studying the transformation and accumulation of iron in this animal model, as iron may travel from the muscle area to the liver through the blood, it is expected that other tissues can also be affected by the iron excess.

In what follows, the magnetic characterisation of selected samples of freeze-dried spleen, heart and kidney tissues obtained 84 days after the iron injection is presented in comparison with control tissues. These results aim to study the degree of iron accumulation in other organs different form the muscle and the liver. The iron-loaded tissues correspond to the same animal whose liver was magnetically characterised in the previous study of the magnetic monitoring of iron with time, for t = 84 days. The AC magnetic measurements of these tissues have been performed at 1Hz.

3.7.1. AC magnetic susceptibility

The in-phase and out-of-phase susceptibility results of the iron-loaded and the control spleen tissues are shown in Fig. 70 and Fig. 71, only up to 100 K. The in-phase susceptibility of the spleen tissues present Curie-type behaviour in the high temperature range together with a low-temperature paramagnetic tail, which is substantially greater in the case of the iron loaded tissue. It can also be observed in the iron-loaded tissue a

small shoulder slightly below 20 K. In the out-of-phase susceptibility of the two spleen samples a clear maximum at around 10 K, similar to the magnetic blocking of the rat liver ferritin standard, is visible (Fig. 71). The higher χ''(T) maximum of the iron-loaded tissue, in comparison with the control one, reveals the accumulation of ferritin-like species in the spleen.

Although the nature of the paramagnetic iron-containing species in the iron-loaded spleen is still unknown, it seems that the origin of the iron in these species, as it is in a greater amount that in the control tissue, may probably be associated to the injected iron dextran.

In Fig. 72 to Fig. 75, the results of the AC susceptibility measurements of the heart and both kidneys corresponding to an animal sacrificed 84 days after the iron administration are shown compared with control tissues. For the sake of clarity data only up to 100 K are shown in the plot although in the high temperature region all the $\chi'(T)$ curves show Curie-type behaviour. At the lowest temperatures the four samples exhibit a $\chi'(T)$ tail whose importance is greater in the iron-loaded rats than the controls, as it happened also in the spleen tissues.

In the case of the control heart and kidney tissues, within the intrinsic noise of the results, the out-of-phase susceptibility is not distinguishable from zero. On the contrary, the iron-loaded rats present a rounded maximum in their $\chi''(T)$ susceptibility curves around 10K, whose temperature location and shapes reminds that of ferritin. These results indicate the accumulation of iron in the kidneys and the heart after the iron dextran injection.

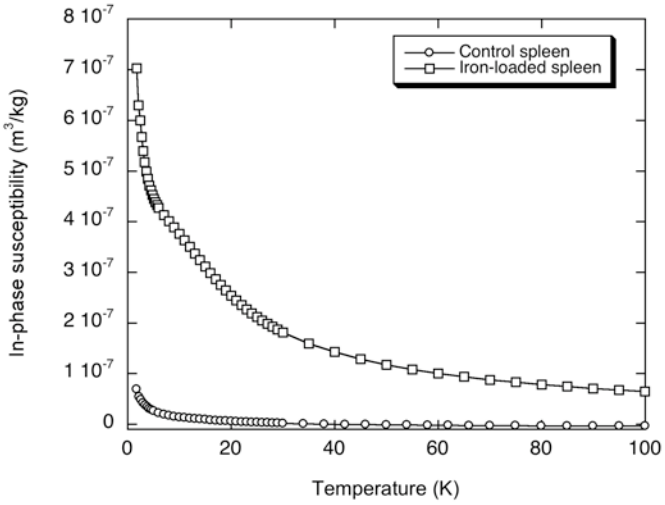

Fig. 70. Temperature dependence of the in-phase susceptibility per mass of freeze-dried spleen tissue corresponding to a control and an iron-loaded rat sacrificed at t = 84 days after iron dextran administration.

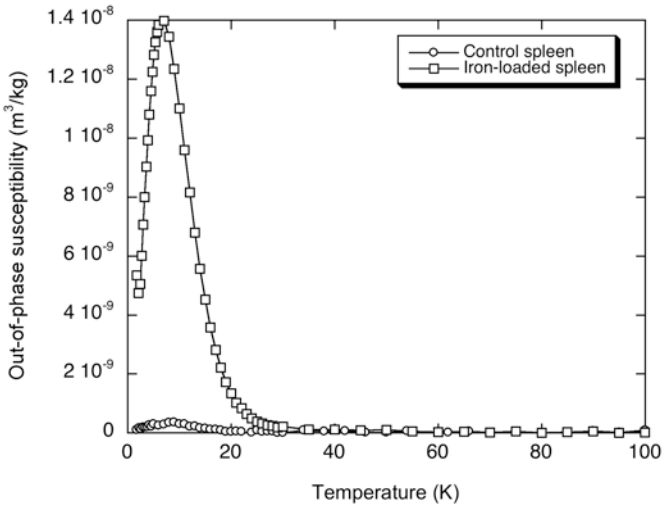

Fig. 71. Temperature dependence of the out-of-phase susceptibility per mass of freeze-dried spleen tissue corresponding to a control and an iron-loaded rat sacrificed at t = 84 days after iron dextran administration.

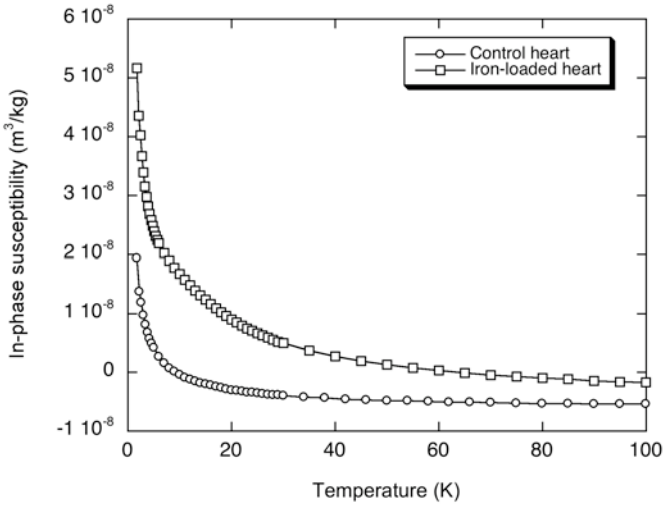

Fig. 72. Temperature dependence of the in-phase susceptibility per mass of freeze-dried heart tissue corresponding to a control and an iron-loaded rat sacrificed at t = 84 days after iron dextran administration.

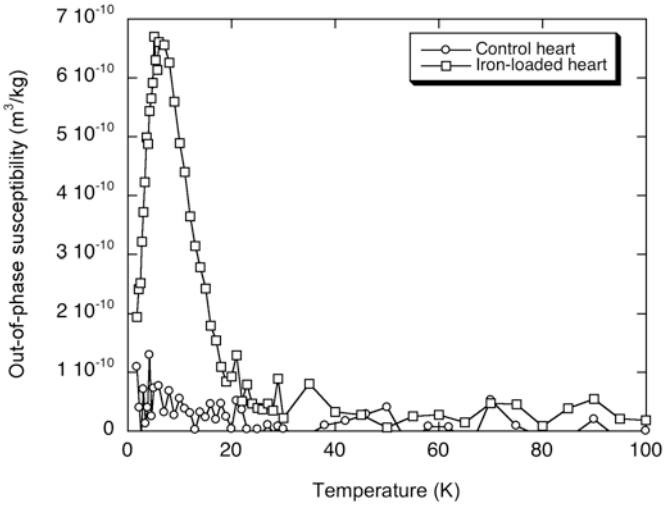

Fig. 73. Temperature dependence of the out-of-phase susceptibility per mass of freeze-dried heart tissue corresponding to a control and an iron-loaded rat sacrificed at t = 84 days after iron dextran administration.

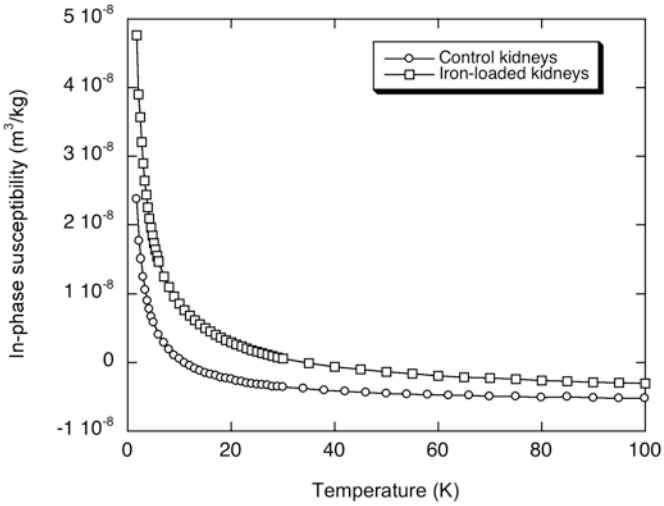

Fig. 74. Temperature dependence of the in-phase susceptibility per mass of freeze-dried tissue of both kidneys of a control and an iron-loaded rat sacrificed at t = 84 days after iron dextran administration.

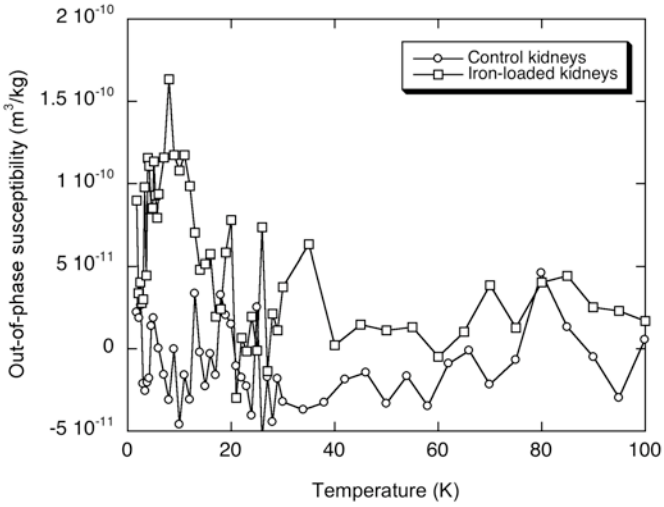

Fig. 75. Temperature dependence of the out-of-phase susceptibility per mass of freeze-dried tissue of both kidneys of a control and an iron-loaded rat sacrificed at t = 84 days after iron dextran administration.

The susceptibility of all the iron-overloaded tissues is significantly higher than the normal ones, especially in the case of spleen, due to its role of iron storage organ. Moreover, from the magnetic results, two different kinds of iron-containing species have been detected to be accumulated in the tissues: paramagnetic and ferritin-like iron-containing species. This result indicates the accumulation of iron in these tissues forming part of species of different nature.

The observation of iron deposits in the heart in this animal model, also described by Carthew et al (Carthew et al. 1991), is of great interest, as iron accumulation has also been observed previously in heart tissues in human diseases of iron-overload (Kaufman et al. 1980; Chua-anusorn et al. 2000).

3.8. Conclusions

In this chapter, the AC susceptibility characterisation of rat liver ferritin has been presented. These data constitute an indispensable element in the interpretation of the AC susceptibility of rat livers, but also from other rat tissues.

The magnetic characterisation of rat liver, muscle, heart, spleen and kidney samples, by measuring the AC susceptibility of the whole tissue, has been also presented in this chapter. The study by magnetic means of liver and muscle tissues at different times after the iron-dextran injection, assisted by TEM observations of the liver tissues, has revealed the transformations of the biomineralised iron, consisting in a progressive degradation and elimination of the administered iron dextran particles together with an increase of the number of ferritin molecules or the

analogous divested cores. The study of spleen, heart and kidney samples at long times after the iron-dextran injection has also shown the accumulation of iron in the form of ferritin or ferritin-like particles also in these tissues. Moreover, slight differences have been observed between the $\chi''(T)$ maxima profiles associated to ferritin among all the characterised tissues, which indicates slight differences in the crystalline structure or particle size.

Not related to the biomineralisation of iron but of special interest for the study of the iron metabolism in this animal model are the changes observed in the low temperature paramagnetic tails of the liver tissues. It seems that the great paramagnetic contribution at short times after the injection, in comparison with the control ones, may be related to the travelling of iron towards the liver.

It has to be mentioned that although this work has studied tissues originated in different rat individuals, the obtained results are remarkably systematic.

In spite of the antiferromagnetic character and the low concentration of most of the iron species found in the rat tissues, the results of this work reveal that enough experimental sensitivity has been achieved in the AC susceptibility measurements, confirming the interest of this technique for iron monitoring in biological and pharmacological studies. Besides, it can be said that there is a huge agreement between the magnetic results and the TEM observations. Furthermore, both techniques provide complementary data as the paramagnetic species can only be observed magnetically and the TEM observations can inform about the crystalline structure and location within the cell of the biomineralised iron.

The fact that not all the iron-containing species present the same contribution to the magnetic susceptibility per iron ion, a direct result from the effective moment values, may help to a better understanding of the obtained data in the clinical application of non-invasive techniques for liver iron assessment based on the magnetic properties of the tissues.

4. Animal models of iron overload II: Hfe Knockout mice

4.1. Introduction and main aims

Genetic haemochromatosis is an autosomal recessive disorder characterized by excessive iron absorption from the duodenum and iron release from the macrophages. In humans, gradual deposition of iron occurs in the liver and in a number of other tissues including the pancreas, joints, skin, heart and the gonadotrophin-secreting cells of the anterior pituitary. Disease manifestations include hepatic fibrosis, diabetes mellitus, arthropathy, pigmentation, cardiomyopathy and

hypogonadotrophic hypogonadism. Liver fibrosis may progress towards cirrhosis, a complication associated with a 200-fold increased risk of hepatocellular carcinoma, the most common cause of death in this condition. Most patients with genetic haemochromatosis are homozygotes for a single point mutation, C282Y, in the HFE gene (Feder et al. 1996). Population studies have shown that genetic predisposition to genetic haemochromatosis was common, with one in 300 homozygotes for the C282Y mutation in populations of Northern European extraction.

Murine models of iron overload, like *Hfe* knockout mice ($Hfe^{-/-}$), provide a useful alternative to humans for a better understanding of the physiologic pathways involved in the disease process (Zhou et al. 1998; Bahram et al. 1999). It has been previously reported that, compared with other mouse strains, DBA/2 mice are particularly susceptible to iron loading in response to *Hfe* disruption (Dupic et al. 2002).

As DBA/2 $Hfe^{-/-}$ mice constitutively become iron overloaded, the model constructed with these animals is expected to be a closer representation of the human disease, at least in terms of genetic origin, than other models like the iron overload induced by parenteral injection of iron dextran used in the previous chapter.

In this chapter, the low temperature AC magnetic susceptibility data of liver, spleen and heart tissues of DBA/2 Hfe knockout (KO) and wild type (WT) mice will be presented with the aim of investigating the tissue iron speciation in iron overload diseases. The magnetic results together with elemental analyses and ultrastructural information of the iron deposits, obtained from Transmission Electron Microscopy and Selected Area Electron Diffraction, will be analysed.

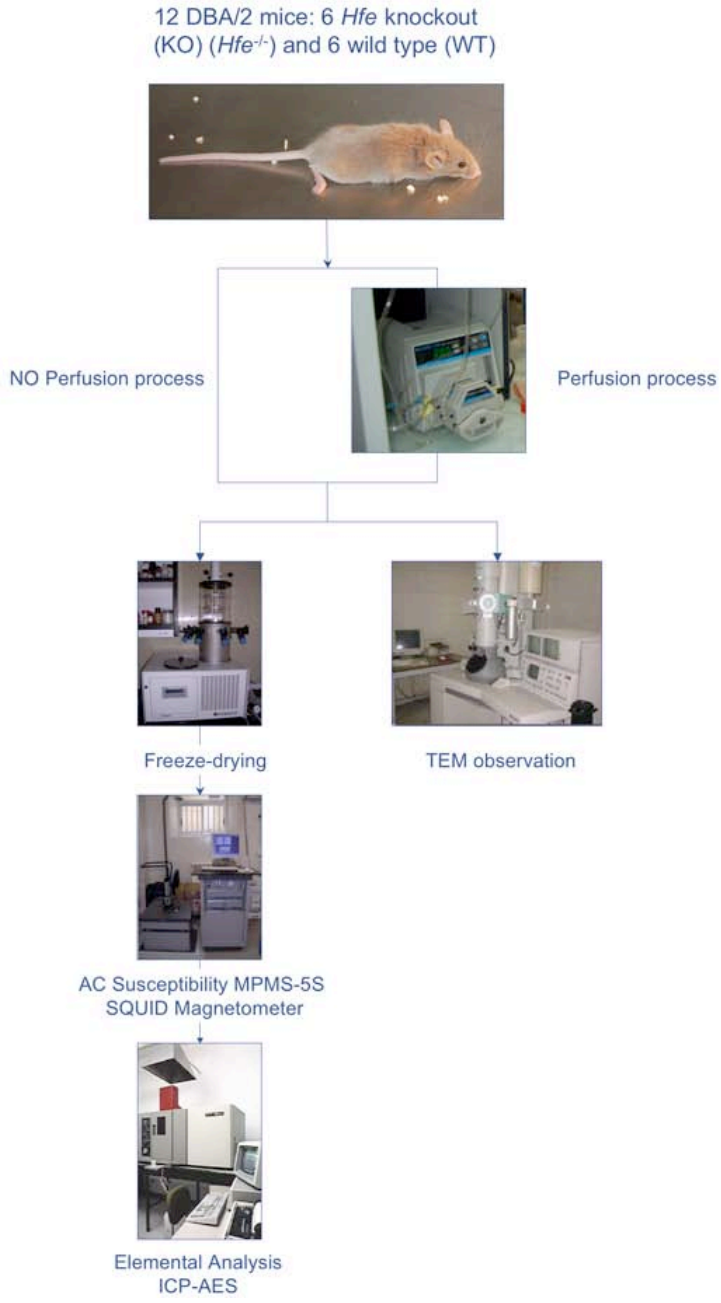

Fig. 76. Work protocol scheme.

4.2. Materials and methods

4.2.1. General considerations

As it has been explained in the previous chapter, in order to avoid metallic sample contamination during all the acquisition and treatments of the tissues, plastic tweezers and ceramic blades have been used.

In Fig. 51, a schematic representation of the different steps carried out in the work presented in this chapter is provided.

4.2.2. Animal model

A total of 12 DBA/2 mice, 8 female and 4 male, have been used in this study. Half of the animals were Hfe knockout and the rest were wild type, in a way that each KO mice had a WT counterpart of the same age and gender (see Table 12 for details).

All the experiments were performed in accordance with institutional and governmental guidelines and the experimental protocols were approved by the Midi-Pyrénées Animal Ethics Committee. WT and KO mice were housed in the IFR30 animal facility (4–6 animals/cage, 12:12 h light-dark cycle; 22 ± 1 °C, 60 ± 5% humidity). The animals had free access to R03 diet (UAR, Epinay-sur-Orge, France) containing 280 mg Fe/kg and distilled water.

4.2.3. TEM observations-fixation protocols

Two different protocols were used for the fixation of the tissues. Half of the animals, were sacrificed under pentobarbitone anaesthesia and portions of the livers, spleens and hearts were prepared for TEM observations immediately after tissue dissection. Fragments of the different tissues were fixed for 2h at room temperature and overnight at 4 ºC in a solution of 2% paraformaldehyde (PAF), 2% glutaraldehyde (Gluta) in 0.1 M phosphate buffer (PB). The rest of the animals were also sacrificed under pentobarbitone anaesthesia although the fixation of the tissues was performed by perfusion. The same fixative (2% PAF, 2% Gluta, 0.1M PB) was injected directly in the heart and pumped during 8 minutes at 20 ml / min. One ventricle was cut in order to eliminate the blood and the fixative solution. Then, a different solution containing 0.1 M phosphate buffer was pumped at the same rate during 2 minutes. A part of the liver was then dissected and left in the fixative at 4 ºC overnight.

All the tissues were then postfixed with 1% osmium tetroxide for 45 min at 4 ºC. After four washes with buffer, samples were treated with 2% uranyl acetate and dehydrated in graded series of acetone (50, 70, 90, 100%) for 15 min each at 4 ºC and embedded in Epon resin at room temperature for 24 h. The polymerization was done at 60 ºC for 48 h.

Ultra-thin sections (40-60 nm) were collected on formvar-coated grids and lightly stained with 2% uranyl acetate for 30-60 s or stained with saturated uranyl acetate and lead citrate by standard procedures.

The TEM characterization was carried out in a Jeol 1010 microscope operated at 100 kV and a Jeol 1200FX.

4.2.4. Freeze drying

The rest of the spleen, heart and liver tissues that were not used for the TEM analysis from the mice without perfusion, were immediately frozen at -80 ºC after their dissection. These tissues were freeze-dried during 48 h in a Telstar-Cryodos equipment and then ground to powder in order to have a homogeneous sample. The fixed liver samples of the perfused animals were stored at 4 ºC, freeze-dried during 24 h in a Heto PowerDry PL3000 and then ground to powder.

4.2.5. Magnetic measurements

The magnetic characterisation has been carried out in a Quantum Design MPMS-5S SQUID magnetometer with an AC susceptibility option. The measurements have always been performed with an AC amplitude of 0.45 mT at a frequency of 1 Hz in the temperature range 1.8-300 K. The presence of adsorbed oxygen in the samples, which would contribute to the susceptibility (Kanoh et al. 1996), has been checked and avoided by repeated runs above and below its boiling temperature in all the cases.

The powder of each liver sample was placed in individual gelatine capsules for the magnetic measurements. Due to the small amount of spleen and heart tissues available from each animal, a pool of samples was prepared for the magnetic characterisation. The spleen tissues of the KO mice (two female and one male) were placed together in the same gelatine capsule, and the same was done with the WT samples. The same procedure was also followed with the heart samples.

4.2.6. Elemental analysis

Inductively-coupled plasma atomic emission spectrometry (ICP-AES) was performed after microwave acid digestion (solution 4:1 (v/v) of HNO_3 (65%) and H_2O_2 (30%)) of the same freeze-dried samples that were magnetically characterised. The elemental analysis was focused on the determination of Fe, but the presence of other magnetogenic elements as Co, Ni, Mn and Cu, which may contribute to the magnetic results, was also included in the analysis.

4.3. Liver tissues

4.3.1. Elemental analysis

The elemental iron content of each liver tissue is shown in Table 12 and varies in a range between 1.729 and 3.903 mg Fe/g dry tissue for KO mice and between 0.371 and 0.636 mg Fe/g dry tissue for the WT ones. The content of other magnetogenic elements (Cu, Co, Mn and Ni) is always less than 0.003 wt% of the freeze-dried tissues.

From the data in Table 12, it can be observed that the KO animals have, as expected, a greater concentration of iron in the tissues than the WT ones. No significant differences are observed between 9 and 14 week old animals, in agreement with unpublished observations that hepatic iron concentration in *Hfe*$^{-/-}$ mice increases sharply after weaning but stabilizes after a few weeks.

The elemental analysis also show that females have higher iron content than those of the corresponding males of the same age, a fact that has been previously observed (Courselaud et al. 2004). The iron contents

of the KO mice tissues obtained from the elemental analysis are also similar to those previously determined by biochemical methods in the same animal model of iron overload (Dupic et al. 2002).

Animal	Genotype	Gender	Age (weeks)	Perfusion	[Fe] (mg/g)
1	WT	M	9	No	0.436
2	KO	M	9	No	2.579
3	WT	F	9	No	0.614
4	WT	F	9	No	0.636
5	KO	F	9	No	3.903
6	KO	F	9	No	2.537
7	WT	M	14	Yes	0.439
8	KO	M	14	Yes	1.729
9	WT	F	14	Yes	-
10	KO	F	14	Yes	2.496
11	WT	F	14	Yes	0.371
12	KO	F	14	Yes	2.764

Table 12. Liver elemental iron content of all the studied animals together with the information about their genotype (Wild Type/Knockout), gender (male/female), age and information about if they were perfused or not.

4.3.2. TEM and SAED

TEM observations of the KO liver tissues show hepatocytes with a dense cytoplasm where the nucleus and all the organelles are well preserved (Fig. 77). In these tissues, in unstained or lightly stained sections, several types of electron dense deposits, in which the presence of iron has been confirmed by in situ X-ray microanalysis, are observed in the cytoplasm of hepatocytes and Kupffer cells and also in intercellular

spaces. It is important to note that, in spite of the iron excess in the KO livers, the physiological tissue structure seems not to be altered.

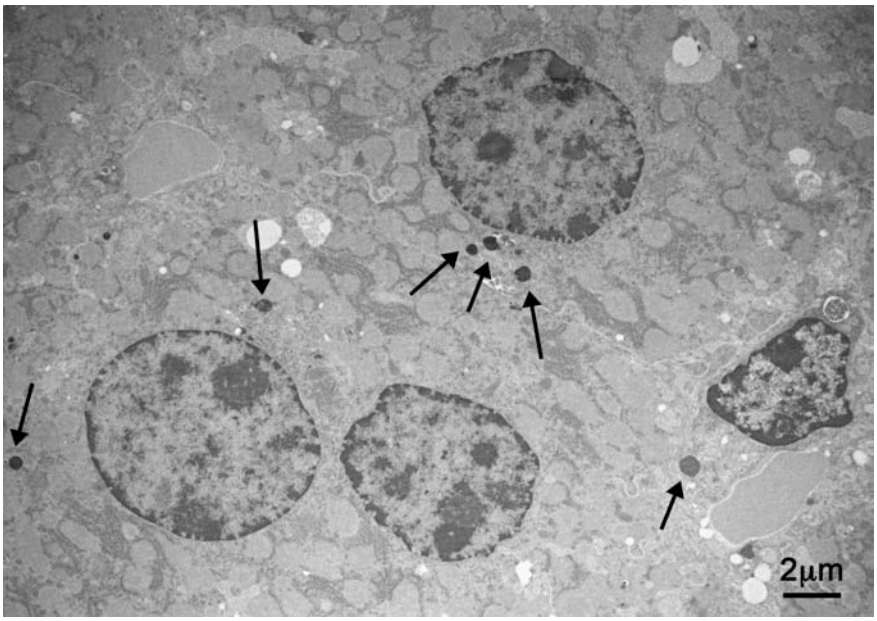

Fig. 77. Liver tissue TEM micrograph of a KO female mouse 9 weeks old. Electron-dense iron deposits (marked with arrows) can be observed in the cytoplasm of the hepatocytes.

Observations at higher magnification (Fig. 78) allow to classify the iron containing deposits into three types: i) cores of ferritin molecules (F) dispersed in the cytoplasm of cells, sometimes localised near the endoplasmic reticulum (ER), ii) cores of ferritin-haemosiderin molecules (#) in lysosomes-sideromes and iii) deposits of heterogeneous shape and size (U), observed mainly in the cytoplasm near the membrane and in the extracellular space.

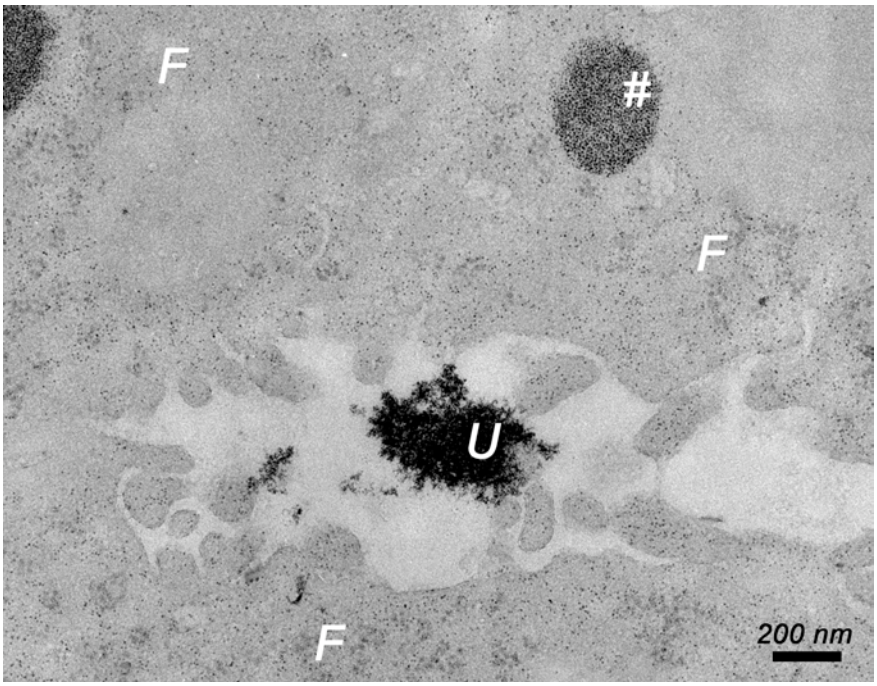

Fig. 78. TEM micrograph at higher magnification of the same liver tissue shown in Fig. 77 corresponding to a KO female mouse. Isolated spherical particles typical of ferritin (F), and lysosomes-siderosomes containing spherical electron-dense particles (#) can be observed in the cytoplasm of the hepatocytes, while very electron-dense deposits (U) are visible in the extracellular space.

The size of the type # aggregates ranges between 0.3 and 0.8 μm. This degree of aggregation seems to be the factor that affects relaxation time shortening in Magnetic Resonance Imaging (Gossuin et al. 2007).

SAED performed on the deposits type F and # show a mineralisation similar to ferrihydrite (Table 2), the most common mineral found in physiological ferritin cores (Cowley et al. 2000). A set of rings, different from those of ferrihydrite and consistent with haematite and/or goethite phases, appear in the diffraction pattern of type U deposits (Table 13), although a deeper study on their nature is still needed.

Six-line Ferrihydrite	Liver iron deposits			Haematite	Goethite
	Type F and #	Type U			
		0.41			0.418
			0.360	0.368	0.338
			0.260	0.270	0.269
					0.258
0.254	0.253	0.25-0.24		0.252	0.249
					0.245
0.223	0.224	0.22	0.210	0.221	0.219
0.197	0.197				
		0.183		0.184	
					0.172
0.172	0.170	0.170	0.171	0.169	0.169
					0.156
					0.151
0.151	0.147	0.147	0.147	0.149	0.147
0.147	0.145	0.145		0.145	0.145

Table 13. Calculated *d* spacings (nm) from the SAED ring data for the different deposits observed in the liver sections. Deposits type F and # correspond to isolated spherical particles and lysosomes-siderosomes containing spherical electron-dense particles respectively, while type U correspond to the very electron-dense deposits shown in Fig. 78 (the two data columns in this group correspond to two different occurrences of this type of deposits). For comparison, the corresponding values for ferrihydrite (a = b = 0.508 nm, c = 0.94 nm), haematite (a = b = 0.503 nm, c = 1.37 nm) and goethite (a = 0.461, b = 0.996 nm, c = 0.302 nm) (Cornell et al. 1996) are indicated.

Although their protein shell is not visible in these TEM micrographs, a large amount of ferritin cores can be observed in the cytoplasm. The actual presence of the ferritin molecules is evidenced from the shape (approximately spherical) and the size (not larger than about 8 nm) of their electron-dense cores that, besides, in unstained or lightly stained sections, appear mutually separated by the non electron-

dense protein shells (Iancu 1992). The presence of ferritin molecules near the ER may indicate a profuse synthesis of this protein in the liver tissues.

The size and shape of the iron-containing particles inside the lysosomes-siderosomes is similar to those of the ferritin cores. However, the apparent mutual contact between them may indicate that the protein shell has undergone certain degradation, analogously to what has been observed in the so-called secondary lysosomes (Iancu 1992; Harrison et al. 1996). This type of deposits have also been observed in the rat liver tissues characterised in the previous chapter and may probably also be related to the degradation sequence of ferritin in the lysosomes to form haemosiderin (Richter 1984; Iancu et al. 1997). In fact, as the mineral structure of these deposits determined by SAED is the same as the corresponding to the ferritins scattered in the cytoplasm, these type # deposits may be another example of the previously mentioned "prehaemosiderin" (St Pierre et al. 1987). Independently of the term used to describe these clusters, it is clear that they contain a large part of the total iron accumulated in the liver.

The intracellular and extracellular type U iron deposits observed in the micrographs show neither morphological nor crystalline similarities with the ferritin cores. Their location near the membranes and in the extracellular space may indicate a process of iron removal from the cell, possibly explaining why the tissues are relatively well preserved in spite of the iron excess. In fact, the beneficial role of biomineralisation processes in preventing iron toxicity has been pointed out in relation to the formation of haemosiderin (Ward et al. 2000). Goethite deposits in tissues have previously been observed in conditions of iron overload (St Pierre et al. 1992; St Pierre et al. 1998; Ward et al. 2000), while haematite, as far as we know, has only been mentioned as a minor phase

in physiological ferritin cores (Cowley et al. 2000; Quintana et al. 2004). It is therefore in this work, in our opinion, the first time that the presence of haematite is detected in iron overload situations.

As previous studies have reported the transformation from ferrihydrite either to haematite or to goethite, we can hypothesize that our type U deposits may be originated from the ferritin ferrihydrite cores. However, while it is known that haematite can be formed from the dehydration of ferrihydrite, the formation of goethite from ferrihydrite would imply its dissolution and further nucleation (Cornell et al. 1996).

As other authors have reported the transformation from ferrihydrite to other iron oxide structures by the effect of the electron beam (Pan et al. 2006), dedicated experiments have been done to assure that the crystalline structure of type U deposits is not due to such effect. In our case, the SAED patterns of ferrihydrite deposits have not been altered after several minutes of irradiation.

4.3.3. AC magnetic susceptibility

The temperature dependence of the AC susceptibility per mass of sample of mice liver samples is shown in Fig. 79 and Fig. 80. For the sake of clarity only the results from six animals are shown in the graphs, however, data from all the characterised tissues have been detailed in Table 14.

A low temperature paramagnetic tail can be observed in $\chi'(T)$ in all the liver samples. The in-phase component of some of the samples also shows a maximum, or a small shoulder, around 11 K that, together with the non-zero out-of-phase susceptibility at the same temperature range,

evidence a magnetic relaxation phenomenon. The out-of-phase susceptibility of all the liver tissues shows a single maximum around 8 K and stays negligible, within the accuracy of the experiments, above approximately 25 K reminding the results obtained for rat liver ferritin presented in the previous chapter. The location in temperature and the value of the susceptibility per mass of sample of the out-of-phase maxima of all the samples is shown in Table 14.

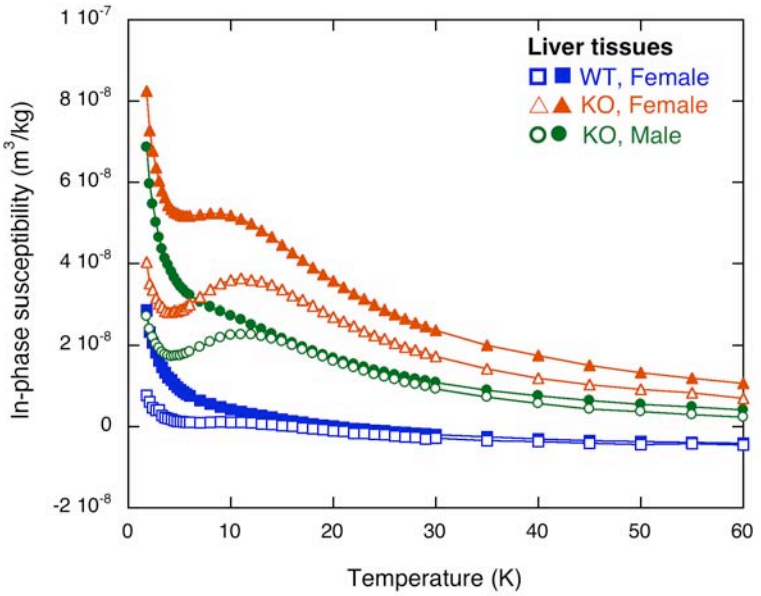

Fig. 79. Temperature dependence of the in-phase susceptibility $\chi'(T)$, at 1 Hz, per mass of freeze-dried liver tissue corresponding to mice of different gender and genotype, some of them subjected to perfusion. Filled symbols correspond to non-perfused animals and empty symbols to the perfused ones.

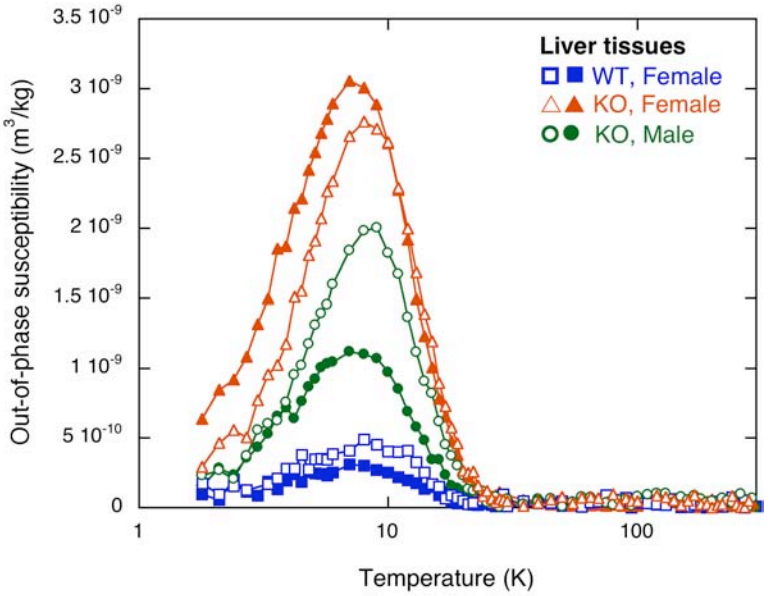

Fig. 80. Temperature dependence of the out-of-phase susceptibility $\chi''(T)$, at 1 Hz, per mass of freeze-dried liver tissue corresponding to mice of different gender and genotype, some of them subjected to perfusion. Filled symbols correspond to non-perfused animals and open symbols to the perfused ones.

From the study of homologous tissues in rats (see previous chapter) and from available AC magnetic susceptibility data of ferritin standards (Luis et al. 1999; Allen et al. 2000) and the characterisation shown in the previous chapter, the $\chi''(T)$ maximum observed in these mice tissues can be assigned to the presence of ferritin or, alternatively, to the cores of partially degraded ferritin whose crystalline structure and size are still similar to those of ordinary ferritin. However, the $\chi''(T)$ maxima of the mice tissues are located at slightly lower temperatures than those previously observed maxima for rat liver ferritin; a phenomenon that may result from small differences in the size of the iron-containing crystallites

inside the ferritin cages or from a qualitative different biomineralisation between the two animal genera.

Animal	Genotype	Gender	χ''_{max} (m^3/kg)	μ_{eff} (μ_B)
1	WT	M	$1.937 \cdot 10^{-10}$	2.43
2	KO	M	$1.119 \cdot 10^{-9}$	2.69
3	WT	F	$3.087 \cdot 10^{-10}$	2.95
4	WT	F	$3.094 \cdot 10^{-10}$	2.92
5	KO	F	$3.056 \cdot 10^{-9}$	3.15
6	KO	F	$1.896 \cdot 10^{-9}$	3.46
7	WT	M	$2.445 \cdot 10^{-10}$	3.72
8	KO	M	$2.002 \cdot 10^{-9}$	3.23
9	WT	F	$4.011 \cdot 10^{-10}$	-
10	KO	F	$2.763 \cdot 10^{-9}$	3.28
11	WT	F	$4.890 \cdot 10^{-10}$	3.61
12	KO	F	$2.987 \cdot 10^{-9}$	3.37

Table 14. Height values of the $\chi''(T)$ maximum for the different liver tissues, genotype (WT / KO), gender and effective moment per iron ion ($\mu_{\#}$). The $\chi''(T)$ maximum is expressed per mass of dry tissue.

With respect to the contribution of type U deposits to the total magnetic susceptibility of the tissues, we expect it to be under the detection limits of the magnetic characterisation. This assumption is based (i) on the fact that these aggregates are quite sparse in the volume in comparison with the ferritin cores and (ii) on the relatively large size of these deposits that, given the antiferromagnetic character of haematite and goethite, result in smaller magnetic moments per iron ion.

When plotting the out-of-phase susceptibility per mass of sample, the height of the χ'' maximum (data in Fig. 80 only for selected samples and in Table 14 for all of them) informs about the amount of iron in the

form of ferritin cores. In Fig. 80, it can be observed that, independently on whether the animals were perfused or not, the $\chi''(T)$ maxima for the KO mice are always higher than for their WT counterparts. This result indicates that the genetically provoked iron overload consists of, not only a greater amount of total iron, but a greater amount of iron in the form of ferritin. When looking at differences between the animal gender, it can be observed that the maximum in the out-of-phase susceptibility per mass of sample is always lower for males than for females in both genotypes, which means that they have a lower ferritin iron content.

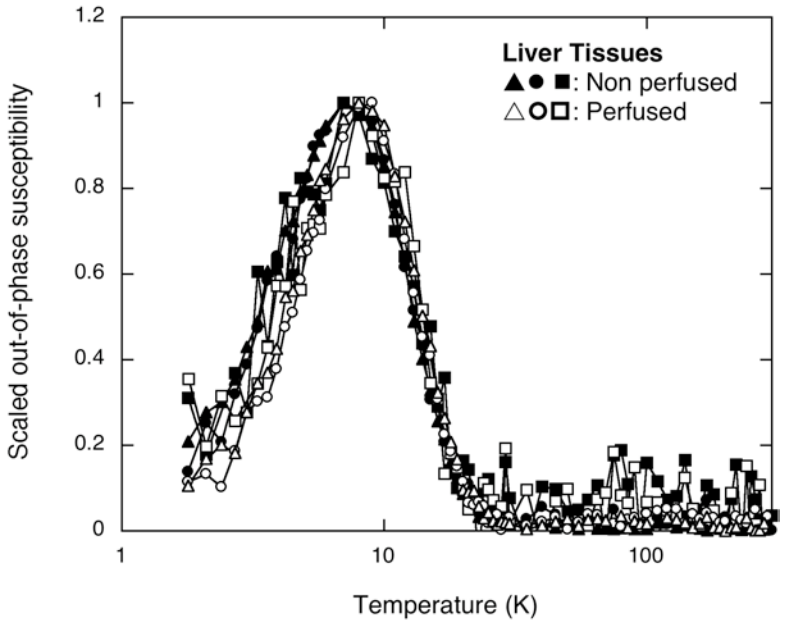

Fig. 81. Comparative plot of the $\chi''(T)$ profiles, scaled to their respective maxima, for the magnetically characterised liver tissues.

In order to study the differences in shape, width and location of the $\chi''(T)$ maxima it is usually adequate to scale the curves to their

maximum height. In Fig. 81 it can be observed that there is a rather good coincidence of the $\chi''(T)$ profile for all the liver samples (perfused and non-perfused, WT and KO) suggesting that in all these cases a very similar biomineralisation, in terms of the formed iron oxide or oxyhydroxide, may exist. However, when looking in more detail, it can be observed that, while the high temperature flank of the $\chi''(T)$ profile very well coincides in all the cases, likely due to the size limitation of the ferritin cavity, there are significant differences in the low temperature flank between perfused and non-perfused animals. This result would indicate that, assuming a similar biomineralisation in all the cases, the size distribution of the iron-containing crystallites in the case of the non-perfused animals is more extended to small sizes than in the case of the perfused ones.

Although, as mentioned, no big differences between the $\chi''(T)$ data for perfused and non-perfused animals, of the same genotype and gender, are observed, they do differ in the in-phase component. The low temperature tail observed in $\chi'(T)$ originates at paramagnetic iron-containing species, that is, molecules or microscopical entities in which the iron atoms may be either bounded to organic ligands (e.g. deoxyhaemoglobin, transferrin) or not, but never in the form of iron oxide or oxyhydroxide nanoparticles. This paramagnetic contribution may correspond either to intracellular iron-containing species or to other substances remaining in the blood vessels. The observed $\chi'(T)$ data for the non-perfused animals, independently of gender and genotype, always present a much greater paramagnetic contribution than for the perfused ones. This result appears logical because in the perfusion process the fixative is introduced through the blood vessels – the iron-containing

species from the blood are substantially removed – reducing their paramagnetic contribution.

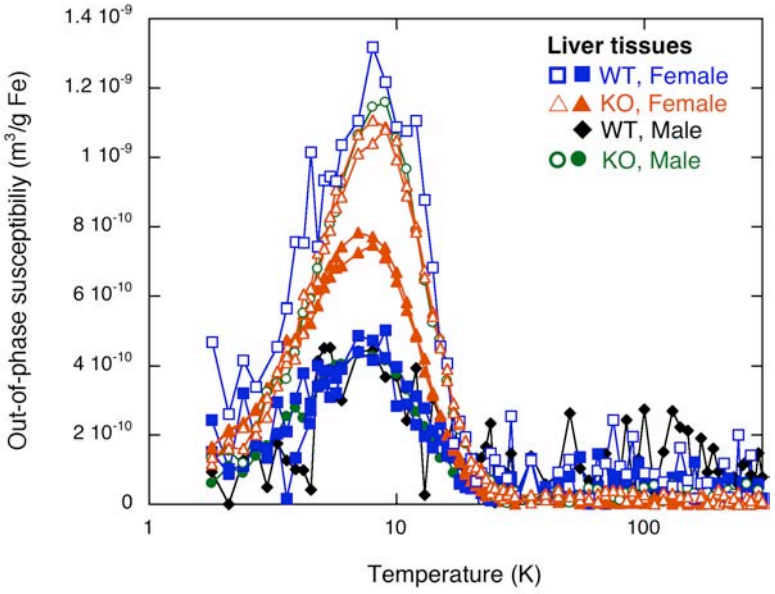

Fig. 82. Temperature dependence of the out-of-phase susceptibility $\chi''(T)$, at 1 Hz, per mass of elemental iron for the liver tissues. Filled symbols correspond to non-perfused animals and open symbols to the perfused ones.

Within a deeper analysis of the iron speciation in the liver tissues, the $\chi''(T)$ data, expressed per mass of iron, are shown in Fig. 82. In this type of representation, if all of the iron atoms in a given tissue were present in the form of a single iron-containing species (e.g. ferritin in this case), the corresponding $\chi''(T)$ data, *per mass of iron*, would coincide with that of isolated species. However, the variable presence of other species not contributing to χ'', like paramagnetic iron, diamagnetic iron, or other weakly magnetic forms of iron as the invoked haematite and/or goethite deposits, will result in that the greater the ratio $Fe_{ferritin}/Fe_{total}$, the higher the $\chi''(T)$ ferritin profile when represented per mass of iron. In particular,

in Fig. 82, the $\chi''(T)$ data points for perfused animals significantly appear higher than for the non-perfused ones. The previously discussed observation of a smaller paramagnetic component in perfused animal tissues (see Fig. 79) independently of their gender or genotype, as it clearly implies removal of iron ions is also consistent with the same idea.

It is also worth to realise that the height of the $\chi''(T)$ maxima per mass of iron for the perfused mice is very similar in all the cases. This coincidence means that the $Fe_{ferritin}/Fe_{total}$ ratio is the same for all those samples. The same thing, with the same interpretation, seems to occur for the non-perfused tissues, although an additional group – the KO females – presents a higher maximum: a fact whose biological explanation is not clear yet.

In the high temperature region of the AC susceptibility, all the $\chi'(T)$ curves show Curie-type behaviour. As it has been previously explained, the high temperature paramagnetic and superparamagnetic contributions are mixed up on a single Curie-law susceptibility whose information is condensed into the value of the effective moment μ_{eff} per iron ion. As each iron-containing species usually has a characteristic effective moment per iron ion, namely, 5.46 μ_B for deoxyhaemoglobin, 0 μ_B for oxyhaemoglobin and 3.4 μ_B for ferritin [(Pauling et al. 1936; Alpert et al. 1975; Pauling 1977) and data from Chapter 3], the effective moment per iron ion determined for the whole tissue sample results from the average of the μ_{eff} values, weighted with the relative abundances of each species.

The effective moments per iron ion of all the characterised samples are shown in Table 14. It can be seen that μ_{eff} = 2.93 ± 0.36 (mean + s.d.) in the case of non-perfused animals and 3.23 ± 0.17 for the

perfused ones. This significant result may indicate that the iron removed in the perfusion process, although being in part of paramagnetic nature, may include an important content of low magnetic moment iron, which may be of diamagnetic and/or antiferromagnetic (large particle size) nature.

4.4. Spleen and heart tissues

4.4.1. Elemental analysis

For spleen and heart tissues, there are no big differences in the iron content between the KO and WT tissue pools (Table 15). This fact indicates that in this animal model, iron is accumulated mainly in the liver.

Animal	Organ	Genotype	Gender	[Fe] (mg/g)
1+3+4	Spleen	WT	2F+1M	1.996
2+5+6	Spleen	KO	2F+1M	1.835
1+3+4	Heart	WT	2F+1M	0.450
2+5+6	Heart	KO	2F+1M	0.375

Table 15. Details of the characterised pools of spleen and heart tissues: genotype (Wild Type/Knockout), gender (male/female) and elemental iron content per mass of dry tissue. All the tissues correspond to 9 weeks old non-perfused animals.

4.4.2. AC magnetic susceptibility

The spleen and heart pools of the KO and WT animals present a low temperature paramagnetic tail in the in-phase susceptibility in all the cases (Fig. 83). The corresponding out-of-phase susceptibility of the four

samples is plotted in Fig. 84. It can be observed that the heart samples show a nearly negligible out-of-phase susceptibility in all the temperature range, while a small and rather noisy maximum at low temperatures can be observed for the spleen samples. For both tissues, the susceptibility results do not show significant differences between the KO and the WT animals.

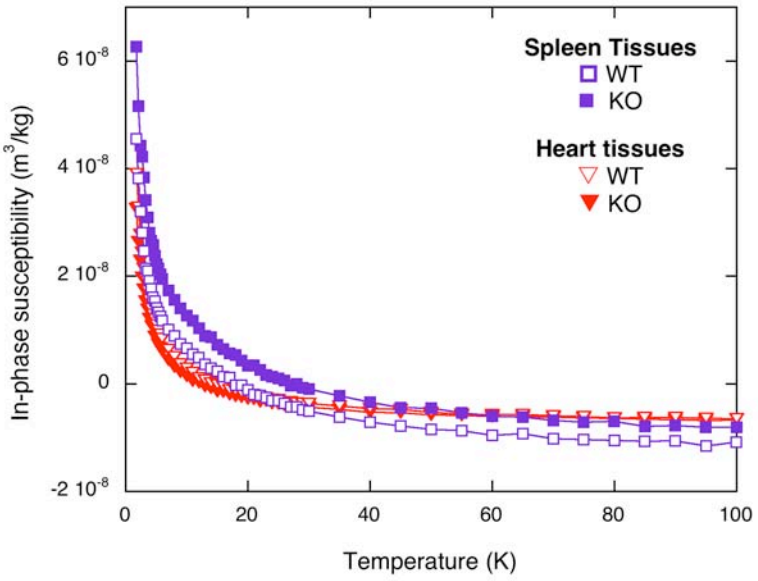

Fig. 83. Temperature dependence of the in-phase susceptibility $\chi'(T)$, at 1 Hz, per mass of freeze-dried tissues of the spleen and heart tissue pools corresponding to mice of different genotype.

The χ'' maximum for spleen tissues (Fig. 84) whose presence very likely corresponds also to ferritin iron, is located at slightly lower temperatures than for liver tissues. This finding may indicate slight differences, in terms of biomineralisation or size of the ferritin core crystallites, between spleens and livers. Similar differences in the out-of-

phase susceptibility between tissues have also been previously observed in rats (see Chapter 3).

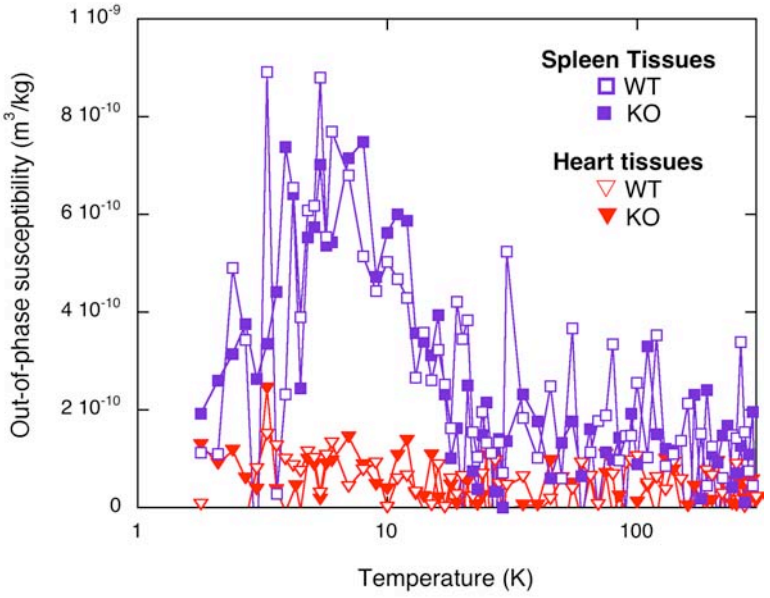

Fig. 84. Temperature dependence of the out-of-phase susceptibility $\chi''(T)$, at 1 Hz, per mass of freeze-dried tissues of the spleen and heart tissue pools corresponding to mice of different genotype.

For heart tissues, $\chi''(T)$ is nearly negligible in all the temperature range meaning that the detection of ferritin iron in these samples is beyond the limits of the technique. For both spleen and heart tissues, the susceptibility of the pool samples in the case of KO animals does not differ significantly from the WT ones indicating that there is no particular iron accumulation in these tissues, in agreement with the determined elemental iron contents (Table 15).

4.5. Conclusions

In this chapter, for the first time, for the first time, AC magnetic susceptibility measurements together with TEM analysis have been used to study the iron deposits formed in the tissues of DBA/2 Hfe KO mice.

No differences between KO and WT mice have been observed in the iron content of spleen and heart tissues. However, a great iron accumulation in liver tissues has been found for the KO mice. Furthermore, when comparing the liver iron accumulation between genders it can also be concluded that females have always a greater iron overload than males.

The differences in shape and location of the $\chi''(T)$ maxima, corresponding to the ferritin cores contribution, observed between different tissues of the same animal and between different animal genera (data of these mice and previous data for rats in the previous chapter) may indicate a slightly different qualitative biomineralisation or different size distribution of the iron-containing crystallites.

The perfusion procedure has revealed that a considerable part of the paramagnetic contribution observed in the non-perfused tissues comes from iron-containing species in the remaining blood.

Iron deposits whose morphology, size and crystalline structure appear different from those of ferritin and those of lysosomes-siderosomes containing ferritin-haemosiderin have been observed in the liver tissues by TEM and SAED analysis. This finding deserves a more profound study, as it may be related with the apparently healthy aspect of the tissues, and opens the way to future studies on biomineralisation processes in cases of iron overload and related to potential treatments of the disease.

The combination of magnetic characterisation and TEM analysis has been proven to be of great usefulness to study the nature and the evolution of tissue iron deposits in conditions of iron overload.

The AC susceptibility results obtained for this model of iron overload can be compared with the previously characterised in Chapter 3 obtained after a single injection of iron dextran in rats. In that model, iron deposits were observed in liver, spleen, muscle, heart and kidney tissues while DBA/2 Hfe KO mice only show liver iron overload.

5.Magnetic carriers: Biodistribution and quantification

5.1. Introduction and main aims

As it was described in the introduction, the magnetic characterisation of biological samples is not free of difficulties, sometimes being near the detection limits of the technique due to the low iron content of the samples in physiological conditions. For this reason, in the previous two chapters, iron overload situations have been explored by magnetic means, being the iron excess the fact that made easier the analysis. In this chapter a completely different situation will be studied:

the analysis of magnetic carriers in tissues. Magnetic carriers are usually composed of ferrimagnetic iron oxides nanoparticles that, due to their high magnetic moment, can be used for biochemical and clinical applications as drug delivery, biosensors, hyperthermia treatments or magnetic resonance imaging (MRI) contrast agents (Häfeli et al. 1997).

Nowadays, many people is working in the development of these compounds, however, most of the work is focused on verifying in vitro that the magnetic carriers fulfil their specific function and there are just a few studies on their biodistribution in tissues. From these previous works, it can be said that there is not a well-established way of studying the magnetic carriers metabolism in the tissues as most of the techniques used present some difficulties. Transmission Electron Microscopy (TEM) can be used if the morphological and crystalline properties of the carriers are known in advance, however the obtained information is intrinsically local and rather qualitative and ^{59}Fe radiolabelling is insensitive to particle degradation (Majumdar et al. 1989). Recent works are making use of relaxometry measurements to quantify iron oxide particles in liver tissues (Briley-Saebo et al. 2006), although special care must be taken in this quantification procedure due to possible intracellular particle aggregation effects. The characterisation of the tissue magnetic susceptibility has also been previously used to monitor the biodegradation of magnetic carriers (Okon et al. 1994), although this study did not include the analysis of the susceptibility in a wide temperature range that can provide more results.

The amount of iron in the form of magnetic carriers typically injected is usually negligible in comparison with the endogenous iron making it difficult their monitoring by conventional elemental analysis of the tissues. However, as these drugs have a magnetic susceptibility much

higher than ferritin, it allows their detection in spite of their low iron content in the tissues. Therefore, it seems interesting the use of AC magnetic susceptibility measurements in order to characterise the biodistribution of magnetic carriers in the tissues, in a similar way to the performed in chapter 3 in the study of the iron-dextran administration to rats. However, the ferrimagnetic character of most of the magnetic carriers enhances the interparticle interactions that induce alterations in the AC susceptibility results (Jonsson et al. 1995; Jonsson et al. 1998). Because of this, a detailed study of the relationship between the concentration and the dipole-dipole interactions in the magnetic carrier must be performed in advance of the administration to the animals. Nevertheless, the alterations of the AC susceptibility properties due to the dipole-dipole interactions will inform about whether the particles are homogeneously distributed in the tissue or, in contrast, they present some degree of local aggregation.

In the first part of this chapter, a description of the low temperature AC susceptibility of a series of dilutions of a magnetic carrier currently used in magnetic resonance imaging (MRI) in order to assess the influence of dipolar interactions on the $\chi''(T)$ curves is provided. Then, a study of the biodistribution of the magnetic carrier in rats is described together with the quantitative analysis of the amount of the magnetic carrier that has travelled to the tissues and the endogenous ferritin present in them.

Magnetic carrier

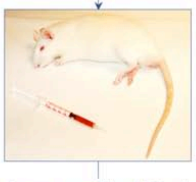

Rats are sacrificed 30 min after the injection

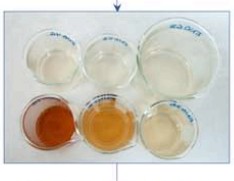

Dilutions of the original product

Freeze-dryer

AC Susceptibility MPMS-5S SQUID Magnetometer

Elemental Analysis ICP-AES

Fig. 85. Work protocol scheme

5.2. Materials and methods

5.2.1. General considerations

As it has previously been explained before, iron is a trace element in the tissues so special care has to be taken to avoid sample contamination during the acquisition and treatments of the tissues using non-metallic instruments.

In Fig. 85 it can be observed a scheme of the work that is presented in this chapter.

5.2.2. Dilutions of the magnetic carrier

The superparamagnetic contrast agent Endorem® (Guerbet laboratories) has been chosen to perform its biodistribution study in the tissues as it is commonly used in the clinical practice. This compound has also been marketed under the name Feridex®, its generic name is *ferumoxide* and the acronym is *AMI-25*. The original product has a nominal iron content of 11.2 mg/ml and is currently known to contain magnetite nanoparticles of a size in the range of 5-10 nm (Jung et al. 1995).

A series of dilutions of the original drug were performed in order to study the effect of dipolar interactions in the AC magnetic susceptibility. This dilution procedure has the objective of generating samples containing the same magnetic carrier but with different number of particles per unit volume. Different volumes of the contrast agent were

added to 1% w/v agar gel solutions (at ~55 ºC) prepared using Milli-Q® water and allowed to cool down to room temperature in a warm water ultrasonic bath. The use of the warm water helps to slow down the solidification procedure while the ultrasonic bath allows having a homogeneous distribution of the particles in the agar gel. More diluted samples were prepared in the same way but starting from a 1/100 dilution of the same contrast agent in Milli-Q® water. The matrix for dispersing the magnetic particles was agar following current methods to simulate biological tissues (Pardoe et al. 2003).

As part of the sample mass of the gels will be lost during the freeze-drying process, for their use in the magnetic characterisation, the iron concentration of each sample must be recalculated after the liophilization. The range of the iron contents of the diluted samples is between 0.0308 mg/g and 58.9 mg/g, while the concentration of the freeze-dried product is 160 mg/g. The specific iron content is listed in Table 16.

5.2.3. Animal model

Three adult male Wistar rats (WIHSIMA200Z), of a weight of the order of 290 g, were purchased from Charles River Laboratories, Spain. Animals were housed at the Universidad de Zaragoza for the acclimatisation process during 7 days under constant environmental conditions on a 12h light-dark cycle, controlled temperature and ventilation. All animals were allowed *ad libitum* access to both food and water. The experiments were performed with the approval of the Ethical Committee for Animal Experiments of the Universidad de Zaragoza.

Animals were sedated under a single dose of sodium pentobarbital anaesthesia (25 mg/ml/kg). Following the doses established for contrast enhancement in humans, a single dose of Endorem® (Guerbet), diluted in glucose, at 15 μmol Fe per kg body weight was administered intravenously to two rats named *rat 1* and *rat 2*. The additional rat, used as control, received 5% glucose solution.

The animals were sacrificed 30 minutes after the drug administration and the different tissues from each rat were removed using nonmetallic instruments, as ceramic blades and plastic tweezers in order to avoid a possible source of iron contamination from the instrumentation. The spleen, kidneys, heart and liver of each animal were dissected, rinsed with isotonic saline solution (0.9% NaCl) to remove excess blood and stored at -20 ºC until being freeze-dried.

The philosophy of this work is not to carry out a statistically significant biodistribution study, which would require a greater number of individuals, instead of the three animals used. In contrast, the main aim is to discuss the usefulness of measuring the AC susceptibility in the qualitative and quantitative determination of the presence of magnetic carriers in biological tissues, for which the consideration of the tissue magnetic properties of selected individuals is enough.

5.2.4. Freeze-drying

The original liquid suspension of the contrast agent as well as the prepared dilutions in agar were freeze-dried in a Telstar-Cryodos equipment. Special care was taken in the weight of the samples before and after the freeze-drying process in order to accurately calculate the

iron content per mass of dry sample. The iron concentrations in the resulting solid agar dilutions were 0.0308, 0.155, 0.793, 3.98, 20.6, 45.5 and 58.9 mg Fe g^{-1} and the corresponding samples were labelled from S1 to S7, respectively. The iron concentration of the freeze-dried original liquid suspension (labelled as E) is 106 mg Fe g^{-1}.

All the tissues were also freeze-dried during 48 h in the same equipment as the agar dilutions of the magnetic carrier. The complete freeze drying was verified by making sure that the samples have lost around 70% of its original weight and also by observation of the tissues. The freeze-dried tissues were then ground to powder in a mortar, to get a homogeneous sample, and stored at room temperature.

5.2.5. Magnetic measurements

The resulting solids obtained after the freeze-drying process were placed into gelatine capsules for the magnetic measurements.

A Quantum Design MPMS-5S SQUID magnetometer with an AC susceptibility option has been used for the magnetic characterisation. The measurements have always been performed in the temperature range between 1.8 and 300K with an AC amplitude of 0.45mT and at a frequency of 1 Hz. Selected samples were also measured at different frequencies.

In order to assure the absence of any magnetic contribution coming from adsorbed oxygen in the samples, repeated runs above and below its boiling temperature were used in the measurements of each sample. These precautions made it increase the duration of the magnetic experiment up to typically 15 hours per sample.

5.2.6. Elemental analysis

After the magnetic characterisation, the freeze-dried tissue powders were submitted to elemental analysis by inductively coupled plasma atomic emission spectrometry (ICP-AES).

The elemental analysis was performed after acid microwave digestion of the samples (dilution 4:1 (v/v) of HNO_3 (65%) and H_2O_2 (30%)).

Although this analysis aims at the determination of the iron content, other elements (Co, Ni, Mn and Cu) have also been studied in order to discard any other contribution to the magnetic results.

5.3. Magnetic carrier characterisation

The knowledge of the magnetic properties of the magnetic carrier that is going to be administered to the rats, with special emphasis in the influence of the interaction effects in the results, is a key step for the understanding of the magnetic properties of the tissues. For this reason, a detailed magnetic characterisation of the dilutions of the magnetic carrier has been performed and is described ahead.

In Fig. 86 to Fig. 89 the in-phase and out-of-phase susceptibility data per mass of sample and per mass of iron of the agar dilutions (S1-S7) together with the freeze-dried original sample (E) are presented. In both kinds of graphs, the samples exhibit a single maximum in the in-phase susceptibility together with a maximum in the out-of-phase susceptibility

located at slightly lower temperatures, indicative of particle magnetic blocking.

As the mass of all the samples introduced in each gelatine capsule is very similar, it is clear that, when representing the data per mass of sample, the height of the maxima increases for increasing concentration in both the in-phase and the out-of-phase components.

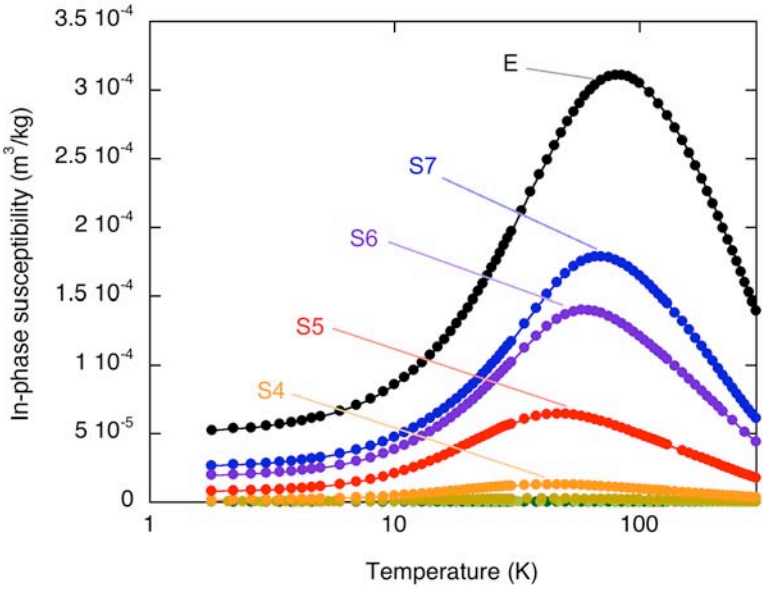

Fig. 86. Temperature dependence of the in-phase susceptibility, at 1 Hz, per mass of freeze-dried dilution of the magnetic carrier corresponding to different particle concentration (S1-S7). The filled circles correspond to the freeze-dried original liquid suspension (E).

In all the samples it is observed that the experimental χ'(T) curves are vertically shifted in a quantity that does not depend neither on temperature nor on the iron content of samples. The low magnetic response of the most diluted samples clearly points to the presence of a

non-negligible diamagnetic contribution, χ'_{dia}. As for the representation per mass of iron it is important to subtract the diamagnetic contribution in the in-phase susceptibility data, Equation 12 has been used to estimate its value.

Sample S2 has been employed for the determination of χ_{dia}, as it meets the compromise between having the best signal to noise ratio while keeping negligible the interaction strength, and the value has been estimated to be $8\pm1 \times 10^{-9}$ m^3 / kg. This diamagnetic susceptibility value has been used to correct the $\chi'(T)$ curves of the rest of the samples.

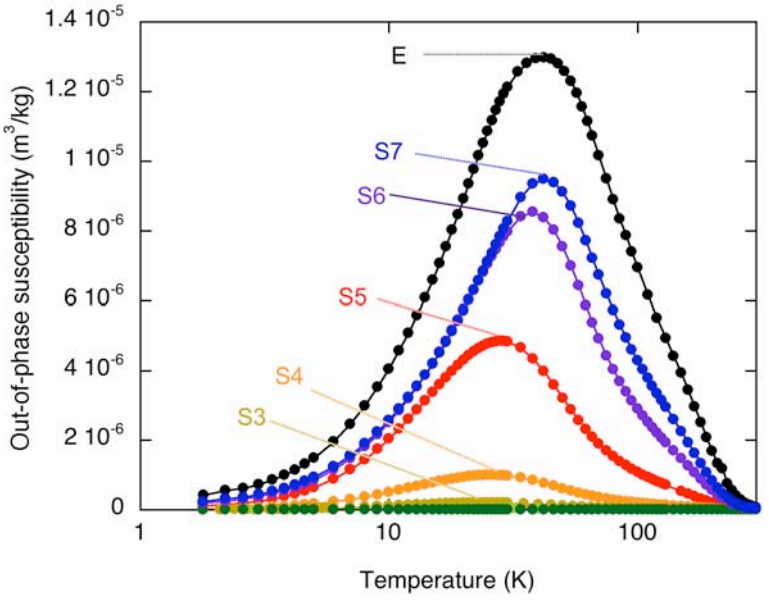

Fig. 87. Temperature dependence of the out-of-phase susceptibility, at 1 Hz, per mass of freeze-dried dilution of the magnetic carrier corresponding to different particle concentration (S1-S7). The filled circles correspond to the freeze-dried original liquid suspension (E).

The height of the maxima in both the in-phase and the out-of-phase components of the susceptibility per mass of iron decrease for increasing concentration and besides a shift towards higher temperatures of the location of the peaks can also be observed. This behaviour has been previously observed (Jonsson et al. 1995; Zhang et al. 1996; Djurberg et al. 1997) and is related to the presence of interparticle interactions. It can be observed that for decreasing concentrations, the $\chi''(T)$ profiles converge to a single profile. The deviations from the behaviour of the most diluted samples are an indication of the interacting particle magnetic dynamics of the more concentrated samples instead of the single particle dynamics of the more diluted ones. Below 0.1 wt% Fe, the interparticle interaction seems not to affect the AC susceptibility.

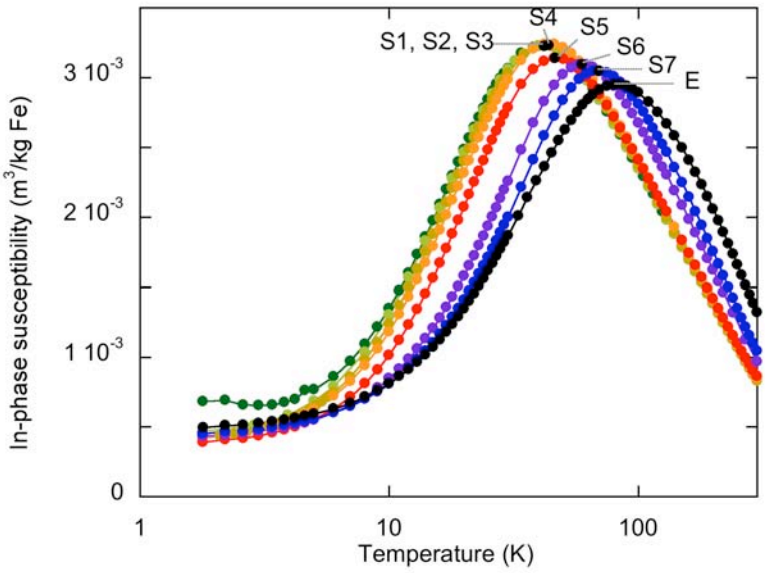

Fig. 88. Temperature dependence of the in-phase susceptibility, at 1 Hz, per mass of iron of the magnetic carrier corresponding to different particle concentration (S1-S7). The filled circles correspond to the freeze-dried original liquid suspension (E).

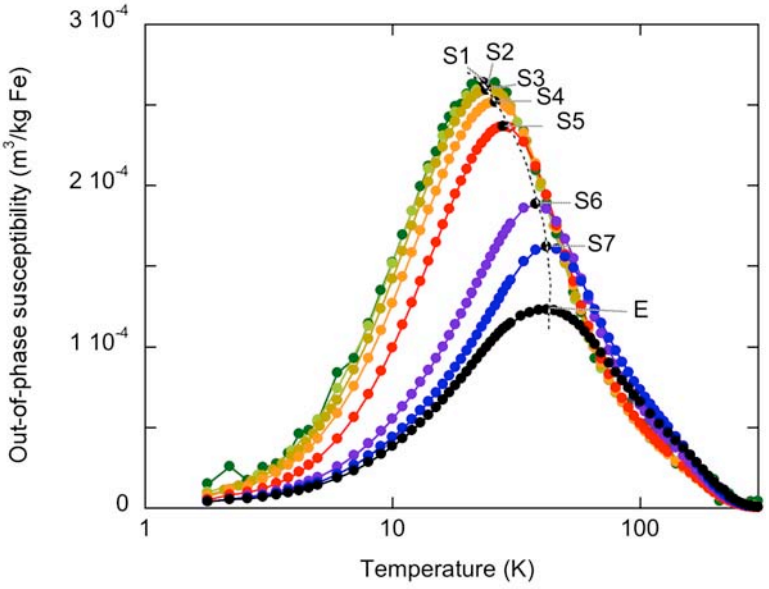

Fig. 89. Temperature dependence of the out-of-phase susceptibility, at 1 Hz, per mass of iron of the magnetic carrier corresponding to different particle concentration (S1-S7). The filled circles correspond to the freeze-dried original liquid suspension (E).

In order to study the interparticle interactions, the value of the preexponential factor of the Arrhenius equation, τ_0, has been calculated. The two different methods for the calculation of τ_0, described in chapter 1, have been applied to sample S2. In Fig. 90, the τ_0 value obtained from the optimum superposition of the curves yields a value of $10^{-12\pm1}$ indicating that the dipolar interaction is negligible at least up to this concentration.

The alternative method for the calculation of τ_0 based on the Equations 12 and 13 that suggest the plotting of $d(T\chi')/dT$ versus χ'' as a way to obtain τ_0 is presented in Fig. 91 for sample S2. The plot clearly shows both the low ($T\rightarrow0$) and high ($T\rightarrow\infty$) temperature tails. Although

in theory both equations can be used to obtain τ_0, in practice the experimental $\chi''(T)$ data does not actually cover the low temperature range as well as the high temperature range. Hence we have used in this case the high temperature approximation. By using Eq. 13 we have estimated from the initial slope (solid line) that τ_0 is around $10^{-12\pm1}$ s, a value consistent with that expected for noninteracting nanoparticle systems and also in agreement with the value obtained from the scaling plot shown in Fig. 90.

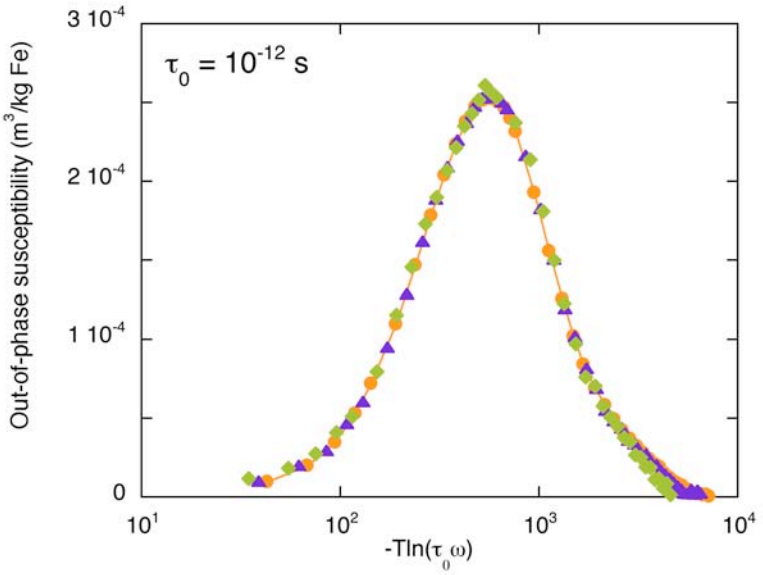

Fig. 90. Scaling plot of the out-of-phase susceptibility at 1 (circles), 10 (triangles) and 120Hz (diamonds) for sample S2. The best superposition is obtained with $\tau_0=10^{-12\pm1}$s. the solid line is just a guide for the eye.

The second method has been used with the rest of the samples to see the deviation of τ_0 from values expected for non-interacting particles assemblies, as shown in Fig. 92. It can be observed that for increasing

particle concentration (increasing dipole-dipole interaction strength) a progressive decrease of the prefactor value towards unphysical values takes place, as it has also been observed in the deviations in temperature location and height of the $\chi''(T)$ maxima per mass of iron.

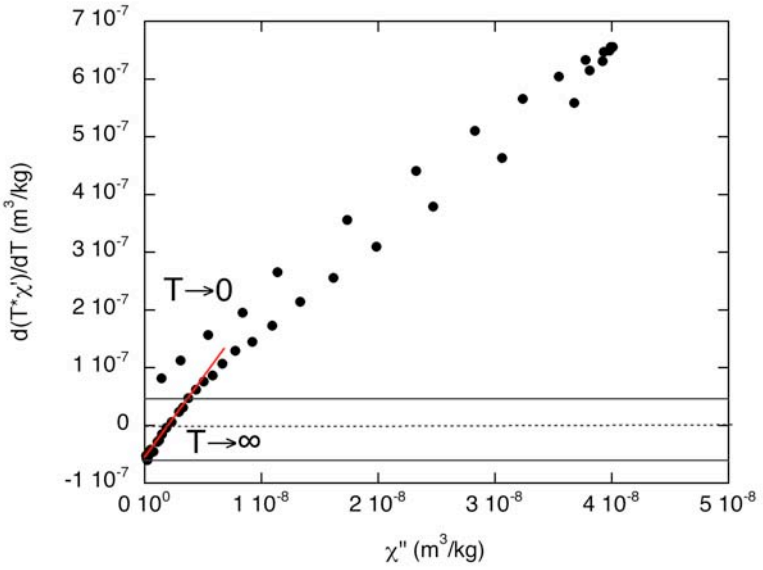

Fig. 91. Alternative method for the determination of τ_0, at 1 Hz, of sample S2. The low and high temperature ends of the curve are explicitly indicated. The horizontal solid lines show the ordinates at the origin of the curve that, according to Eq. 12 and 13, can be used to estimate χ'_{dia} and M_s^2/K.

The overall data provide clear evidence that changes in particle concentration, (and therefore in dipolar interaction) shift the susceptibility peaks, $\chi'(T)$ and $\chi''(T)$, to higher temperatures. Our experiments suggest that the increase in the interaction strength causes the average energy barrier of particles to become higher, in agreement with previous experimental studies (Jonsson et al. 1995, Zhang et al. 1996, Djurberg et

al. 1997, Taketomi 1998, Jonsson et al. 1998). Some authors have resolved numerically the stochastic Langevin equations to obtain the temperature dependence of χ'' for interacting nanoparticle systems (Berkov and Gorn 2001). They have defined a reduced parameter $\beta = 2K/M^2_s$ in order to classify systems according to the single-particle anisotropy value. They demonstrated that the AC susceptibility peak could move with the increasing particle concentration (dipolar interaction strength) towards both lower and higher temperatures, depending on β. The behaviour observed in our samples agrees very well with the predictions for systems with low single-particle anisotropies, $\beta = 0.2\text{-}0.5$ (in our case the estimated value of $\beta = 0.2$).

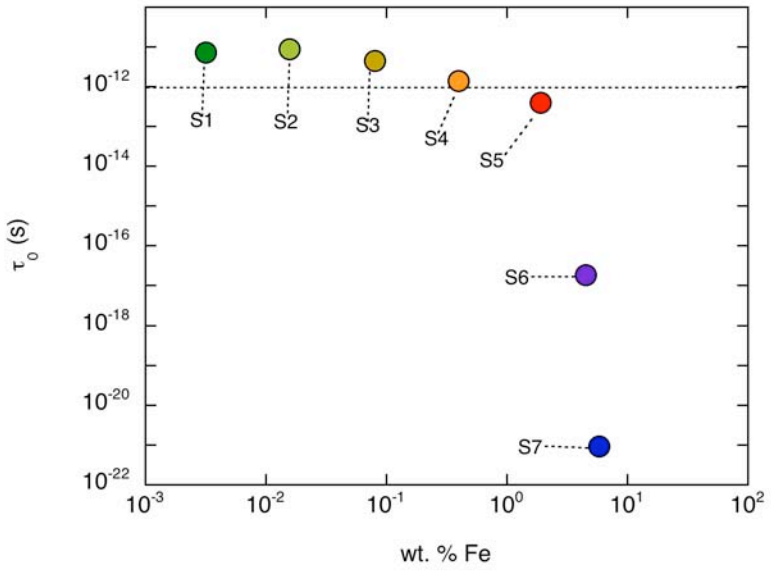

Fig. 92. Depending of the τ_0 prefactor on the particle concentration. See that for increasing particle concentration (increasing dipole-dipole interaction strength) a progressive decrease of the prefactor value towards unphysical values takes place.

By using Eq. 12, a value for M^2_s /K can be estimated from the intercept of the extrapolated experimental curve, as shown in Fig. 91. Taking $M_s = 4.8 \times 10^5$ A m^{-1} as the spontaneous magnetization for bulk magnetite (Cornell et al. 1996), we obtain $K = 26.7 \pm 0.7 \times 10^3$ J m^{-3}, in agreement with other previous characterizations of magnetite (Cornell et al. 1996; Arelaro et al. 2005). From Fig. 87, we can see that the maximum of $\chi''(T)$, occurs at ~23 K for sample S2. Using this value as representative of the magnetic blocking process and according to equation 15, it results in an estimate of 8.1 ± 0.1 nm for the magnetite particles diameter, which is in good agreement with the typical sizes previously determined for Endorem® by TEM observations (Jung et al. 1995; Lima et al. 2006).

5.4. Tissues characterisation (Liver, spleen, heart and kidneys)

Once the magnetic carrier has been magnetically characterised it is possible to identify it in the tissues after its administration to animals. In this case, the magnetic carrier was injected to two rats, and a different one was used as control. The liver, spleen, heart and kidney tissues of the three animals were dissected 30 minutes after the administration and magnetically characterised, providing results about the biodistribution of the drug among the different tissues.

In the next sections, the results of the magnetic characterisation of the different tissues are presented.

5.4.1. Liver

The temperature dependence of the AC susceptibility per mass of sample of the three liver samples is shown in Fig. 93 and Fig. 94.

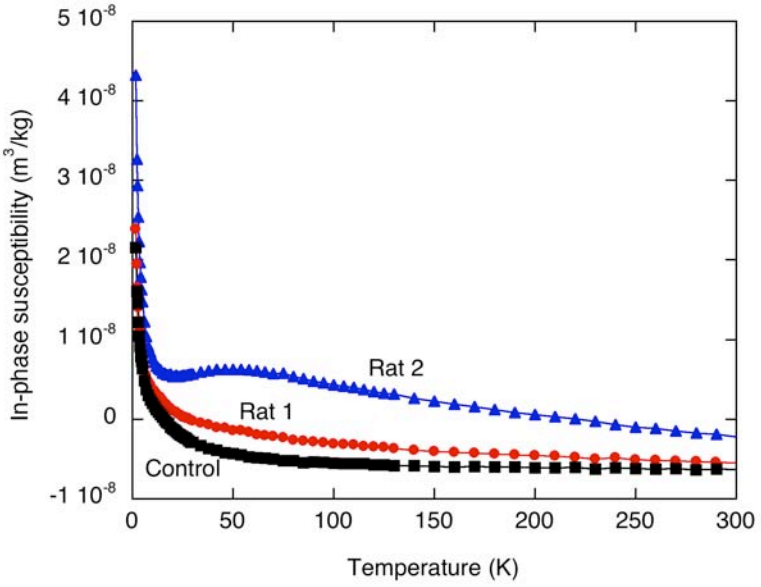

Fig. 93. Temperature dependence of the in-phase susceptibility, at 1 Hz, per mass of freeze-dried liver tissue corresponding to two rats sacrificed after the magnetic carrier administration and a control one.

A low temperature paramagnetic tail can be observed in the in-phase component of all the liver samples, similar to what has been observed previously in the control rat characterised in Chapter 3. The origin of these low-temperature tails comes from the paramagnetic iron-containing species present in the tissues but also from those coming from the blood contained in the blood vessels. A maximum around 50 K can also be clearly observed in the in-phase susceptibility of *rat 2*.

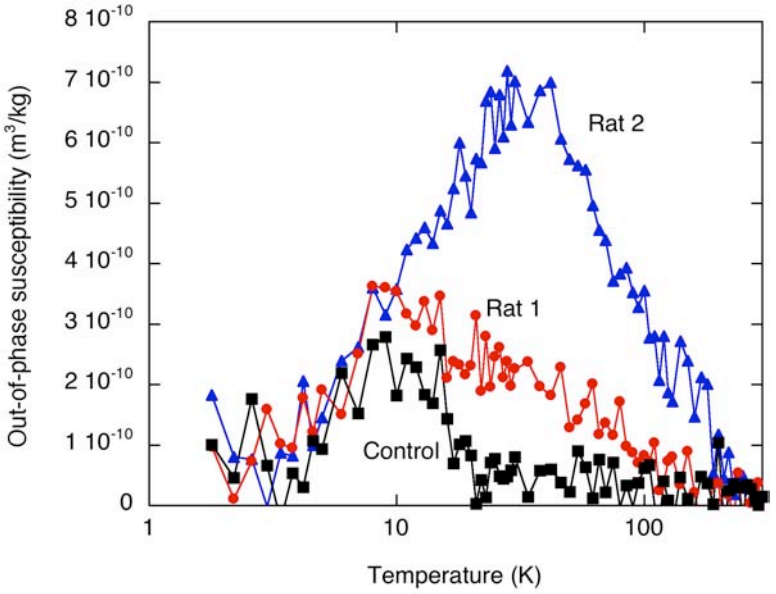

Fig. 94. Temperature dependence of the out-of-phase-phase susceptibility, at 1 Hz, per mass of freeze-dried liver tissue corresponding to two rats sacrificed after the magnetic carrier administration and a control one.

The out-of-phase susceptibility of the liver tissue of the *control rat* shows a single maximum around 9 K and becomes negligible above ≈ 25 K, within the accuracy of the experiments. The shape and location in temperature and the value of the susceptibility per mass of sample reminds that of the rat liver ferritin standard previously characterised (see Chapter 3). A similar maximum associated to the presence of ferritin should also be present in *rat 1* and *rat 2*. The $\chi''(T)$ data of *rat 1* reveals also the presence of ferritin (maximum at around 9 K), however, the non-zero out of phase susceptibility above 25K can be related with the presence of the contrast agent. The out-phase-susceptibility of *rat 2* shows a maximum at around 32 K, which indicates that the magnetic

carrier content is higher than that of the liver of *rat 1*. The high magnetic contribution of the magnetic carrier to the out-of-phase susceptibility of *rat 2* makes it difficult to observe the maximum corresponding to the presence of ferritin.

Measurements at different frequencies (1, 10 and 120 Hz) have been performed for the liver tissues in order to calculate the value of τ_0. Nevertheless, due to the intrinsic noise of the out-of-phase susceptibility data it is difficult to obtain a good superposition of the data at the three frequencies and for that reason, the alternative method, described in Chapter 1, for the calculus of the preexponential factor has been used. The τ_0 values, obtained from the slope of the $d(T\chi')/dT$ versus χ'' representation (Fig. 95), are not higher than 10^{-16} s, an unphysical value that indicates that dipole-dipole interactions are important.

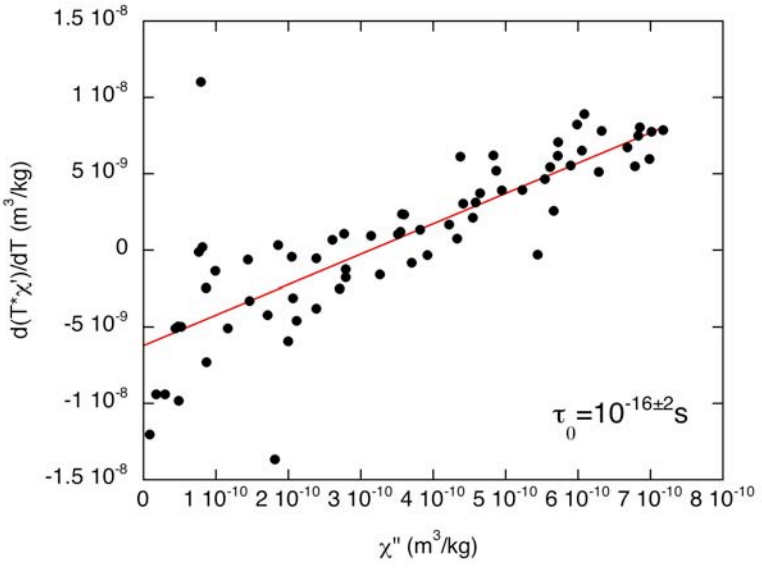

Fig. 95. Alternative method for the determination of τ_0, at 1 Hz, of the liver of *rat 2*. τ_0 values not higher than 10^{-16} s are obtained.

Both the location in temperature of the out-of-phase susceptibility maxima together with the τ_0 value of the liver of *rat 2* are similar to the agar dilution S6, which is one of the most concentrated ones that has been characterised in the previous section. This fact may indicate a similar degree of dipolar interactions in the liver tissue, as the one observed in sample S6 indicating that the particles may present some degree of local aggregation in the liver.

5.4.2. Spleen

In Fig. 96 and Fig. 97 the in-phase and out-of-phase susceptibility data of the spleen tissues are shown.

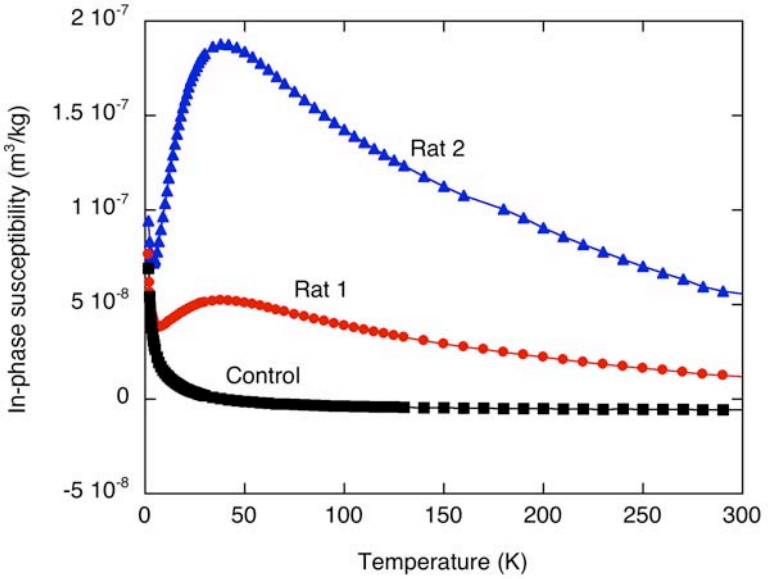

Fig. 96. Temperature dependence of the in-phase susceptibility, at 1 Hz, per mass of freeze-dried spleen tissue corresponding to two rats sacrificed after the magnetic carrier administration and a control one.

In all the cases, the susceptibility contains a low-temperature tail that can be assigned to paramagnetic iron-containing species present in the tissues or in rests of blood from the blood vessels as it has also been observed in the liver tissues. Conspicuous maxima are observed in the χ' (T) of the spleens of the treated rats which, together with the non-zero out-of-phase susceptibility at slightly lower temperatures, evidences a magnetic relaxation phenomenon, associated to the presence of the injected magnetic carrier.

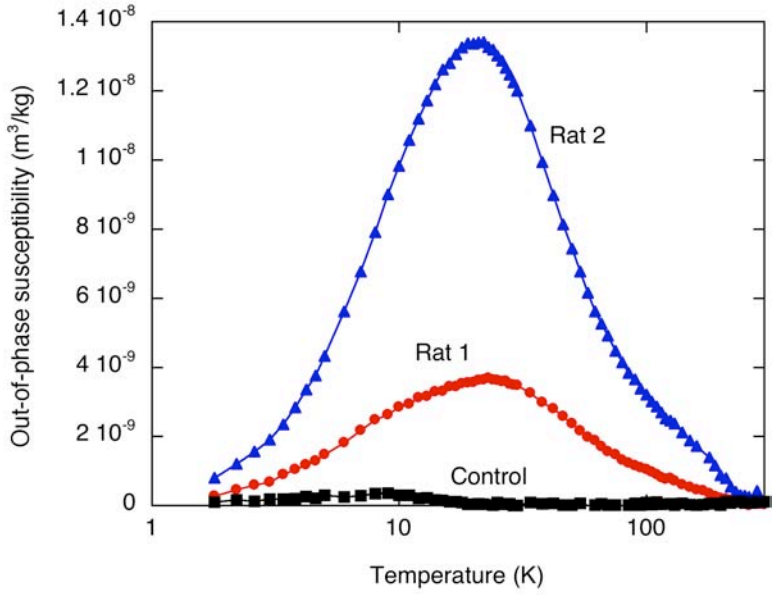

Fig. 97. Temperature dependence of the out-of-phase susceptibility, at 1 Hz, per mass of freeze-dried spleen tissue corresponding to two rats sacrificed after the magnetic carrier administration and a control one.

The presence of a maximum similar to the observed in the rat liver ferritin standard is visible in the out-of-phase susceptibility data of the *control rat*. Nonetheless, a slight discrepancy either in the maximum temperature location and width, in comparison with the rat liver ferritin

standard, point to differences in the biomineralisation of ferritin between both tissues.

The spleen samples of the treated rats present a maximum at around 22 K in the out-of-phase susceptibility, which very much resembles that of the most diluted magnetic carrier preparations. However, in addition to the contrast agent, a small shoulder at about 10K can also be observed in the $\chi''(T)$ data for *rat 1*, revealing the presence of ferritin. Very likely the spleen of *rat 2* does also contain ferritin but it is not so clearly detected due to the higher content of the magnetic carrier.

Measurements at three different frequencies (1, 10 and 120 Hz) of the spleen of *rat 2* have been performed in order to calculate the preexponential factor, τ_0, to estimate the interparticle interactions of the magnetic carrier in the tissue. The best superposition of the curves has been achieved with $\tau_0=10^{-11}$ s (Fig. 98a). The alternative method for the calculation of τ_0, detailed in Chapter 1 has also been used with the same sample (Fig. 98b) in order to compare the results from both methods.

It has to be stood out the good agreement of the preexponential factor values obtained by the two methods.

The location in temperature of the out-of-phase susceptibility maxima together with the τ_0 value of the spleens of *rat 1* and *rat 2* are similar to samples S1 and S2, which are the most diluted agar dilutions of the magnetic carrier characterised in the previous section. Then, a similar degree of dipolar interactions can be considered in the four samples indicating that the injected particles may be sparely distributed in the spleen tissues.

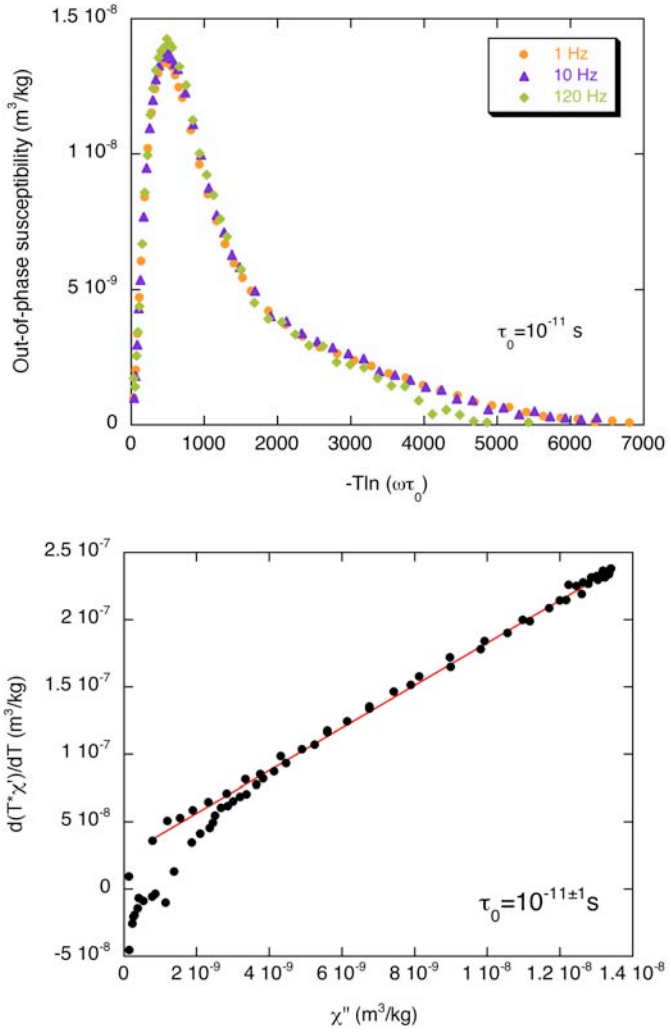

Fig. 98. a) Scaling plot of the out-of-phase susceptibility at 1 (circles), 10 (crosses) and 120Hz (diamonds) for the spleen of *rat 2*. The best superposition is obtained with $\tau_0=10^{-11}$s. b). Alternative method for the determination of τ_0, at 1 Hz, of the same sample according to Eq. 12 and 13. The value of τ_0 obtained is similar to the obtained from the method in graph a).

5.4.3. Heart and kidneys

The tissue samples of the heart and the kidneys of *rat 1* present a low temperature paramagnetic tail in the in-phase susceptibility (Fig. 99). The corresponding out-of-phase susceptibility of both samples is plotted in Fig. 100. It can be observed that the kidney samples have a nearly negligible out-of-phase susceptibility in all the temperature range, while a small and rather noisy maximum at low temperatures can be observed in the heart sample. The shape and location in temperature of this maximum reminds that of the rat liver ferritin standard. However, due to the negligible out-of-phase susceptibility above 20K in both tissues, it can be said that the concentration of the carrier in both tissues is under the detection limits of the technique.

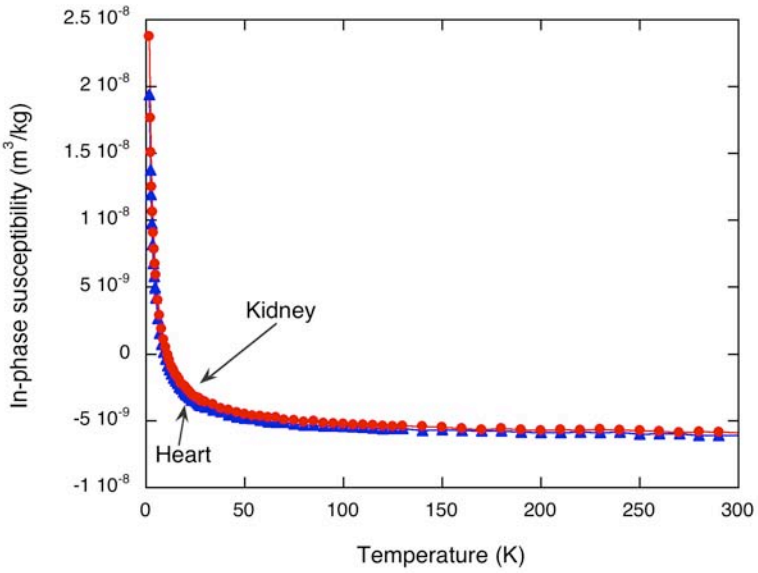

Fig. 99. Temperature dependence of the in-phase susceptibility, at 1 Hz, per mass of freeze-dried heart and kidney tissues corresponding to two rats sacrificed after the magnetic carrier administration and a control one.

As the magnetic carrier has been injected intravenously, it can be assumed that rests of the drug are still in the blood. As it has been observed that the iron-containing species present in the blood vessels of the tissues also contribute to the magnetic susceptibility of the tissue samples (see Chapter 4) the fact of not observing the magnetic carrier in none of both heart and kidney tissues indicates that the presence of the carrier detected in the liver and the spleen tissues is not due to rests of the drug in the blood vessels, and that the carrier has been incorporated to these tissues.

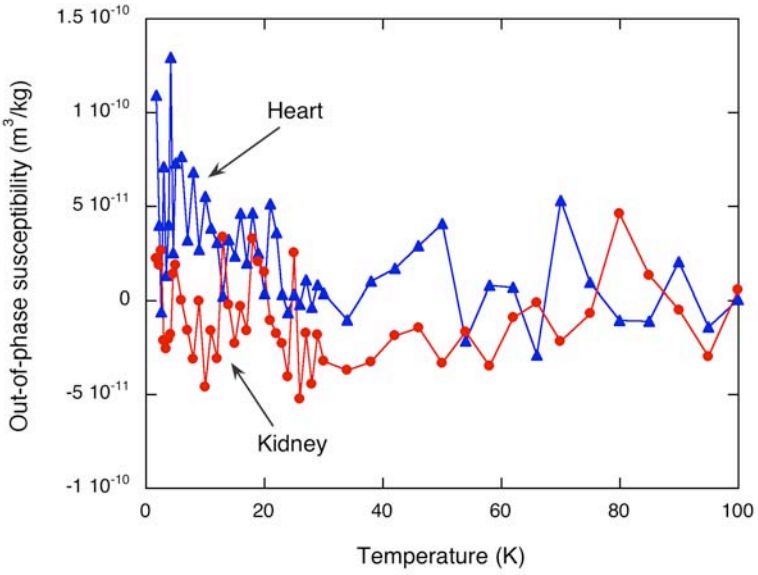

Fig. 100. Temperature dependence of the out-of-phase susceptibility, at 1 Hz, per mass of freeze-dried heart and kidney tissues corresponding to two rats sacrificed after the magnetic carrier administration and a control one.

5.5. Quantification protocol

The study of the magnetic characterisation results of the tissue samples has provided qualitative information about the biodistribution of the injected magnetic carrier among the different tissues, however it will be desirable to obtain quantitative details. With this purpose, a protocol for the quantification of ferritin and Endorem® in the animal tissues has been developed with the aim of using the magnetic susceptibility measurements as an analytical technique for the characterisation of iron-containing species in biological media.

5.5.1. Introduction to the quantification process

As it has been explained in previous chapters, when representing the out-of-phase susceptibility data per mass of iron, if all of the iron atoms in a given sample were present in the form of a unique iron-containing species (e.g. ferritin), the corresponding $\chi''(T)$ profile per mass of iron would coincide with that of the corresponding standard.

Inversely it can be said that it is possible to determine the iron concentration of a given species from the proportionality factor that relates its mass out-of-phase susceptibility to that of a reference sample with a known iron content.

At this point of the discussion it is important to emphasize that, as the diamagnetic and paramagnetic contributions constitute a rather important part of the in-phase susceptibility, it becomes advantageous to perform these calculations with the out-of-phase susceptibility data, as this component is totally insensitive to diamagnetism and paramagnetism.

5.5.2. Verification of the protocol: Quantification of the magnetic carrier concentration in agar dilutions

In order to investigate the range of applicability of the magnetic quantification process, it has been applied to samples whose iron concentration is known in advance: The agar dilutions of Endorem®. The iron content in these samples has been calculated by just considering the proportionality factor of the height of the $\chi''(T)$ maxima, with sample S1, which has been used as a reference as it shows the weakest dipolar interaction. The iron concentrations obtained by the magnetic quantification are compared with the nominal value of each sample in Table 16. The table shows that, while for the most diluted samples the iron content determined from the magnetic data is in very good agreement with the nominal one, for increasing concentration the error induced by using a $\chi''(T)$ reference profile, that has not got the maximum at the same temperature due to interparticle interactions, is also increasing progressively.

Sample	χ''_{max} (m^3/kg)	T_{max} (K)	[Fe] $_{prepared}$ (mg Fe/g)	[Fe] $_{calculated}$ (mg Fe/g)	% Error
S1	$8.128 \cdot 10^{-9}$	23	0.0308	-	-
S2	$4.032 \cdot 10^{-8}$	24	0.155	0.154	0.787
S3	$2.008 \cdot 10^{-7}$	24.9	0.793	0.784	1.18
S4	$1.002 \cdot 10^{-6}$	26	3.98	3.92	1.42
S5	$4.872 \cdot 10^{-6}$	28.5	20.6	19.8	4.1
S6	$8.576 \cdot 10^{-6}$	38	45.5	33.8	25.8
S7	$9.545 \cdot 10^{-6}$	43	58.9	37.6	36.2
E	$1.297 \cdot 10^{-5}$	42	106	51.5	51.4

Table 16. Characteristics of the $\chi''(T)$ maximum for the different agar dilutions of the original contrast agent. In the last columns the iron content used in the preparation, the calculated one from the scaling of the χ'' maxima and the percentage error of this calculation are shown.

In Fig. 101, the same data as the presented in Fig. 86 are shown as scaled to their maxima. It can be observed that when the differences between the profiles of the samples with respect to the sample S1, used as standard, increase, the percentage error in the quantification procedure is also increased (Table 16).

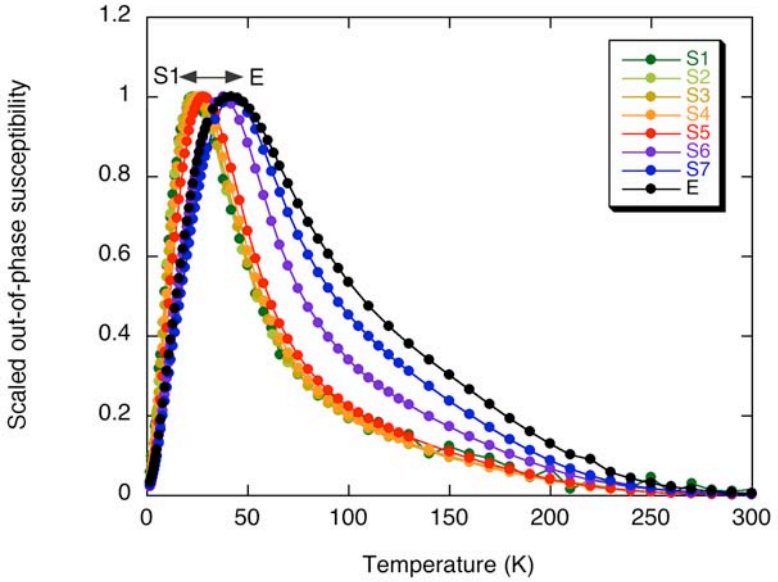

Fig. 101. Comparative plot of the χ"(T) profiles for the freeze-dried original liquid suspension of Endorem® and all the prepared dilutions as scaled to their respective maxima.

From the variation of the error in the quantification of the iron in the form of the magnetic carrier in the agar dilutions it is observed the importance of the use of the appropriated standard for the quantification procedure. Agar samples in which the particles are near enough to interact cannot be submitted to the quantification procedure using as standard the diluted agar solution in which there are no interactions between the particles. The quantification procedure should be improved by using as a

reference the standard whose profile and location in temperature better approaches the unknown one.

Summarizing, the magnetic data of the Endorem® dilutions presented here constitute a necessary calibration step in the determination, through appropriate scaling of the AC susceptibility, of the content of this magnetic carrier in unknown tissues.

5.5.3. Description of the quantification protocol applied to tissues: previous requirements and list of steps

The application of the quantification protocol of the iron-containing species from their magnetic characterisation results, which has been checked out to work with the agar dilutions of the magnetic carrier in the previous section, can also be applied to tissue samples, as a technique for the monitorization of the iron metabolism and the biodistribution of iron-containing drugs. However, due to the complexity of the tissue matrix and to the fact that the particles in the body may be degraded in their travel to the tissue, the magnetic quantification of the iron-containing species in tissues must fulfil some previous requirements.

Moreover, additional information about the sample is needed in advance to perform the quantification of the iron-containing species from the magnetic characterisation results. The knowledge of the details listed below would simplify the quantification analysis.

Requirements:

Identification of the iron-containing species present in the sample and characterisation of the standards. It is important to know the species that will be present in the sample in order to characterise the analogous standards. The knowledge of the magnetic behaviour per mass of iron of

the standard is the key factor in order to quantify the species in the different samples.

Study of the interaction of the different iron-containing species. As the concentration of a given species may affect to its magnetic behaviour by means of interaction processes, it is important to know whether these processes are occurring in the samples whose iron content is desired to determine.

Study of the presence of other magnetogenic elements. When quantifying the iron speciation it is important to know that there are no other magnetogenic elements in the sample that may have a magnetic contribution.

Study of the degradation of the injected particles. In the case of the quantification of particles in a tissue, the time after the administration of the particles matters, as the degradation processes will change the magnetic behaviour of the iron-containing species and therefore new standards will be required.

Once the previously detailed requirements are fulfilled by the sample whose iron speciation is going to be quantified, the quantification process may be started.

The sequence of steps to perform the magnetic quantification of iron-containing species in tissues samples is detailed ahead. Although it has been tried to define a general protocol for its use in a wide variety of cases, the quantification of ferritin and a magnetic carrier in a tissue has been used as an example of some of the steps.

Steps of the quantification protocol:

1. Selection of the appropriated standard. The most similar standard available must be used for the quantification. For the quantification of ferritin in a tissue, a standard of the ferritin of the same animal and tissue should be used. For the quantification of a magnetic carrier, a standard with the most similar degree of interparticle interactions as in the sample should be used. To choose the appropriated standard the value of τ_0 and the location in temperature of the maxima will be taken into account.

2. Scaling of the data from the unknown sample and the standard. In the case of a tissue sample, the proportionality factor that relates the out-of-phase susceptibility per mass of sample of the tissue with the out-of-phase susceptibility per mass of iron of the standard provides the value of the iron content in the form of the standard in the tissue sample.

$$\underset{(m^3/kg)}{\chi''_{sample}} = \underset{(kgFe/kg)}{[Fe]_{standard}} \cdot \underset{(m^3/kgFe)}{\chi''_{standard}} \qquad \text{Eq. 18}$$

In the case of having more than one iron-containing species, the previous equation will be modified by adding the contributions of all the species:

$$\underset{(m^3/kg)}{\chi''_{sample}} = \underset{(kgFe/kg)}{[Fe]_1} \cdot \underset{(m^3/kgFe)}{\chi''_1} + \underset{(kgFe/kg)}{[Fe]_2} \cdot \underset{(m^3/kgFe)}{\chi''_2} + \ldots \qquad \text{Eq. 19}$$

3. Use of controls. When quantifying two different iron-containing species in a tissue (e.g. ferritin and the magnetic carrier), if one of them has a bigger magnetic contribution, the other one may be difficult to quantify. A reference value of the presence of endogenous species (e.g. ferritin) can be obtained from the use of control animals, which should have a similar value of ferritin.

4. Determination of the total iron content. This value may allow the use of the values of the endogenous species obtained from the control animals for the treated ones, if they present a similar total iron content. It has to be said that the amount of iron in the form of the magnetic carrier in some of the tissues is negligible in comparison with the endogenous one.

5. Error check. There are two main sources of error in the quantification process: The experimental noise and the fact of choosing a standard of a magnetic carrier of a given concentration. The first one provides an interval of values of the concentration of each species that may fit the experimental data, so these deviations must be included in the result value. To check the error due to having standards of the magnetic carrier at specific concentrations (specific degree of dipole-dipole interactions) once that the dilution of the carrier that is going to be used as standard has been chosen (similar location in temperature of the χ'' maxima and τ_0) the nearest dilutions can also be used as standards to see the differences in the concentration obtained.

5.5.4. Application of the quantification protocol to tissue samples

The concepts developed above have been applied to rat tissues, obtained 30 min after a single injection of Endorem®, whose AC susceptibility has been presented in the previous sections. In these samples, the iron-containing species that will have a magnetic contribution to the out-of-phase susceptibility will be the endogenous ferritin and the injected magnetic carrier. The presence of other magnetogenic elements different from iron has been discarded by elemental analysis as it has been determined to be lower than 0.001 wt%. As the animals were sacrificed at a very short time after the injection, it is reasonable to assume that the magnetic carrier particles have not had enough time for degradation in their travel to the tissue.

5.5.4.1. Livers

In Fig. 102(a), the out-of-phase susceptibility of the control liver tissue is shown. The ferritin iron content of this sample has been quantitatively determined by scaling the $\chi''(T)$ single maximum with respect to a ferritin standard (commercial rat liver ferritin previously characterized (see Chapter 3), resulting in 0.14 mg Fe g^{-1} dry tissue. Contrarily to the case of ferrimagnetic particle assemblies, as the agar dilutions described above, the $\chi''(T)$ profile of ferritin is not affected by dipolar interactions given the antiferromagnetic character of the ferritin cores. In the figure, the rather good fit of the liver tissue $\chi''(T)$ is apparent with respect to the standard, not only in terms of maximum temperature but also of maximum width. The obtained ferritin iron value is lower than

the total iron content (Table 17) which indicates that the rest of the iron may not be in the form of ferritin.

As the three liver samples have a very similar total iron content (see Table 17), which means that the injected iron represents a very small amount compared to the physiological one in that organ, it has been assumed that the ferritin content in the livers of the treated rats is similar to the control one. The $\chi''(T)$ data of the treated rats liver tissues present a maximum at ~32 K and τ_0 values, obtained from the slope of the $d(T\chi')/dT$ versus χ'' representation, not higher than 10^{-16} s. Therefore, to estimate the iron content in the form of magnetic carrier particles in the treated rat livers, we have used as reference the agar dilution S6 because it presents the most similar τ_0 and T_{max} values (Fig. 92 and Table 16).

Sample	$[Fe]_{Total}$ (mg Fe/g dry tissue)	$[Fe]_{Endorem}$ (μg Fe/g dry tissue)	$[Fe]_{Ferritin}$ (mg Fe/g dry tissue)
Control liver	0.39	-	0.14 ± 0.01
Liver 1	0.40	1.3 ± 0.7	0.14 ± 0.01
Liver 2	0.38	3.5 ± 1.2	0.13 ± 0.01
Control spleen	1.00	-	0.2 ± 0.02
Spleen 1	1.38	14.5 ± 0.1	0.3 ± 0.05
Spleen 2	1.05	53.2 ± 0.4	0.2*

Table 17. Iron content determined by elemental analysis by ICP-AES ($[Fe]_{Total}$) of all the tissues together with the magnetic quantification results obtained for Endorem® and ferritin following the algorithm described in the text. * The same value as the one obtained for the control spleen

In Fig. 102(c), it can be observed that although the tissue ferritin-iron concentration is nearly three orders of magnitude higher than the tissue magnetic-carrier-iron concentration (Table 17), both magnetic contributions are of the same order, a clear consequence of the different

intraparticle arrangement of the atomic spins that ferri- and antiferromagnetic particles have. Incidentally, in this figure, it can be said that the differences between the experimental curve and the calculated one at the lowest temperatures have no significance due to the intrinsic experimental noise.

The $\chi''(T)$ profile of the liver of *rat 2* (Fig. 102(e)) indicates that its magnetic carrier particles content is higher than that of the liver of *rat 1*. In any case, a satisfactory interpretation of the complete profile can only be achieved with the concurrence of a sizeable amount of ferritin. It appears that the $\chi''(T)$ profile is able to give account of interindividual variations in the content of magnetic carrier and endogenous liver ferritin with a surprising good fit of the calculated profiles with respect to the experimental ones.

In Table 17, the results of the quantitative determination of iron in the form of magnetic carrier and in the form of ferritin are shown for all the considered tissues. The error bars of this determination have been estimated from the quality of the fit between the calculated $\chi''(T)$ curves and the experimental ones. The contribution to the total error coming from the choice of the magnetic carrier dilution standard, which represents the degree of dipolar interaction, has been observed to be of the same order as that caused by the experimental $\chi''(T)$ noise.

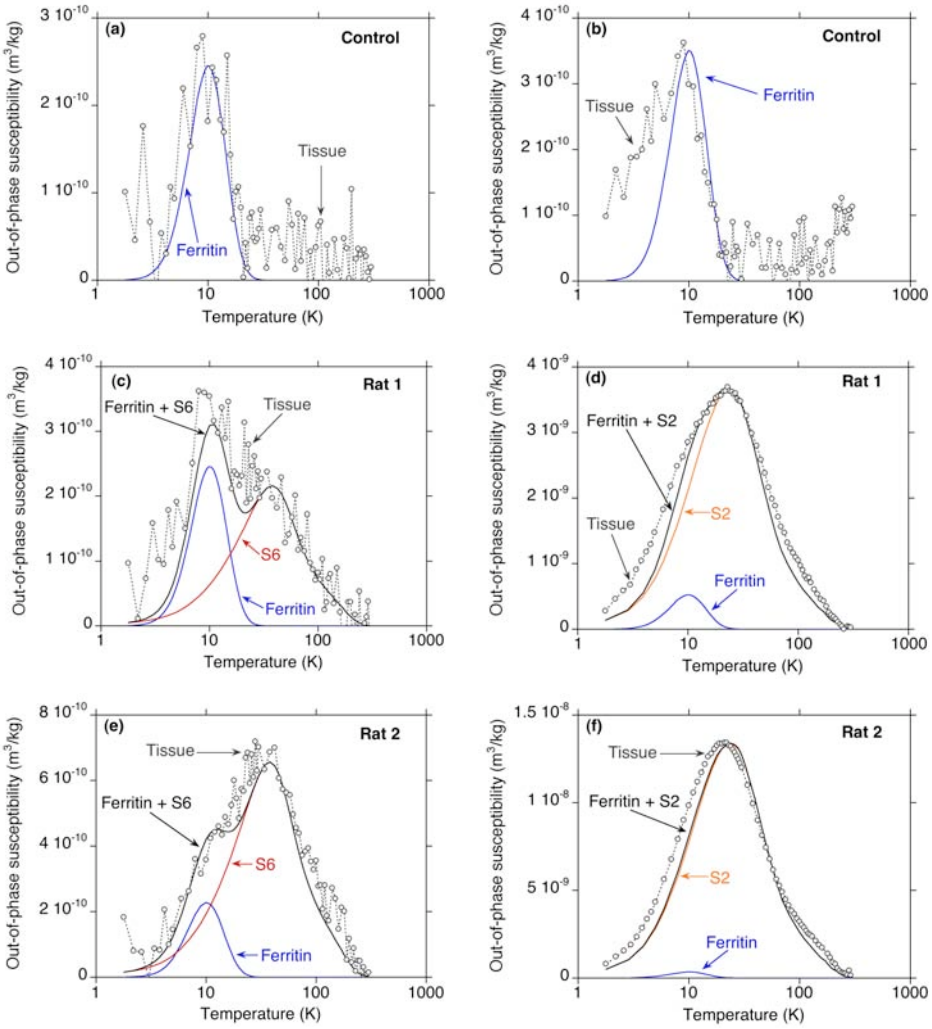

Fig. 102. a, b, c, d, e, f: Quantification procedure to determine the particulate content from the out-of-phase susceptibility of the rat liver and spleen tissues. In the figure, the calculated χ"(T) contributions of rat liver ferritin, the magnetic carrier, and the sum of both are shown together with the actual result for the tissue (circles). The agar dilution standards chosen for livers and spleens were S6 and S2, respectively.

5.5.4.2. Spleens

The spleen tissues whose magnetic data have been used for quantitative analysis of the magnetic carrier content correspond to the *control rat*, *rat 1* and *rat 2*, whose livers have been considered in the previous section.

In Fig. 102(b), the $\chi''(T)$ data of the control spleen is plotted together with that of commercial rat liver ferritin, which has been used as a reference, in the estimated quantity. In the figure, a slight discrepancy either in the maximum temperature and in the shape of the left flank of the profile seems to occur, suggesting that the biomineralisation of spleen ferritin may differ from that of the liver. The use of the rat liver ferritin magnetic data as a reference to quantify spleen ferritin may therefore be understood just as an approximation.

The $\chi''(T)$ data of the treated rat spleens (Fig. 102(d) and (f)) present conspicuous maxima at around 22–23 K that very much resemble that of the most-diluted magnetic carrier preparations. As the τ_0 values, calculated by any of the two methods described in Chapter 1, result of the order of 10^{-11} s for the two spleen samples, it seems adequate to choose S1 or S2 as a reference to quantify the magnetic carrier (Fig. 92 and Table 16). To obtain the calculated profiles we have considered for spleen 2 the same ferritin content as in the control one due to their very similar total iron concentration. For Spleen 1 a slightly higher ferritin content, suggested by the higher total iron determined from elemental analysis, has been chosen, also contributing to a better fit quality. The discrepancy in the left flank of the profile between the tissues and the sum of the contributions of the isolated species may very likely have the same origin as in the case of the control spleen. From the obtained quantitative results

(Table 17), it can be observed that the determination of the magnetic carrier content in spleen tissues is much more accurate than that of ferritin.

5.6. Biodistribution of the magnetic carrier

In this section, the information obtained from the magnetic characterization of the different tissues is discussed in the frame of previous studies on the same MRI contrast agent in rats.

Through consideration of the injected iron and the wet weights of the respective organs, the percentages of the total injected iron that have travelled to the tissues, determined from the data in Table 17, result in 1.8 and 1.2% (*rat 1*), and 5.3 and 3.8% (*rat 2*), for the whole livers and spleens, respectively. Although the iron content per mass of sample in the spleens results higher than in the livers (Table 17), as the wet weight of the whole liver is around 16 times more than the spleens, the livers accumulate a bigger percentage of the total administered iron. These results agree with previous experiments with radiolabelled ^{59}Fe AMI-25 (Majumdar et al. 1989) in that the fraction of the total injected iron in the whole liver results higher than in the whole spleen.

It has also to be noted that no rest of the magnetic carriers have been detected magnetically in the heart and the kidneys of the rats 30 min after the injection.

From the analysis of the tissue AC susceptibility data, presented above, it follows that the magnetic behaviour of the injected Endorem® nanoparticles corresponds to the noninteracting and interacting regime for spleens and livers, respectively. This result, which is independent of the

determined concentration of the magnetic carrier in each tissue, suggests that a different spatial organization of the magnetic particles exists in each organ. More specifically, it suggests that the particles may present some degree of local aggregation in the liver, while in the spleen they seem to be sparely distributed. This magnetically detected difference in biodistribution, at tissue level, is in full accordance with previous findings using fluorescent markers-assisted intravital laser microscopy that contemplated the influence of the different degree of aggregation of superparamagnetic iron oxide (SPIO) particles in the liver and spleen and its effect on the MRI contrast (Tanimoto et al. 2001). The aggregation of AMI-25 nanoparticles in the liver tissue at an ultrastructural level is also an already observed phenomenon (Na et al. 2003).

5.7. Conclusions

The study of the biodistribution of magnetic carriers in tissues has been achieved by the use of a detailed magnetic characterisation. For this purpose, a deep study of the magnetic behaviour of the injected magnetic carrier, with special interest in the influence of the dipolar interaction effects in the AC susceptibility, has been performed in advance to the administration to rats.

The magnetic characterisation of the different tissues after the magnetic carrier administration has revealed, together with the existence of endogenous iron, the incorporation of the carrier in the spleen and liver tissues, while no rests of the drug have been observed in the heart or the kidneys.

It appears that the measurement of the temperature dependence of the AC susceptibility in the cryogenic range, in particular its out-of-phase component (χ''), of the tissues is able to resolve the contribution of administered particles from that of physiological particulate minerals (e.g., inside ferritin).

A protocol that allows the quantitative analysis of the iron-containing nanoparticles present in the tissues (the ferritin cores and the injected magnetic carriers) has been developed. It has been shown that an iron amount of the order of 1 μg Fe/g dry tissue in the form of Endorem® magnetite nanoparticles can be detected from a careful analysis of $\chi''(T)$. The singular adequacy of using $\chi''(T)$ for this purpose, as this quantity is not affected by either the presence of paramagnetic or diamagnetic iron containing species, has been shown.

As typical applications of particulate magnetic carriers involve low doses (of the order of 0.5 wt% Fe in the wet tissue); the contribution of the injected particles to the tissue total iron concentration is usually not detectable by elemental analysis so, in these cases, the magnetic quantification will be of great relevance for the study of the biodistribution of the particles,

Furhermore, if the calibration of a particulate magnetic carrier, as the one that has been performed in this work for Endorem®, is previously accomplished, it will be possible to apply the concepts developed in this chapter for the study of its biodistribution and pharmacokinetics by magnetic means. In a more general sense, studies on the chemical speciation of biological iron may also take advantage of the developed quantification protocol.

In addition, the calculation of the τ_0 value, as it informs about the nanoparticle magnetic dynamics, appears to be an interesting indicator of the degree of particle aggregation with special relevance in the understanding of the magnetic carrier spatial distribution at tissue level.

6. Conclusions

In the work presented in this thesis, techniques commonly employed in the characterisation of materials have been used in a novel and combined way to study the bioinorganic aspects of the iron metabolism, being a new example of multidisciplinary work.

The magnetic behaviour of the most common iron supplements used nowadays for the treatment of iron deficiency anaemia has been studied and related to their composition. Special attention has been paid to those compounds that have been observed to contain iron oxyhydroxide nanoparticles. In these compounds, the relationship between their magnetic behaviour and the size and crystalline structure of the particles has been studied.

Provided the good results obtained in the characterisation of iron oxyhydroxide nanoparticles by magnetic means, the study of the iron-containing deposits in tissues from two different animal models of iron overload has been performed.

In the first studied animal model of iron overload, different tissues were magnetically characterised after a single injection of iron dextran to rats. Among other results, the degradation of the injected drug together with the increase of iron in the form of ferritin has been observed at different times after the iron dextran administration.

In the second studied animal model of iron overload, mice constitutively became iron loaded after genetic modification exemplifying human conditions of iron overload. The accumulation of iron in the liver but not in the spleen or heart has been observed in these mice. Furthermore, different kinds of iron deposits have been identified by TEM in the liver tissues.

With the monitorisation of iron dextran in the first animal model of iron overload as a starting point, the biodistribution of a different iron-containing drug, a magnetic carrier used as a contrast agent for MRI, has been studied also in rats. A special protocol for the quantification of iron in the form of the different iron-containing nanoparticles present in the tissues (those coming from endogenous ferritin and the injected magnetic carrier) has been developed.

Nowadays, in order to characterise the different iron-containing species present in the tissues, some chemical processes or isolation procedures are commonly used. The use of whole tissue samples in order to characterise the iron-containing species by magnetic means is specially interesting as it implicates a great diminution of the procedures that may alter the iron speciation.

The magnetic point of view provided in this thesis in order to study the iron speciation in biological systems opens the way to future research in different situations in which the iron metabolism is being studied (different organisms, diseases, etc.). Moreover, in a wider scenario, the protocols for the study of biological samples by magnetic means presented in this thesis may be of much relevance for monitoring different processes of the biogeochemical cycle of iron.

Thinking about future applications of the magnetic characterisation techniques applied to the study of biological samples, one can also think about the magnetic properties of the iron-containing species as a crucial issue in the development of new clinical techniques based on magnetism for the study of the iron metabolism.

7. References

Adams, P. C., D. M. Reboussin, J. C. Barton, C. E. McLaren, J. H. Eckfeldt, G. D. McLaren, F. W. Dawkins, R. T. Acton, E. L. Harris and V. R. Gordeuk (2005). Hemochromatosis and Iron-Overload Screening in a Racially Diverse Population. 352**:** 1769-1778.

Allen, P. D., T. G. St Pierre, W. Chua-anusorn, V. Strom and K. V. Rao (2000). "Low-frequency low-field magnetic susceptibility of ferritin and hemosiderin." Biochimica Et Biophysica Acta-Molecular Basis of Disease 1500(2): 186-196.

Alpert, Y. and R. Banerjee (1975). "Magnetic susceptibility measurements of deoxygenated hemoglobins and isolated chains " Biochimica Et Biophysica Acta 405(1): 144-154.

Andrews, S. C., M. C. Brady, A. Treffry, J. M. Williams, S. Mann, M. I. Cleton, W. de Bruijn and P. M. Harrison (1988). "Studies on haemosiderin and ferritin from iron-loaded rat liver." Biol Met 1(1): 33-42.

Arelaro, A. D., A. L. Brandl, E. Lima, L. F. Gamarra, G. E. S. Brito, W. M. Pontuschka and G. F. Goya (2005). "Interparticle interactions and surface contribution to the effective anisotropy in biocompatible iron oxide nanoparticles used for contrast agents." Journal of Applied Physics 97(10): 3.

Atanasova, B. D., A. C. Y. Li, I. Bjarnason, K. N. Tzatchev and R. J. Simpson (2005). "Duodenal ascorbate and ferric reductase in human iron deficiency." American Journal of Clinical Nutrition 81(1): 130-133.

Azároff, L. V. (1968). "Elements of X-ray Crystallography " McGraw-Hill, New York.

Bahram, S., S. Gilfillan, L. C. Kuhn, R. Moret, J. B. Schulze, A. Lebeau and K. Schumann (1999). Experimental hemochromatosis due to MHC class I HFE deficiency: Immune status and iron metabolism, National Acad Sciences. 96**:** 13312-13317.

Bean, C. P. and I. S. Jacobs (1956). "Magnetic granulometry and super-paramagnetism." Journal of Applied Physics 27(12): 1448-1452.

Berkov, D. V. and N. L. Gorn (2001). "Susceptibility of the disordered system of fine magnetic particles: a Langevin-dynamics study." Journal of Physics-Condensed Matter 13(41): 9369-9381.

Berman, H., K. Henrick and H. Nakamura (2003). "Announcing the worldwide Protein Data Bank." Nature Structural Biology 10(12): 980-980.

Blaise, A., J. Feron, J. L. Girardet and J. J. Lawrence (1967). "Contribution to study of magnetic properties of ferritine." Comptes Rendus Hebdomadaires Des Seances De L Academie Des Sciences Serie B 265(20): 1077-&.

Blakemore, R. P. (1982). "Magnetotactic Bacteria." Annual Reviews in Microbiology 36(1): 217-238.

Brem, F., A. M. Hirt, C. Simon, H. G. Wieser and J. Dobson (2005). "Characterization of iron compounds in tumour tissue from temporal lobe epilepsy patients using low temperature magnetic methods." Biometals 18(2): 191-197.

Briley-Saebo, K. C., L. O. Johansson, S. O. Hustvedt, A. G. Haldorsen, A. Bjornerud, Z. A. Fayad and H. K. Ahlstrom (2006). "Clearance of iron oxide particles in rat liver - Effect of hydrated particle size and coating material on liver metabolism." Investigative Radiology 41(7): 560-571.

Bush, C. H. (2000). "The magnetic resonance imaging of musculoskeletal hemorrhage." Skeletal Radiology 29(1): 1-9.

Caroli, S., M. Spagnoli, G. Forte, M. Alessandrelli, R. Cresti, S. D'Ilio, J. Pauwels, G. N. Kramer and G. Zaray (2000). "Trace elements in bovine muscle: an ongoing project for a new certified reference material." Microchemical Journal 67(1-3): 235-243.

Carthew, P., R. E. Edwards, A. G. Smith, B. Dorman and J. E. Francis (1991). "Rapid induction of hepatic fibrosis in the gerbil after the parenteral administration of iron-dextran complex." Hepatology 13(3): 534-539.

Chasteen, N. D. and P. M. Harrison (1999). "Mineralization in ferritin: An efficient means of iron storage." Journal of Structural Biology 126(3): 182-194.

Chua-anusorn, W., K. C. Tran, J. Webb, D. J. Macey and T. G. St Pierre (2000). "Chemical speciation of iron deposits in thalassemic heart tissue." Inorganica Chimica Acta 300: 932-936.

Chua-anusorn, W., J. Webb, D. J. Macey, P. D. M. Hall and T. G. St Pierre (1999). "The effect of prolonged iron loading on the chemical form of iron oxide deposits in rat liver and spleen." Biochimica Et Biophysica Acta-Molecular Basis of Disease 1454(2): 191-200.

Chuaanusorn, W., T. G. St Pierre, G. Black, J. Webb, D. J. Macey and D. Parry (1994). "Mossbauer spectroscopic study of iron-oxide deposits in liver-tissue from the marine mammal dugong dugong." Hyperfine Interactions 91(1-4): 899-904.

Cohen, J., K. M. Creer, Srivasta.K and R. Pauthenet (1962). "Proprietes magnetiques des substances antiferromagnetiques en grains fins." Journal of the Physical Society of Japan 17: 685-&.

Cornell, R. M. and U. Schwertmann (1996). The Iron oxides: Structure, Properties, Reactions, occurrences and uses, Wiley-VCH.

Courselaud, B., M. B. Troadec, S. Fruchon, G. Ilyin, N. Borot, P. Leroyer, H. Coppin, P. Brissot, M. P. Roth and O. Loréal (2004). "Strain and gender modulate hepatic hepcidin 1 and 2 mRNA expression in mice." Blood Cells, Molecules and Diseases 32(2): 283-289.

Cowley, J. M., D. E. Janney, R. C. Gerkin and P. R. Buseck (2000). "The structure of ferritin cores determined by electron nanodiffraction." Journal of Structural Biology 131(3): 210-216.

Crichton, R. (2001). Inorganic Biochemistry of Iron Metabolism, From molecular mechanisms to clinical consequences, John Wiley & Sons, LTD.

Danielson, B. G. (2004). "Structure, chemistry, and pharmacokinetics of intravenous iron agents." Journal of the American Society of Nephrology 15(12): S93-S98.

Deugnier, Y., P. Brissot and O. Loréal (2008). "Iron and the liver: Update 2008." Journal of Hepatology.

Dickson, D. P. E., R. K. Pollard, B. Borchiohnsen, R. J. Ward and T. J. Peters (1988a). "Mossbauer spectroscopic studies of hemosiderins from different sources." Hyperfine Interactions 42(1-4): 889-892.

Dickson, D. P. E., N. M. K. Reid, S. Mann, V. J. Wade, R. J. Ward and T. J. Peters (1988b). "Mossbauer-spectroscopy, electron-microscopy and electron-diffraction studies of the iron cores in various human and animal hemosiderins." Biochimica Et Biophysica Acta 957(1): 81-90.

Djurberg, C., P. Svedlindh, P. Nordblad, M. F. Hansen, F. Bodker and S. Morup (1997). "Dynamics of an interacting particle system: Evidence of critical slowing down." Physical Review Letters 79(25): 5154-5157.

Dobson, J. and P. Grassi (1996). "Magnetic properties of human hippocampal tissue - Evaluation of artefact and contamination sources." Brain Research Bulletin 39(4): 255-259.

Dubiel, S. M., B. Zablotna-Rypien, J. B. Mackey and J. M. Williams (1999). "Magnetic properties of human liver and brain ferritin." European Biophysics Journal with Biophysics Letters 28(3): 263-267.

Dupic, F., S. Fruchon, M. Bensaid, N. Borot, M. Radosavljevic, O. Loreal, P. Brissot, S. Gilfillan, S. Bahram and H. Coppin (2002). "Inactivation of the hemochromatosis gene differentially regulates duodenal expression of iron-related mrnas between mouse strains." Gastroenterology 122(3): 745-751.

Evans, M. E. and F. Heller (2003). Environmental magnetism, principles and applications of enviromagnetics.

Feder, J. N., A. Gnirke, W. Thomas, Z. Tsuchihashi, D. A. Ruddy, A. Basava, F. Dormishian, R. Domingo, M. C. Ellis and A. Fullan (1996). "A novel MHC class I-like gene is mutated in patients with hereditary haemochromatosis." Nature Genetics 13(4): 399-408.

Fischbach, F. A., D. W. Gregory, P. M. Harrison, T. G. Hoy and J. M. Williams (1971). "On the structure of hemosiderin and its relationship to ferritin." J Ultrastruct Res 37(5): 495-503.

Funk, F., G. J. Long, D. Hautot, R. Buchi, I. Christl and P. G. Weidler (2001). "Physical and chemical characterization of therapeutic iron containing materials: A study of several superparamagnetic drug formulations with the beta-FeOOH or ferrihydrite structure." Hyperfine Interactions 136(1-2): 73-95.

Garcia-Palacios, J. L. (2000). On the statics and dynamics of magnetoanisotropic nanoparticles. Advances in Chemical Physics, Vol 112. New York, John Wiley & Sons Inc. **112:** 1-210.

Gider, S., D. D. Awschalom, T. Douglas, S. Mann and M. Chaparala (1995). "Classical and quantum magnetic phenomena in natural and artificial ferritin proteins." Science 268(5207): 77-80.

Gilles, C., P. Bonville, H. Rakoto, J. M. Broto, K. K. W. Wong and S. Mann (2002). "Magnetic hysteresis and superantiferromagnetism in ferritin nanoparticles." Journal of Magnetism and Magnetic Materials 241(2-3): 430-440.

Gossuin, Y., P. Gillis, R. N. Muller and A. Hocq (2007). "Relaxation by clustered ferritin: a model for ferritin-induced relaxation in vivo." Nmr in Biomedicine 20(8): 749-756.

Guyodo, Y., S. K. Banerjee, R. L. Penn, D. Burleson, T. S. Berauo, T. Seda and P. Solheid (2006). "Magnetic properties of synthetic six-line ferrihydrite nanoparticles." Physics of the Earth and Planetary Interiors 154(3-4): 222-233.

Hackett, S., W. Chua-anusorn, P. Pootrakul and T. G. St Pierre (2007). "The magnetic susceptibilities of iron deposits in thalassaemic spleen tissue." Biochimica Et Biophysica Acta-Molecular Basis of Disease 1772(3): 330-337.

Häfeli, U., W. Schutt, J. Teller and M. Zbrowoski (1997). "Scientific and Clinical Applications of Magnetic Carriers." New York: Plenum Pub Corp.

Hamburger, A. E., A. P. West, Z. A. Hamburger, P. Hamburger and P. J. Bjorkman (2005). "Crystal structure of a secreted insect ferritin reveals a symmetrical arrangement of heavy and light chains." Journal of Molecular Biology 349(3): 558-569.

Harrison, P. M. and P. Arosio (1996). "Ferritins: Molecular properties, iron storage function and cellular regulation." Biochimica Et Biophysica Acta-Bioenergetics 1275(3): 161-203.

Hider, R. C. (2002). "Nature of nontransferrin-bound iron." European Journal of Clinical Investigation 32(s1): 50-54.

Hoy, T. G. and A. Jacobs (1981). "Changes in the characteristics and distribution of ferritin in iron-loaded cell-cultures." Biochemical Journal 193(1): 87-92.

Hubbard, S. R., W. A. Hendrickson, D. G. Lambright and S. G. Boxer (1990). "X-ray crystal structure of a recombinant human myoglobin mutant at 2.8 A resolution." J Mol Biol 213(2): 215-218.

Hudson, J. Q. and T. J. Comstock (2001). "Considerations for optimal iron use for anemia due to chronic kidney disease." Clinical Therapeutics 23(10): 1637-1671.

Hylton, T. L. (1993). "Limitations of magnetoresistive sensors based on the giant magnetoresistive effect in granular magnetic composites." Applied Physics Letters 62(19): 2431-2433.

Iancu, T. C. (1992). "Ferritin and hemosiderin in pathological tissues." Electron Microscopy Reviews 5(2): 209-229.

Iancu, T. C. (1993). "Animal-models in liver research - Iron overload." Animal Models in Liver Research 37: 379-401.

Iancu, T. C., Y. Deugnier, J. W. Halliday, L. W. Powell and P. Brissot (1997). "Ultrastructural sequences during liver iron overload in genetic hemochromatosis." Journal of Hepatology 27(4): 628-638.

Janney, D. E., J. M. Cowley and P. R. Buseck (2000). "Transmission electron microscopy of synthetic 2-and 6-line ferrihydrite." Clays and Clay Minerals 48(1): 111-119.

JCPDS (1974). "International Centre for Diffraction Data." Natl. Bur. Stand.(US) Monogr. 25(11): 66.

Jensen, P. D. (2004). "Evaluation of iron overload." British Journal of Haematology 124(6): 697-711.

Jiles, D. (1991). Introduction to magnetism and magnetic materials, Chapman & Hall.

Jonsson, T., J. Mattsson, C. Djurberg, F. A. Khan, P. Nordblad and P. Svedlindh (1995). "Aging in a magnetic particle system." Physical Review Letters 75(22): 4138-4141.

Jonsson, T., P. Nordblad and P. Svedlindh (1998). "Dynamic study of dipole-dipole interaction effects in a magnetic nanoparticle system." Physical Review B 57(1): 497-504.

Jung, C. W. and P. Jacobs (1995). "Physical and chemical-properties of superparamagnetic iron-oxide mr contrast agents - ferumoxides, ferumoxtran, ferumoxsil." Magnetic Resonance Imaging 13(5): 661-674.

Kanoh, H. and K. Kaneko (1996). "Magnetic spin states of O-2 confined in a graphitic slit-shaped nanospace at low temperature." Journal of Physical Chemistry 100(2): 755-759.

Kaufman, K. S., G. C. Papaefthymiou, R. B. Frankel and A. Rosenthal (1980). "Nature of iron deposits on the cardiac walls in beta-thalassemia by mossbauer-spectroscopy." Biochimica Et Biophysica Acta 629(3): 522-529.

Kilcoyne, S. H. and R. Cywinski (1995). "Ferritin - A model superparamagnet." Journal of Magnetism and Magnetic Materials 140: 1466-1467.

Kirschvink, J. L., M. M. Walker and C. E. Diebel (2001). "Magnetite-based magnetoreception." Current Opinion in Neurobiology 11(4): 462-467.

Lázaro, F. J., A. R. Abadía, M. S. Romero, L. Gutiérrez, J. Lázaro and M. P. Morales (2005). "Magnetic characterisation of rat muscle

tissues after subcutaneous iron dextran injection." Biochimica Et Biophysica Acta-Molecular Basis of Disease 1740(3): 434-445.

Lázaro, F. J., A. Larrea and A. R. Abadía (2003). "Magnetostructural study of iron-dextran." Journal of Magnetism and Magnetic Materials 257(2-3): 346-354.

Lázaro, F. J., A. Larrea, A. R. Abadía and M. S. Romero (2002). "Magnetic study of iron sorbitol." Journal of Magnetism and Magnetic Materials 250(1-3): 256-259.

Lima, E., A. L. Brandl, A. D. Arelaro and G. F. Goya (2006). "Spin disorder and magnetic anisotropy in Fe3O4 nanoparticles." Journal of Applied Physics 99(8): 10.

López, A., L. Gutiérrez and F. J. Lázaro (2007). "The role of dipolar interaction in the quantitative determination of particulate magnetic carriers in biological tissues." Physics in Medicine and Biology 52(16): 5043-5056.

López, A., F. J. Lázaro, J. L. GarcíaPalacios, A. Larrea, Q. A. Pankhurst, C. Martinez and A. Corma (1997). "Superparamagnetic particles in ZSM-5-type ferrisilicates." Journal of Materials Research 12(6): 1519-1529.

Lucotte, G. and F. Dieterlen (2003). "A European allele map of the C282Y mutation of hemochromatosis: Celtic versus Viking origin of the mutation?" Blood Cells, Molecules and Diseases 31(2): 262-267.

Luis, F., E. del Barco, J. M. Hernandez, E. Remiro, J. Bartolome and J. Tejada (1999). "Resonant spin tunneling in small antiferromagnetic particles." Physical Review B 59(18): 11837-11846.

Majumdar, S., S. Zoghbi, C. F. Pope and J. C. Gore (1989). "A quantitative study of relaxation rate enhancement produced by iron-oxide particles in polyacrylamide gels and tissue." Magnetic Resonance in Medicine 9(2): 185-202.

Makhlouf, S. A., F. T. Parker and A. E. Berkowitz (1997). "Magnetic hysteresis anomalies in ferritin." Physical Review B 55(22): 14717-14720.

Mann, S. (2001). Biomineralization, principles and concepts in bioinorganic materials chemistry, Oxford chemistry masters, University press.

Mann, S., V. J. Wade, D. P. E. Dickson, N. M. K. Reid, R. J. Ward, M. Oconnell and T. J. Peters (1988). "Structural specificity of hemosiderin iron cores in iron-overload diseases." Febs Letters 234(1): 69-72.

Martin, D. H. (1967). Magnetism in solids. Cambridge, Massachussets, The M.I.T press.

Massover, W. H. (1993). "Ultrastructure of ferritin and apoferritin - a review." Micron 24(4): 389-437.

Michaelis, L., C. D. Coryell and S. Granick (1943). "Ferritin III. The magnetic properties of ferritin and some other colloidal ferric compounds." Journal of Biological Chemistry 148(3): 463-480.

Mohieeldin, M. E. Y., R. B. Frankel and L. Gunther (1994). "A comparison of the magnetic-properties of polysaccharide iron complex (PIC) and ferritin." Journal of Magnetism and Magnetic Materials 135(1): 65-81.

Na, J. B., J. S. Suh, Y. M. Huh, S. J. Kim, S. H. Kim, S. W. Cha and S. H. Lee (2003). "Pharmacokinetic modeling of phagocytic activity of

the liver using superparamagnetic iron oxide nanoparticles in dynamic MR imaging." Yonsei Medical Journal 44(3): 429-437.

Neel, L. (1962). "Proprietes magnetiques des grains fins antiferromagnetiques - superparamagnetisme et superantiferromagnetisme." Journal of the Physical Society of Japan 17: 676-&.

Okon, E., D. Pouliquen, P. Okon, Z. V. Kovaleva, T. P. Stepanova, S. G. Lavit, B. N. Kudryavtsev and P. Jallet (1994). "Biodegradation of magnetite dextran nanoparticles in the rat - A histologic and biophysical study." Laboratory Investigation 71(6): 895-903.

Pan, Y., A. Brown, R. Brydson, A. Warley, A. Li and J. Powell (2006). "Electron beam damage studies of synthetic 6-line ferrihydrite and ferritin molecule cores within a human liver biopsy." Micron 37(5): 403-411.

Pardoe, H., W. Chua-anusorn, T. G. St Pierre and J. Dobson (2003). "Detection limits for ferrimagnetic particle concentrations using magnetic resonance imaging based proton transverse relaxation rate measurements." Physics in Medicine and Biology 48(6): N89-N95.

Pauling, L. (1977). "Magnetic-properties and structure of oxyhemoglobin." Proceedings of the National Academy of Sciences of the United States of America 74(7): 2612-2613.

Pauling, L. and C. D. Coryell (1936). "The magnetic properties and structure of hemoglobin, oxyhemoglobin and carbonmonoxyhemoglobin." Proceedings of the National Academy of Sciences of the United States of America 22: 210-216.

QuantumDesign (1997). "Oxygen contamination." MPMS Application Note 1014-210.

Quintana, C., S. Bellefqih, J. Y. Laval, A. Gloter and A. Croisy (2005). "In situ visualization of ferritin and hemosiderin in Alzheimer's disease hipocampus by tem and X-ray nanoanalysis." Modern Pathology 18: 339A-339A.

Quintana, C., J. M. Cowley and C. Marhic (2004). "Electron nanodiffraction and high-resolution electron microscopy studies of the structure and composition of physiological and pathological ferritin." Journal of Structural Biology 147(2): 166-178.

Quintana, C., T. D. Wu, B. Delatour, M. Dhenain, J. L. Guerquin-Kern and A. Croisy (2007). "Morphological and chemical studies of pathological human and mice brain at the subcellular level: Correlation between light, electron, and NanoSIMS microscopies." Microscopy Research and Technique 70(4): 281-295.

Richter, G. W. (1959). "The cellular transformation of injected colloidal iron complexes into ferritin and hemosiderin in experimental animals - A study with the aid of electron microscopy." Journal of Experimental Medicine 109(2): 197-&.

Richter, G. W. (1984). "Studies of iron overload - Rat-liver siderosome ferritin." Laboratory Investigation 50(1): 26-35.

Robards, A. W. and A. J. Wilson Procedures in electron microscopy, Wiley.

Roder, H., J. Berendzen, S. F. Bowne, H. Frauenfelder, T. B. Sauke, E. Shyamsunder and M. B. Weissman (1984). "Comparison of the magnetic properties of deoxydissociated and photodissociated

myoglobin." Proceedings of the National Academy of Sciences of the United States of America-Biological Sciences 81(8): 2359-2363.

St Pierre, T. G., W. Chua-anusorn, J. Webb, D. Macey and P. Pootrakul (1998). "The form of iron oxide deposits in thalassemic tissues varies between different groups of patients: a comparison between Thai beta-thalassemia/hemoglobin E patients and Australian beta-thalassemia patients." Biochimica Et Biophysica Acta-Molecular Basis of Disease 1407(1): 51-60.

St Pierre, T. G., W. Chua-anusorn, J. Webb and D. J. Macey (2000). "Iron overload diseases: the chemical speciation of non-heme iron deposits in iron loaded mammalian tissues." Hyperfine Interactions 126(1-4): 75-81.

St Pierre, T. G., D. P. E. Dickson, J. K. Kirkwood, R. J. Ward and T. J. Peters (1987). "A mossbauer spectroscopic study of the form of iron in iron overload." Biochimica Et Biophysica Acta 924(3): 447-451.

St Pierre, T. G., K. C. Tran, J. Webb, D. J. Macey, P. Pootrakul and D. P. E. Dickson (1992). "Core structures of haemosiderins deposited in various organs in beta-thalassemia hemoglobin-e disease." Hyperfine Interactions 71(1-4): 1279-1282.

Steinberg, K. K., M. E. Cogswell, J. C. Chang, S. P. Caudill, G. M. McQuillan, B. A. Bowman, L. M. Grummer-Strawn, E. J. Sampson, M. J. Khoury and M. L. Gallagher (2001). Prevalence of C282Y and H63D Mutations in the Hemochromatosis (HFE) Gene in the United States, Am Med Assoc. 285**:** 2216-2222.

Tame, J. R. H. and B. Vallone (2000). "The structures of deoxy human haemoglobin and the mutant Hb Tyr[alpha]42His at 120 K." Acta Crystallographica Section D 56(7): 805-811.

Tanimoto, A., K. Oshio, M. Suematsu, D. Pouliquen and D. D. Stark (2001). "Relaxation effects of clustered particles." Journal of Magnetic Resonance Imaging 14(1): 72-77.

Tarling, D. H. and F. Hronda (1993). The magnetic anisotropy of rocks, Chapman&Hall.

Tejada, J. and X. X. Zhang (1994). "On magnetic-relaxation in antiferromagnetic horse-spleen ferritin proteins." Journal of Physics-Condensed Matter 6(1): 263-266.

Testa, U. (2002). Proteins of iron metabolism. Boca Raton, Florida, CRC Press.

Wally, J., P. J. Halbrooks, C. Vonrhein, M. A. Rould, S. J. Everse, A. B. Mason and S. K. Buchanan (2006). "The Crystal Structure of Iron-free Human Serum Transferrin Provides Insight into Inter-lobe Communication and Receptor Binding." Journal of Biological Chemistry 281(34): 24934.

Ward, R. J., A. L. Florence, D. Baldwin, C. Abiaka, F. Roland, M. H. Ramsey, D. P. E. Dickson, T. J. Peters and R. R. Crichton (1991). "Biochemical and biophysical investigations of the ferrocene-iron-loaded rat - An animal-model of primary hemochromatosis." European Journal of Biochemistry 202(2): 405-410.

Ward, R. J., R. Legssyer, C. Henry and R. R. Crichton (2000). "Does the haemosiderin iron core determine its potential for chelation and the development of iron-induced tissue damage?" Journal of Inorganic Biochemistry 79(1-4): 311-317.

Ward, R. J., M. Ramsey, D. P. E. Dickson, C. Hunt, T. Douglas, S. Mann, F. Aouad, T. J. Peters and R. R. Crichton (1994). "Further characterization of forms of hemosiderin in iron-overloaded tissues." European Journal of Biochemistry 225(1): 187-194.

Webb, J., T. G. St Pierre, K. C. Tran, W. Chuaanusorn, D. J. Macey and P. Pootrakul (1996). "Biologically significant iron(III) oxyhydroxy polymers: Mossbauer spectroscopic study of ferritin and hemosiderin in pancreas tissue of beta-thalassemia hemoglobin E disease." Inorganica Chimica Acta 243(1-2): 121-125.

Wixom, R. L., L. Prutkin and H. N. Munro (1980). "Hemosiderin: nature, formation, and significance." Int Rev Exp Pathol 22: 193-225.

Zhang, J. L., C. Boyd and W. L. Luo (1996). "Two mechanisms and a scaling relation for dynamics in ferrofluids." Physical Review Letters 77(2): 390-393.

Zhou, X. Y., S. Tomatsu, R. E. Fleming, S. Parkkila, A. Waheed, J. Jiang, Y. Fei, E. M. Brunt, D. A. Ruddy and C. E. Prass (1998). HFE gene knockout produces mouse model of hereditary hemochromatosis, National Acad Sciences. 95**:** 2492-2497.

8. Publications

Most of the work presented here has been already published in scientific journals and just the work presented in chapter 4 has been recently submitted to publication. A list of the publications in which I have participated is listed ahead.

Magnetostructural study of iron sucrose, L. Gutiérrez, M. P. Morales, F.J. Lázaro, Journal of Magnetism and Magnetic Materials 293, 69-74 (2005)

Magnetic characterisation of rat muscle tissues after subcutaneous iron dextran injection, F.J. Lázaro, A.R. Abadía, M.S. Romero, L.

Gutiérrez, L. Lázaro, M. P. Morales, Biochimica et Biophysica Acta-Molecular Basis of Disease 1740, 434-445 (2005)

Magnetic and structural study of the state of iron in the oral haematinic ferrimannitol ovoalbumin, L. Gutiérrez, M.P. Morales, F.J. Lázaro, Journal of Inorganic Biochemistry, 100 (3), 413-417 (2006)

Bioinorganic transformations of liver iron deposits observed by tissue magnetic characterisation in a rat model, L. Gutiérrez, F.J. Lázaro, A. R. Abadía, M. S. Romero, C. Quintana, M. P. Morales, C. Patiño, R. Arranz, Journal of Inorganic Biochemistry, 100 (11), 1790-1799 (2006)

Comparative study of iron containing haematinics from the point of view of their magnetic properties, L. Gutiérrez, F.J. Lázaro, Journal of Magnetism and Magnetic Materials 316 (2), 136-139 (2007)

Biological tissue magnetism in the frame of iron overload diseases, F.J. Lázaro, L. Gutiérrez, A.R. Abadía, M.S. Romero, A. López, Journal of Magnetism and Magnetic Materials, 316 (2), 126-131 (2007)

Whole tissue AC susceptibility after superparamagnetic iron oxide contrast agent administration in a rat model, F.J. Lázaro, L. Gutiérrez, A.R. Abadía, M.S. Romero, A. López, M.J. Muñoz, Journal of Magnetism and Magnetic Materials, 311, 460-463 (2007)

The role of dipolar interaction in the quantitative determination of particulate magnetic carriers in biological tissues, López, L. Gutiérrez and F.J. Lázaro, Physics in Medicine and Biology, 52, 5043-5056 (2007)

The speciation of iron in desert dust collected in Gran Canaria (Canary Islands): Combined chemical, magnetic and optical analysis, F.J. Lázaro, L. Gutiérrez, V. Barrón and M.D. Gelado, Atmospheric Environment (In press)

Iron speciation study of Hfe knockout mice tissues: Magnetic and ultrastructural characterisation, L. Gutiérrez, C. Quintana, C. Patiño, J. Bueno, H. Coppin, M. P. Roth, F. J. Lázaro (submitted to Biochimica et Biophysica Acta - Molecular Basis of Disease)

9. Acknowledgements

Quiero expresar mi gratitud a las siguientes personas e instituciones por su apoyo durante la realización de esta tesis:

A la Diputación General de Aragón por la concesión de una beca para la realización de la tesis doctoral.

Al Instituto de Salud Carlos III y a la Diputación General de Aragón por la concesión de fondos para la realización de este trabajo.

A Pacho por su dedicación, apoyo y entusiasmo.

Al resto de miembros del Grupo de Análisis Magnético de MAteria Nanodispersa (γN): Antonio López, Marisol Romero y Ana Rosa Abadía, sin los cuales este trabajo no podría haberse realizado.

A Carmen Quintana, Cristina Patiño y Rocío Arranz por explicarme los detalles del TEM de tejidos.

A Mª Puerto Morales y el resto de gente del ICMM que me acogieron una temporada en Madrid.

A Helene Coppin y Marie-Paule Roth por la colaboración para estudiar los ratones "transgénicos" y al resto del grupo de Toulouse por la estancia allí.

A Ana Arauzo, Enrique Guerrero por estar siempre dispuestos para solucionar cualquier problema con el SQUID.

A Mª Jesús Muñoz y José Ignacio Rivera por su ayuda con las ratas.

A Octavio Alda por prestarnos el liofilizador en los inicios y a Marta aguantar el ruido que hace.

A mis compañeros del departamento de Ciencia y Tecnología de Materiales y Fluidos de la Universidad de Zaragoza.

Al personal de limpieza del centro, especialmente a Milagros.

A mi familia y amigos por estar siempre ahí.

A Miguel.